SOME STUDIES IN SINGLE PARTICLE AND PLASMA CONFINEMENTS IN MAGNETIC MIRROR

A THESIS

SUBMITTED FOR THE DEGREE OF

DOCTOR OF PHILOSOPHY

OF THE

GUJARAT UNIVERSITY

BY

DHIRAJ BORA

OCTOBER 1979

PHYSICAL RESEARCH LABORATORY
AHMEDABAD 380 009
INDIA

TO MY PARENTS

C O N T E N T S

STATEMENT

The primary aim of the work described in this thesis is to study the behaviour of charged particles in magnetic field with spatial variations. The work describes the experiments conducted to study the single reflection of charged particles and plasma from a magnetic mirror as well as the leakage of charged particles due to nonadiabaticity from an adiabatic trap with different magnetic field scale lengths during confinement.

The escape of particles from the mirror traps is regarded as being due to departure of the magnetic moment from adiabaticity. As a consequence of this departure, the value of the magnetic moment changes as the particle traverses certain region of the magnetic field variation. The expression for such a change has been obtained in literature. From the expressions it is seen that even for a single reflection the change in magnetic moment, $\Delta\mu$, depends on various parameters of the system. The nonadiabatic escape of particles from magnetic trap is usually explained as a consequence of the cumulative change in $\Delta\mu$, that makes the particles fall in the loss cone and escape. In a theoretical work by Varma nonadiabatic leakage of particles have been studied and it is shown that there exist multiple e-folding times in the leakage of the particles having same energy and initial value of the magnetic moment. A literature survey of the earlier theoretical, numerical and

experimental works pertinent to the problem, described in the thesis, is done and presented in Chapter I.

With an aim to investigate the possible existence of multiple life times in the leakage of the charged particles, an experimental system was set up. The design considerations of different subsystems and their integration along with the different diagnostics used are described in Chapter II.

A single reflection experiment was conducted for a low energy electron beam at high vacuum conditions. The experiment was repeated with a simple plasma gun. Chapter III describes the experimental techniques and results obtained from the single reflection experiment. It is observed that the reflectivity of the mirror goes through a minimum, as the nonadiabaticity parameter is increased, and attains a value less than the value for an adiabatic mirror configuration. Based on the experimental observations, it is concluded that nonadiabatic mirror traps can be as effective as the adiabatic mirror trap for sufficiently high density electron beams and plasma streams.

Charged particle confinement in magnetic mirror and the life time measurements for charged particles of different energies under various different conditions are described in Chapter IV. Along with other experimental techniques, numerical analysis of the data is described in detail. The main result obtained from the sets of experiments performed is the

observation of two life times for particles with specified energy and initial magnetic moment, leaking out of the magnetic mirror. Most of the results concerning the variation of the life times with different parameters of the system can be explained with the help of the theoretical work of Varma[47].

The results obtained from the experimental works are recapitulated in Chapter V.

ACKNOWLEDGEMENTS

The work presented in this thesis was carried out under the supervision of Professor R.K. Varma. I am sincerely grateful to him for his guidance and encouragement throughout the course of the work. I also thank him for critically going through the manuscript and for important suggestions towards its improvement.

I gratefully acknowledge the help and constant encouragement extended by Professor P.I. John without which it would have been difficult to complete the work. I thank Dr. Y.C. Saxena for his interest in the work and friendly advice, specially during the numerical analysis of the results. I also thank both of them for their useful suggestions during the preparation of the manuscript.

I have academically benefited a lot from Drs. S.K. Mattoo, M. Sinha, A.M. Punithavelu, B.N. Goswami and P.N. Guzdar.

I thank Dr. V.Sheorey for making the programmes of function minimization available to us and Dr. K.S. Rao for help during the computation. The assistance of Mr. V.R. Choksi during data handling and analysis is acknowledged.

The experimental work presented in this thesis was supplemented by the efficient technical assistance of M/s.K.S. Lali, H.D. Pujara, H.A. Pathak, S.B. Bhatt, A.H. Shaikh and D.R. Vinchi. The help rendered by M/s. M.P.K. Kurup and

K.K. Sivsankaran from the glass blowing section and M.M. Mistry and D.M. Suthar from the workshop staff during the installation of the experimental system is greatly appreciated.

I owe immensely to my friends and colleagues K.K, K.K. Jain, Venkat, Manab, Jiten, Bhatta, Mohan, Nirjhari and P.K. Bhattacharji for their cooperation and help during the course of the work in some way or the other.

I sincerely thank Mr. T.T. Chacko for neat and efficient typing of the thesis. My thanks are also due to M/s. H.S. Panchal, S.K. Bhavsar, N.D. Dave and D.R. Ranpura for their efficient and skilfull drafting and photography. I also thank Mr. Ghanashyam Patel for speedy cyclostyling of the thesis.

LIST OF FIGURES

LIST OF TABLES

Table 4 The values of $T_{eff\ 1,2}/\ T_b$ for different values of total energies E, magnetic field scale lengths $\mathcal{L}^{-1}$ and pitch angles. 127

CHAPTER 1

INTRODUCTION

1.1. Magnetic Mirrors:

Confinement of plasma for sufficient time is one of the major problems in the field of plasma research. The schemes for magnetic confinement of plasma are conveniently grouped as having closed or open magnetic lines of force. As candidates for fusion reactors, each type of device possesses different advantages and disadvantages.

As the name suggests, in closed line systems, the magnetic lines of force do not leave the volume and are confined to a family of nested, toroidal flux surfaces. Confinement is achieved as the plasma loaded surfaces are isolated from the material wall. However, the particle or energy loss are due to the mechanisms which transport them across the magnetic lines. Therefore, this loss is associated with transport in space and confinement time can be increased by increasing the physical dimension of the system. The principal toroidal confinement device at the present time is the Tokamak.

Magnetic Mirror trap is one of the examples of the open field line systems. These open line systems present an entirely different picture, although the basic aim is the same. The magnetic lines of force leave the plasma volume to pass through the material walls. The axial confinement of the particles is achieved either because they are mirror trapped by

virtue of the adiabatic invariance of the magnetic moment or in the case of long, straight reactor concept simply because of the time of flight. The life time of a particle in a mirror trap is limited by the time for velocity space scattering from regions where a particle is trapped to one where it is not. Therefore by increasing the physical dimensions, no direct life time advantage is gained. Many examples of mirror effect in confinement of particles can be cited in nature also. One such example is the particle confinement in the Van Allen belts. The magnetic field of the earth being strong at the poles and weak at the equator forms a natural mirror. In rest of this section, we will discuss the basic features of this confinement mechanism.

The particle confinement in a magnetic mirror field is based upon the conservation of the magnetic moment, μ. It is defined as

$$\mu = m v_{\perp}^2 / 2B \qquad (1.1.1)$$

where m is the mass of the charged particle, $V_{\perp}$ is the component of the velocity perpendicular to the magnetic field lines. The constancy of the magnetic moment is an asymptotic result as a consequence of the slow variation of the magnetic field in the frame of the particle's motion. Thus, while calculating the change in the magnetic moment μ, a

smallness parameter is often defined in relation to the relative change of the magnetic field over a distance of the order of Larmor radius (r_L/R), where r_L is the Larmor radius of the particle and R is the radius of curvature of the magnetic lines of force. Therefore, in a static inhomogeneous magnetic field, the adiabaticity condition is expressed in the following way

$$\gamma_L \nabla_\mu B/B \ll 1 \qquad (1.1.2) .$$

The motion of charged particles in static magnetic field has been studied extensively [4,6,40].

In a mirror trap, the magnetic field configuration has a minimum at the midplane of the system and the two field values at the ends are maximum. In such a static, inhomogeneous magnetic field the total energy of particles is an invariant. Some of the particles injected into a magnetic mirror have trajectories which encircle the magnetic axis of symmetry while other particles have trajectories which do not encompass the axis. The nature of trajectories is determined not only by the radial position of injection but by the particle energy, the angle of particle injection and the field value at the point of injection.

In a cylindrically symmetric system, the canonical angular momentum is an absolute invariant of the motion. As argued below, a particle that encircles the magnetic axis can be permanently confined if its energy and canonical angular momentum are suitably chosen. In cylindrical coordinates (r, θ, z), the

Hamiltonian for a charged particle in an axially symmetric mirror field is given by[48]

$$H = (2m)^{-1}\left\{P_r^2 + P_z^2 + \frac{1}{r^2}\left[P_\theta - (e/c)\,rA_\theta\right]^2\right\} \qquad (1.1.3)$$

where $P_\theta = mr^2\dot{\theta} + e/c\, rA_\theta$ is a constant of motion in the axis symmetric field.

From the expression (1.1.3) it is seen that if P_θ, the canonical angular momentum, could be negative, then the last term in the Hamiltonian would be large. When P_θ is sufficiently negative, it follows that in some regions the last term in the Hamiltonian may be larger than the total energy of the particle, and the particle is trapped regardless of the conservation of its magnetic moment.

From the expression of the canonical angular momentum, it is clear that for $e > 0$, the canonical momentum can be negative only through the term $mr^2\dot{\theta}$ with $\dot{\theta} < 0$. In the cylindrical coordinates $\dot{\theta} < 0$ implies that the particles encircle the axis of symmetry. Thus, particles can be permanently trapped if they have the appropriate energy and circle the axis of symmetry. It also follows that greater the energy of the particle, the more negative will be the canonical momentum needed to trap it and larger will be the Larmor radius of the particle.

If the particles have small Larmor radius, the P_θ itself vanishes as $\sim r^2$ and the term involving P_θ in the Hamiltonian

vanishes as $\sim r^2$ and therefore provides a well of vanishing depth as $r \rightarrow 0$. This means that permanent trapping becomes unimportant as Larmor radius becomes small.

Apart from the special case of absolute confinement in the axisymmetric systems, the confinement is usually adiabatic in nature and occurs in consequence of the adiabatic invariance of the magnetic moment and the constancy of the total energy in a static magnetic field. By virtue of the fact that the magnetic moment of the particle remains constant, the perpendicular energy of the particle increases at the expense of the parallel kinetic energy as the particle moves from a weak field region into a stronger field region. Thus at a sufficiently strong magnetic field, the particle looses its parallel energy completely and because of the parallel force $F_{11} = -\mu \nabla_{11} B$ ($\nabla_{11} B$ is the magnetic field gradient along the direction of motion), the particle is reflected back towards the weaker field. Thus, the particles can be reflected back and forth between the two strong magnetic field regions seperated by a weaker field in between. The two points of reflection in strong field regions are known as the mirror points. Particles injected into the minimum field region with a total kinetic energy W can be made to travel to and fro between the mirror points provided the following condition is satisfied:

$$W/W_{\perp} \leqslant R_m \qquad (1.1.4)$$

Here $W_{\perp}$ is the perpendicular energy of the particle at the

minimum of the magnetic field and R_m is the mirror ratio defined as

$$R_m = B_{max} / B_{min} \quad . \qquad (1.1.5)$$

This constraint on the relative magnitude of perpendicular energy and total energy for confinement, can alternately be expressed as

$$1/\sin\theta \leq \sqrt{R_m} \qquad (1.1.6)$$

where the pitch angle θ is the angle that the velocity vector of the particles makes with the lines of force at the minimum of the magnetic field B_{min}. This pitch angle θ, has a critical value θ_m, determined by $\sin\theta_m = R_m^{-\frac{1}{2}}$, such that particles having $\theta < \theta_m$ will not be reflected back from the mirror point and will therefore, escape the trap. The equation (1.1.6) above thus defines a boundary in the velocity space in the form of a cone which is known as the loss cone. Fig.1(a) depicts the loss cone in the velocity space. θ_m is known as the "loss cone angle" and particles having velocity vector within this "loss cone" are not trapped in the magnetic mirror where as those with velocity vectors outside the cone are trapped. Fig. 1(b) shows the motion of a charged particle in a magnetic mirror.

Such a picture of trapping can also be visualized in terms of the particles residing in a potential well of height μB_{max}, so that those particles with total energy less than the well height are confined and those with higher values of energy manage to escape from the well.

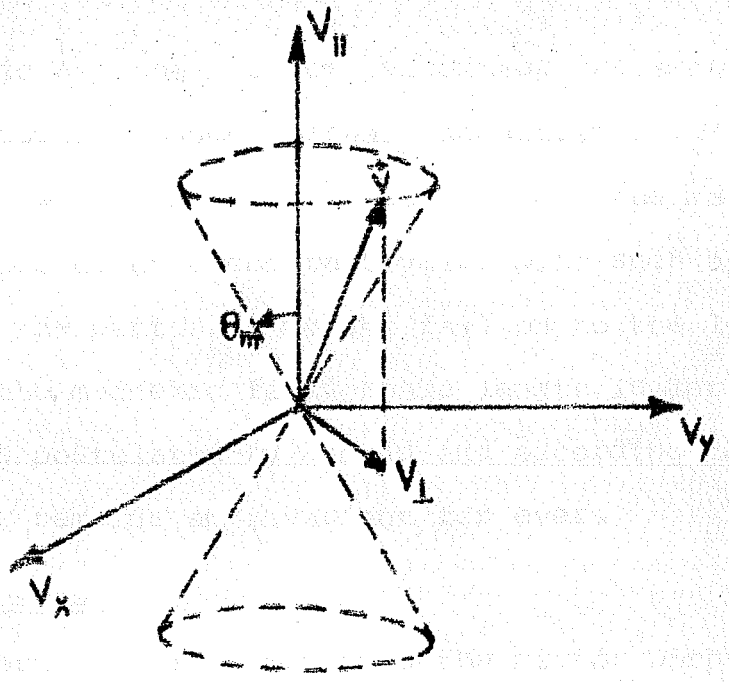

Fig. 1a. Schematic representation of the loss cone in the velocity space configuration. θ_m defines the boundary of the loss cone.

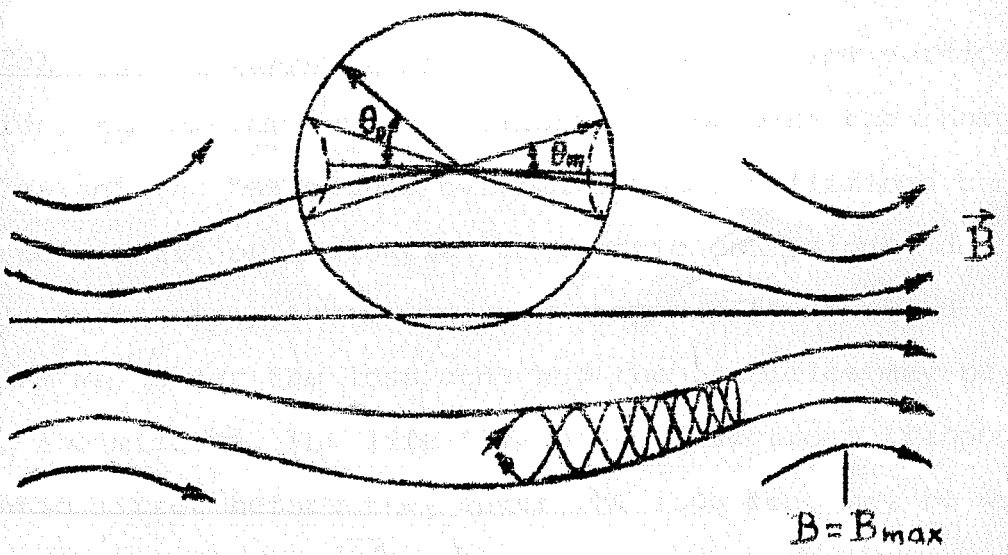

Fig. 1b. Particle motion in a magnetic mirror.

The particles, that do not encompass the axis also can be trapped perpetually under certain conditions. In an axially symmetric trap, which is a non-linear system, the magnetic moment oscillates about a constant value with such a small amplitude that the particles do not fall on to the loss cone, provided that the magnetic field scale length is large. This hypothesis[2] was postulated by Arnold and according to this, the magnetic moment remains an invariant for ever.

1.2. Loss Processes:

The particles injected into the mirror with parameters satisfying the trapping condition do not in general get trapped perpetually. For low particle densities, there are primarily two processes which may lead to the particle leakage from the trap. i) Collisions between particles; ii) Departure from the adiabatic invariance of the magnetic moment.

1.2.1. Collisions between particles: In case of low particle densities, the predominant collisions are between the charged particles and the background neutrals. These collisions can either be elastic or inelastic. In elastic collisions, due to multiple scattering, the velocity vector of the charged particles may enter the loss cone and the particles may be lost through the mirrors. The life time of the electrons trapped in a magnetic mirror before they enter the loss cone may be written as[19]

$$\tau_{scat} = \frac{\overline{\alpha^2}\, V^3}{8\pi N_0 (Z^2+Z)\, r_0^{*2}\, c^4 \ln \frac{V^2}{2\alpha^* Z^{4/3} c^2}} \qquad (1.2.1)$$

where $\overline{\alpha^2} = 2\left[\arccos\left(1/\sqrt{R_m}\right) - \theta\right]^2$, Z is the atomic number and N_o is the number density of the gas, r^* is the classical electron radius, θ is the initial pitch angle at the midplane of the mirror system, V is the velocity of the electrons and α^* is the fine structure constant. When the background gas is air, this equation reduces to

$$\tau_{scat} = 2 \times 10^{-9} \frac{\overline{\alpha^2} E^{3/2}}{P \ln(2.7E)} \qquad (1.2.2)$$

Here τ_{scat} is expressed in seconds, E in kev and P, the residual gas pressure, in Torr.

From (1.2.2) one can observe that the scattering time increases as the residual gas pressure in the working volume reduces and the energy of the particles is increased. By reducing the pressure and increasing the energy, it is thus possible to confine the particles for longer time provided the nonadiabatic effects are negligible.

Inelastic collisions affect the life time of the particles in the trap to a much lesser extent as compared to elastic collisions. As the atomic number Z of the gas increases, the elastic collision cross section $\sigma_{elast.}$ increases as Z^2, where as the inelastic collision cross section $\sigma_{inelast.}$ is directly proportional to the atomic number Z. Moreover, the ratio of the differential cross section for inelastic collisions to those for elastic collisions through a given angle falls sharply as the scattering angle increases.

Therefore, the probability of any marked change in the direction of motion of the particles due to inelastic collisions is small compared to the probability of a change in the direction of motion as a result of elastic collisions.

1.2.2. Departure from the adiabatic invariance of the magnetic moment: In the absence of collisions, particles which satisfy the trapping condition initially should remain trapped for ever. However, this does not happen, as the magnetic moment is only an approximate constant of motion valid only under the condition for the adiabaticity. Whenever the condition (1.1.2) is violated, variations in the magnetic moment are likely to occur as the particles travel to and fro in the inhomogeneous magnetic mirror field. Whether these variations in magnetic moment accumulate over long periods of particle residence in the mirror or whether there are limits to the variations so that the magnetic moment oscillates about some mean value are questions which have not been understood very well so far. These questions have been the subjects of many theoretical, numerical and experimental studies, some of which are summarised in the following sections.

1.3. Theoretical Studies Related to the Nonadiabatic Behaviour of charged particles in Magnetic Mirror traps:

The escape of particles from a magnetic mirror trap in the absence of collisions can be regarded as being due to the departure from adiabaticity. There have been various approaches to calculations of nonadiabatic changes in the magnetic moment and the related phenomena. Classical theoretical calculations[1,33,34] as well as quantum mechanical treatments[18] have been used to estimate the departure from adiabaticity. Following another line, resonance theory[10] of energy transfer between different degrees of freedom has been also invoked to explain the non-adiabatic effects.

Following the treatment used by Dykhne[18], change in the magnetic moment, $\Delta\mu$, for a spatially nonuniform magnetic field can be written as

$$\Delta\mu/\mu = A\ \mathrm{Re}\left[\exp i\left(\int^{S} \frac{\omega(s)}{V_{11}(s)}\, ds\right)\right] \qquad (1.3.1)$$

where ω is the Larmor frequency and V_{11} is the particle velocity parallel to the lines of force S. The pre exponential factor A is weakly dependent on the adiabaticiy parameter.

Unlike the analysis of Kulsrud[34], the work of Dykhne[18] has established a relation between the finite value of the smallness parameter (ρ_L/R) and $\Delta\mu/\mu$. With the help of (1.3.1), the change in the adiabatic invariant can be investigated as a function of pitch angle, mirror width etc.

In another approach[10] invoking resonance energy transfer among different degrees of freedom of particles, the redistribution of energy has been explained in the following way: the charged particles, which are trapped in a magnetic mirror, oscillate between the two mirror points. Resonance can occur between the Larmor gyration of the particles and the slow oscillations (or its harmonics), depending upon the prevailing conditions in a mirror trap. In the vicinity of the separatrix of each resonance there appears the so called stochastic layer, which constitutes a certain region of unstable motion. If the smallness parameter increases, the resonance layer broadens to the dimensions of their resonances as a result of which neighbouring resonances overlap in phase space and strong stochastic instability results[28]. The magnetic moment, therefore, can change and it can allow a redistribution of energy among the longitudinal and transverse degrees of freedom of the particles. As a consequence, the particles can fall into the loss cone and thus leak out of the magnetic trap. Following this argument Chirikov[10] calculated the systematic change in μ and its spread. For different values of $\Delta B/B$, the number of reflections for the particles was calculated. The draw back in this theory is that it has been given only in the approximation of straight lines of force and thus deals only with systems having infinite scale sizes for magnetic field variations.

It is possible to determine the life time using $\Delta\mu$ by solving the Fokker-Planck equation in the magnetic moment space. This would give the evolution of the particle density as a function of μ and time. However, in another formalism, Fokker-Planck diffusion treatment[7,11] has been used to study the diffusion in velocity space associated with the nonadiabatic changes in the magnetic moment of a particle. This formalism describes the temporal behaviour of the distribution function and therefore leads to a diffusion rate due to nonadiabaticity.

The diffusion coefficient $\langle(\Delta\mu)^2\rangle$, which has been calculated is given by[7]

$$\frac{\langle\Delta\mu^2\rangle}{\mu^2} \simeq \frac{AE}{\mu B} \exp\left[-r_L g\left(\frac{E_{th}}{E}\right)^{1/2}\right] \qquad (1.3.2)$$

where A is a slowly varying function of pitch angle with a magnitude of order 5, g is another slowly varying function of pitch angles less than $\pi/4$, r_L is the particle Larmor radius calculated in terms of the thermal energy E_{th} of the particles.

The "diffusion" due to nonadiabaticity can be compared with the classical diffusion constant. It is observed that the nonadiabatic effects are dominant for large values of E/E_{th}. Because of the pitch angle dependence of g, small pitch angle particles are most susceptible to nonadiabatic diffusion.

These are some of the approaches made to understand the nonadiabatic behaviour of charged particles in an inhomogeneous

magnetic field. However, so far in these works, the question of the determination of the life time in a magnetic trap has no where been explicitly discussed, and as a consequence no specific relationships between the time of residence of the particles in the mirror trap to various parameters of the particles and the mirror trap have been obtained.

1.4. Numerical Calculations of Particle Trajectories in Magnetic Mirrors:

One of the problems requiring greater understanding is the extent to which particles obey predictions of the adiabatic theory. Particle trajectories have been followed numerically and the results have been compared with the adiabatic predictions[21,25,40]. The magnetic moment (μ) and the change in it per reflection ($\Delta\mu$) is calculated in these numerical works as a function of the different parameters of the system.

In one of these works[21], the effect of different parameters like velocity, the initial phase angle etc,, on the change $\Delta\mu/\mu$ has been extensively studied. The dependence on the velocity can be well approximated by a function of the form A exp $(-b/v)$, where A and b are constants.

The variations in μ was investigated for different orbit sizes. This was found to be large in case of the large orbit sizes. The magnetic moment oscillates at the gyration frequency about a fixed value until the particle crosses the median plane in magnetic mirror, near which μ suffers a large transient change. Then μ oscillates about a new mean value; the residual change in μ between successive reflections, depends on the various parameters that define the orbit.

Cumulative effect on the change $\Delta\mu$ after many traversals in the machine have also been investigated. To investigate this effect, such orbits have been computed for which the particle

made many reflections[21,40]. At each traversal of the median plane, the pitch angle (δ) is plotted as a function of the phase angle λ. Fig.2 shows the plot of δ as a function of λ[40]. In fact, instead of δ, δ or $\pi-\delta$ which ever is smaller is plotted. In this phase plot the numbered points represent the successive travel through median plane. Zero indicates the initial point. From the plot it is quite evident that there are two types of particle behaviour. One of the behaviours can be termed as stable where the successive traversals of the median plane can be connected by smooth curve of the type A or B. The other can be termed as unstable and the successive traversals are shown by X. The pitch angle δ of the stable particles may undergo severe variations. It is seen that the variations are larger for larger gyro radius. However, these variations are highly self cancelling and the phase points always appear to fall on a well defined curve such as A or B.

In contrast to the stable particles, the unstable particles do not fall on a well defined curve. Successive points in the phase plot meander in a rather erratic way and after a few reflections the particles escape through the loss cone.

The constancy of the magnetic moment is an asymptotic result as a consequence of the slow variation of the magnetic field in the frame of the particle's motion. The stable curves of the phase plot can be qualitatively predicted with the help of the first two terms of the magnetic moment series.

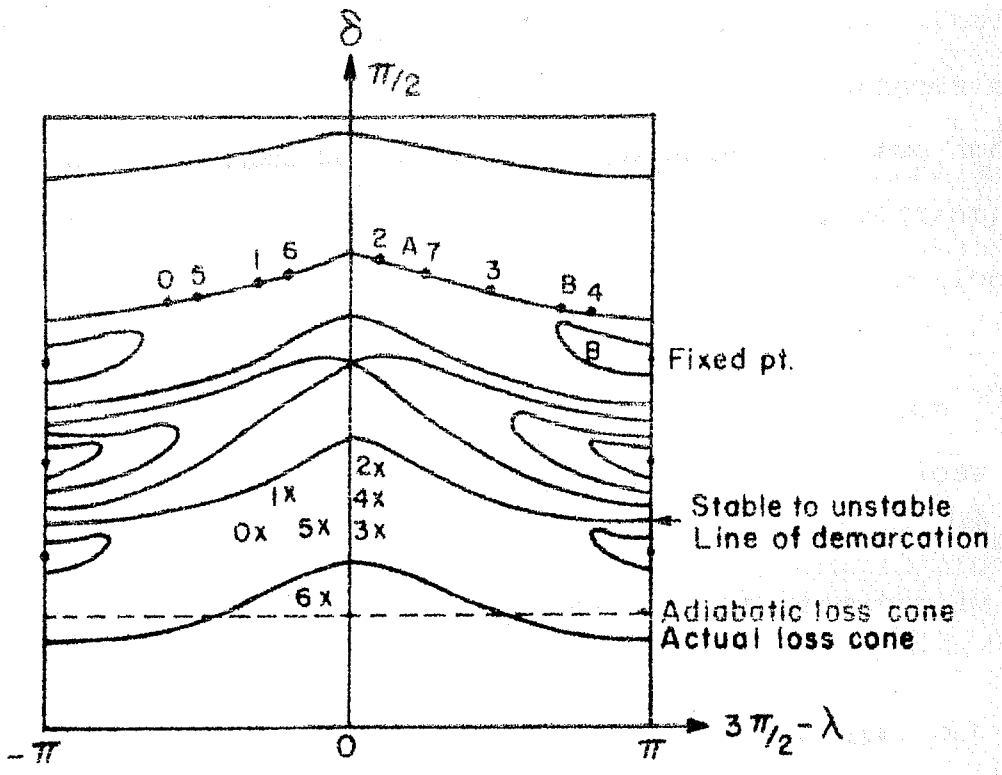

Fig. 2. Phase plots for a particle in a mirror geometry.

Fig.2 can be plotted as a polar diagram[21], in which case the curves A would be closed curves. One can probably state that these smooth curves represent the intersection with the median plane of two dimensional surfaces, which are invariant. They are invariant in the sense that all particles on such surfaces at any time would stay on them for ever. It is possible to have among curves of type A, which appear numerically to be invariant, some curves that are not really invariant, but the deviation is much less than the numerical errors.

In an azimuthally asymmetric system, the invariant curves cannot "seal off" non invariant curves from the loss cone. As a consequence of not "sealing off" of the surfaces, the particles are lost at a faster rate than in the azimuthally symmetric case.

From the results of these numerical experiments, one can conclude that even beyond the adiabatic loss cone, there exists a region where the particle motion is not stable and the particles in this region are lost after a few reflections, thus the residence time for such particles is considerably reduced. There lies a line of demarcation between the stable and the unstable region which can be termed as the effective loss cone which is slightly larger than the adiabatic loss cone.

Usually in the numerical calculations, the charged particles can be followed only for a limited number of reflections. As the number of reflections increases, the

computational error creeps in and the calculations become unreliable. Therefore, it is difficult to follow the charged particles for very many reflections before they are lost through the loss cone.

1.5. Experiments in Magnetic Mirror Traps:

The behaviour of charged particles in an adiabatic mirror trap has also been a topic of experimental studies since long. One of the possible consequences of the nonadiabatic behaviour is the leakage of charged particles from adiabatic confinement in the mirror traps. This will result in the particles having a finite life time in the trap. The earlier experiments[22,23,44] were mainly conducted with the motivation of studying the life time as a function of different parameters such as mirror ratio, residual gas pressure etc. and these results were compared with the predictions of scattering theories. Experiment[8] has also been conducted to study the effect of local perturbation of the magnetic field on the life time. In the more recent experiments[5,16,41], the critical value of the adiabaticity parameter has also been investigated. There has been another approach to study the transition from adiabatic to nonadiabatic motion of charged particles[42,43]. These studies have been done experimentally and numerically simultaneously.

1.5.1. Nonadiabatic behaviour with single reflection: Experimental studies of a single interaction of a beam of charged particles with a magnetic barrier under steady state conditions were conducted[42]. An ion beam was used during the experiment.

It was possible to detect

experimentally the transition from adiabatic to nonadiabatic reflection of the ion beam and these results were compared with the results of numerical computation. The percentage of particles, which were adiabatic, was plotted as a function of the mirror ratio R_m and $\langle R_L \rangle / Z_o$ for the average radius about which the particle gyrated during its reflection or escape, α_1 . Here $R_m = B_{min}/B_{max}$; $\langle R_L \rangle$ is the average Larmor radius, based on the constant speed of the particle and average magnetic field, Z_o is the distance from the midplane to one end of the mirror. It was observed that the percentage of nonadiabatic particles increased with larger orbit sizes.

1.5.2. Particle confinement experiments in Magnetic Mirrors: The source of the charged particles in the confinement experiments were different in different cases. In most of the experiments, the charged particles were produced over a large volume of the experimental chamber. For instance, in one of the earliest experiment, Rodionov[44] studied the motion of β particles from the radio active decay of tritium in an adiabatic trap. In another set of experiments Gibson et al.[22,23] studied the confinement of energetic positrons emitted from Ne^{19} isotropically and uniformly in a mirror geometry.

In these experiments, the life time was measured as a function of different parameters of the system and the particles themselves. Variation of the life time on the minimum of the magnetic field was also investigated by Rodionov and

for a fixed maximum magnetic field, a maximum of life time was observed. In the works of Gibson et al.[22,23] very large containment time was observed. The life time in the symmetric as well as in the asymmetric magnetic mirrors was measured as a function of different parameters. In these experiments the loss of particles was entirely collisional.

The draw back of these experiments were that the pitch angle and the mirror ratio for all the particles were not identical since the particles were produced at different regions of the system as mentioned in the begining of this discussion.

Localized introduction of charged particles was done in a machine called "Ogryonok", where Brevnov and Tomashchuk[8] studied the effect of local perturbations of the magnetic field on the life time. An ion beam was led into the injection radius with the help of a magnetic channel. The magnetic channel gave rise to the non uniformities in the magnetic field of the mirror machine. Controlled local perturbations also could be produced with the help of a magnetic dipole.It was observed that the life time was shortened drastically due to the perturbations in the magnetic field. These perturbations could shift the centre of gyration of the ions across the magnetic field by a distance of the order of magnitude of the Larmor radius also.

There have been a few more refined experiments[5,16,41] to study the nonadiabatic behaviour of charged particles in a magnetic mirror. The methodology in all these experiments were conceptually similar. Charged particles, all having specified energy and initial value of the magnetic moment were injected off axis into a magnetic mirror trap and confined in it adiabatically. The particles escaping the trap were collected at one end and the leakage current was measured as a function of time. The current signals were then analysed to determine characteristic leakage time for the particles. Besides determining the leakage time, the spectra were taken after different intervals of time after the particles were captured in the trap for different magnetic field strengths and different field configurations[41].

The ratio $\Delta\mu/\mu$ was calculated from the experimentally obtained inflection points on the curves $\bar{\tau}(H_{max})$, where $H_{max} = H_{cr}$. This ratio of change in the magnetic moment to the magnetic moment exhibited a functional dependence of the form $\exp(-\chi H_{max})$[41]. The maximum value of the nonadiabaticity parameter at the critical magnetic field $H_{critical}$ was calculated and was found to depend on the magnetic field configuration. Thus, the behaviour of nonadiabatic process appeared to depend not only on the nonadiabaticity parameter but also on the field geometry.

The effect of nonadiabaticity is manifested as an exponential decrease of the life time with the reduction of the magnetic field for fixed residual gas pressure and beam energy[5]. As the magnetic field is decreased the Larmor radius of charged particles increases. Therefore after a certain critical magnetic field, it is possible to have such Larmor radius for the particles that they would encircle the axis of symmetry of the system. This could happen even for initially off axis particles. In such cases, large confinement times at lower magnetic field values would be expected as were observed by Balebanov and Semashko[5]. The mechanism for such large confinement times has been already discussed in the begining of the chapter.

Besides the effect of nonadiabaticity on particles, some more interesting results were obtained during the course of these experiments. Ponomarenko et al.[41] observed that the leakage current as a function of time indicated two characteristic life times. However this was interpreted as due to particles in the trap with different magnetic moments. Those with magnetic moments in the neighbourhood of the critical value of the magnetic moment for confinement would leave the trap in a short time; while those with larger magnetic moment would leave the trap after a longer time.

Another interesting result was the observation of very large confinement times of the order of a few minutes by Dubinina et al.[16]. $\ln \tau$ Vs B curve showed an abrupt steepening signifying

this fact. Authors explained this with the help of the Arnold's hypothesis[2], which has been discussed briefly in the begining of this chapter.

There have been many other experiments[14,15,26,27,28] which were conducted basically to study the critical value of the adiabaticity parameter. Since near the midplane, the dipole trap is very much similar to an ordinary mirror trap, one can just mention about the study of nonadiabatic loss [26,27,28] in such a trap. It has been observed that at large values of the adiabaticity parameter, escape of particles, due to nonadiabaticity of the magnetic moment, loss from the dipole trap enhances and the containment time reduces.

From all these experiments, one can conclude that beyond a critical value of the adiabaticity parameter, the nonadiabatic loss of particles occur from a magnetic mirror. The decrease in lifetime as a consequence of the increase in nonadiabaticity follows an exponential behaviour[5]. The nonadiabatic behaviour not only depends on the nonadiabaticity parameter but also depends on the field geometry.

1.6. Wave Mechanical Model for Nonadiabatic loss from Magnetic Mirror.

Most of the theories and the models that have been used to interpret the experimental results are based on the adiabatic loss cone concept. A suggestion usually made[5,16,10] for the mechanism of nonadiabatic escape of particles from magnetic

traps is that they suffer a cumulative change in their action invariant until they finally fall into the loss cone and escape.

Therefore, discarding the adiabatic loss cone concept, a wave mechanical model for the nonadiabatic loss of particles from magnetic mirror traps was considered by Varma[47]. The nonadiabatic loss is a consequence of the exact equations of motion and these equations constitute the only mechanism of escape. Since the adiabatic concept is discarded, one can work in terms of the exact trajectories of the particles. To describe the distribution of particles, the adiabatic action $\mu = m v_\perp^2 / 2\Omega$ is introduced as a variable, which is nothing but the time integral of the adiabatic Lagrangian. Here Ω is the electron gyro frequency. Even though the exact trajectories are very complicated, the distribution in action has some simple properties which are fully utilized in the theory. The slight nonadiabaticity that is considered guarantees that the distribution in μ at any subsequent time will be centered around the initial value $\bar{\mu}$. The trap is considered axi-symmetric and the particles are injected away from the axis of symmetry.

The guiding centre equation of motion

$$m \frac{dv_\parallel}{dt} = -\nabla_\parallel (\bar{\mu} \Omega) \qquad (1.6.1)$$

can be obtained by minimising the action S. Action S can be written in the following fashion.

$$S = \int dt \left(\frac{1}{2} m v_{\perp}^2 - \bar{\mu} \Omega \right) = \int L \, dt \qquad (1.6.2)$$

where L is the Lagrangian. The magnitude of the action S at a given time as calculated for an exact trajectory will be in general different from the adiabatic value S_A at that space point x at a time t. But as $\bar{\mu} \to 0$ the action S will approach the latter if the changes in action S are infinitesimal. At an adiabatically accessible point (x, t), the distribution of particles in S would peak around the adiabatic value S_A. Thus it can be noted that the action appears as a very significant label because for a trajectory to end up outside the trap at the end of a time t, it must have its action different from the minimum for that time.

The problem of determining the probability of nonadiabatic escape of particles then reduces to finding the fraction of trajectories labeled by the action that end up outside the trap at each instant of time. The action phase ϕ is introduced as a variable, instead of the action, which is defined as $\phi = S/\bar{\mu} = \varphi + \int \frac{1}{2} m v^2 dt / \bar{\mu}$. Density of the trajectory end points are given by f (x, ϕ_t, t) at the time interval t per unit interval Δx at x and with their action phases in $\Delta \phi_t$ at ϕ_t. The particle density at (x, t) is given by

$$G(x,t) = \int d\phi_t \, f(x, \phi_t, t) \qquad (1.6.3)$$

The following equation for f can be written down

$$f(x, \phi_{t+\zeta}, t+\zeta) = \int d(\Delta x) f(x-\Delta x, \phi_t, t) \times P(x, t+\zeta, \phi_{t+\zeta} \mid x-\Delta x, \phi_t, t) \quad (1.6.4)$$

where p represents the probability that a particle at $(x-\Delta x, t)$, with action phase ϕ_t goes to the point $(x, t+\zeta)$ with action phase $\phi_{t+\zeta}$. For infinitesimal changes

$$\phi_{t+\zeta} = \phi_t + L\zeta/\bar{\mu} \quad . \quad (1.6.5)$$

It can be mentioned that in the adiabatic limit $\mu \to 0$, the equation (1.6.4) yields the equation of continuity.

A very useful and natural choice for P with this property emerges if we write for f a positive definite expression;

$$f(x, \phi_t, t) = \psi^*(x, \phi_t, t)\psi(x, \phi_t, t) \quad (1.6.6)$$

since f as a function of ϕ_t, peaks around the value $\phi_A(x,t)$, one can write in the adiabatically accessible region:

$$\psi = \sum_n \tilde{\psi}(x, n, t) \exp\{in[S_t - S_A(x,t)]/\bar{\mu}\} \quad (1.6.7)$$

For an arbitrary space point, Fourier analysis of ψ is carried out with respect to ϕ_t as

$$\psi(x, \phi_t, t) = \sum_n \Psi(x, n, t) \exp(in S_t/\bar{\mu}) \quad (1.6.8)$$

The following differential equation is obtained for $\Psi(x,n,t)$

$$-i\frac{\bar{\mu}}{n}\frac{\partial\Psi}{\partial t}=-\left(\frac{\bar{\mu}}{n}\right)^2\frac{1}{2m}\frac{\partial^2\Psi}{\partial x^2}+(\bar{\mu}\Omega)\Psi(x,n,t) \quad (1.6.9)$$

The relation between the density and the solutions Ψ (x,n,t) of the above equation is

$$G(x,t)=\int d\Phi_t\, f(x,\Phi_t,t)=\sum_{n\neq 0}\Psi^*(x,n,t)\Psi(x,n,t) \quad (1.6.10)$$

It is seen that the form of the solution for Ψ resembles Schrödinger theory in quantum mechanics. Here the role of $\hbar$ is played by the first action invariant $(\bar{\mu}/n)$, $\bar{\mu}$ is the value at injection, $\bar{\mu}\Omega$ that occurs in place of the potential is precisely the potential which describes the adiabatic motion. The nonadiabatic escape of particles from the adiabatic traps, which can be calculated from these equations, then appears to be of the nature of the "tunneling effect" in quantum mechanics.

If the potential $\bar{\mu}\Omega$ is of the form $\bar{\mu}\Omega=\bar{\mu}\Omega_{max}[\mathrm{sech}(\alpha x)]^2$ in the region of the mirrors along a certain field line, then the probability of transmission per unit time across the potential hill is given by

$$P=1/T_{eff}\sum_n C(n)\exp\left\{-(2m)^{1/2}\frac{2\pi n}{\alpha\bar{\mu}}\left[(\bar{\mu}\Omega_{max})^{1/2}-\sqrt{E}\right]\right\}$$

$$=1/T_{eff}\sum_n C(n)\exp\left(-m(n)\right) \quad (1.6.11)$$

where T_{eff} is the effective bounce period between two adiabatic turning points and $c(n)$ are appropriate constants. The dominant contribution comes from $n = 1$. But the presence of other values of n shows that there exist various e-folding times in the decay of the particle density.

The life time corresponding to this probability can be written as

$$\tau_n = T_{eff_n} \exp\left\{(2m)^{1/2} \frac{2n}{\alpha\mu}\left[(\mu\Omega_{max})^{1/2} - \sqrt{E}\right]\right\} \quad (1.6.12)$$

Since the Schrödinger-like equations are uncoupled linear equations, the probability coefficients are related to the initial conditions[49].

The exponent in the expression for τ_n gives the slope $m(n)$ of $\ln \tau_n$ variation with magnetic field. The expression for τ_n predicts following features of dependence of τ_n on various parameters.

1) $\ln \tau_n$ vs B curve would be straight line with a slope of m_n which would be n times the slope of $\ln \tau_1$ vs B.

2) The magnitude of the slope would decrease with increasing energy as $E^{-\frac{1}{2}}$ and increase with increasing magnetic field scale length α^{-1}.

These predictions can be subjected to experimental verifications. These theoretical predictions[47] were infact compared with some of the experimental results from[5,16,41]. The

experimental values of the exponents were obtained from the steepest section of $\ln \tau_n$ vs B curve for $n = 1$. In most of the cases the theoretical values were in good agreement with the experimentally observed values. Thus the experimentally observed variations of life time could be compared with theoretical values.

1.7. Motivation of the Present Experimental Work:

In the previous sections of this chapter, we have reviewed the theoretical, numerical and experimental works on particle confinement in, and leakage out of mirror traps. From this overview one can observe that these works have led to important observations and conceptual informations on particle interaction with inhomogeneous magnetic fields. However, inspite of all these efforts, there remains a number of significant questions about the particle behaviour in such confinement devices. The prediction of multiple life times in such devices is another interesting and fascinating aspect of the problem.

From the theoretical considerations, it is apparent that the conventional life time measurements cannot be directly compared with the theories, barring the theory described in the previous section. Therefore, the possibility of observing multiple lifetimes for particles with same initial pitch angle and energy as postulated by Varma[47] was considered to be a challenging problem, well worth the design and construction of a complex experiment. Main motivation behind the experiments has been the effort to observe multiple e-folding times for particles

with specific energy and initial value of the magnetic moment. Other behaviour of charged particles, such as the motion of charged particles in highly nonadiabatic mirror configurations has also been studied. The same experimental system was also used to study plasma reflection from a nonadiabatic mirror with the necessary modifications demanded by the particular experiment.

CHAPTER II

EXPERIMENTAL ARRANGEMENT

The specific objective of the experiment, as defined earlier was the study of single particle behaviour in magnetic mirror geometry, with slow spatial variation. The particle field interaction manifests itself in modification of particle trajectories and ultimately in loss of particles from the trap. Hence, the processes such as interparticle collision, which would also result in particle loss have to be minimised in this experiment. The primary experimental requirements could thus be defined as low particle densities, ultra high vacuum, high particle energy, adiabatic mirror magnetic field and fast electronics.

This chapter describes an experimental system designed and constructed to fulfill the parameter constraints as defined above. The experimental set up can be broadly divided into the following sub systems:

i) Vacuum system

ii) Magnetic field system

iii) Source of charged particles (Electron gun)

iv) Diagnostics and data acquisition system

2.1. Vacuum System :

With a mirror seperation of 120 cm and an additional length of 30 cm for diagnostic instruments etc a vacuum chamber of 150 cm in length and 15 cm diameter is used for the experiment.

The vacuum system is constructed entirely from 304 stainless steel. The vacuum system along with the magnetic field system is depicted schematically in fig.3. The main experimental region of the chamber was made up of a seamless stainless steel tube. The whole system was evacuated with the help of a LN_2 trapped oil diffusion pump upto a pressure of $\sim 10^{-5}$ torr. After attaining this pressure, the system was further evacuated to a pressure of $\sim 5 \times 10^{-8}$ torr with the help of a sputter ion pump which has a speed of 300 liters/sec. While pumping was continued with the help of the sputter ion pump, the oil diffusion pump along with the backing system was isolated from the experimental chamber with the help of a mechanical valve.

An isolation valve of 4" diameter was designed and fabricated for use between the ion pump and the experimental apparatus. The isolation valve consisted of a piston placed at 45^{o} with a spring attached to it. The piston was pulled out with the help of a solenoid, thus connecting the pump to the system. This was possible since the stem of the piston was constructed out of magnetic stainless steel.

To attain ultra high vacuum (UHV) the system was baked to a temperature of $150^{o}C$ for a period of 10-12 hrs. This was done with the help of tape heater wrapped on the main experimental system. The ion pump was also baked at the same time.

For any modifications necessitating the opening of vacuum system, the system was filled with nitrogen by continuously

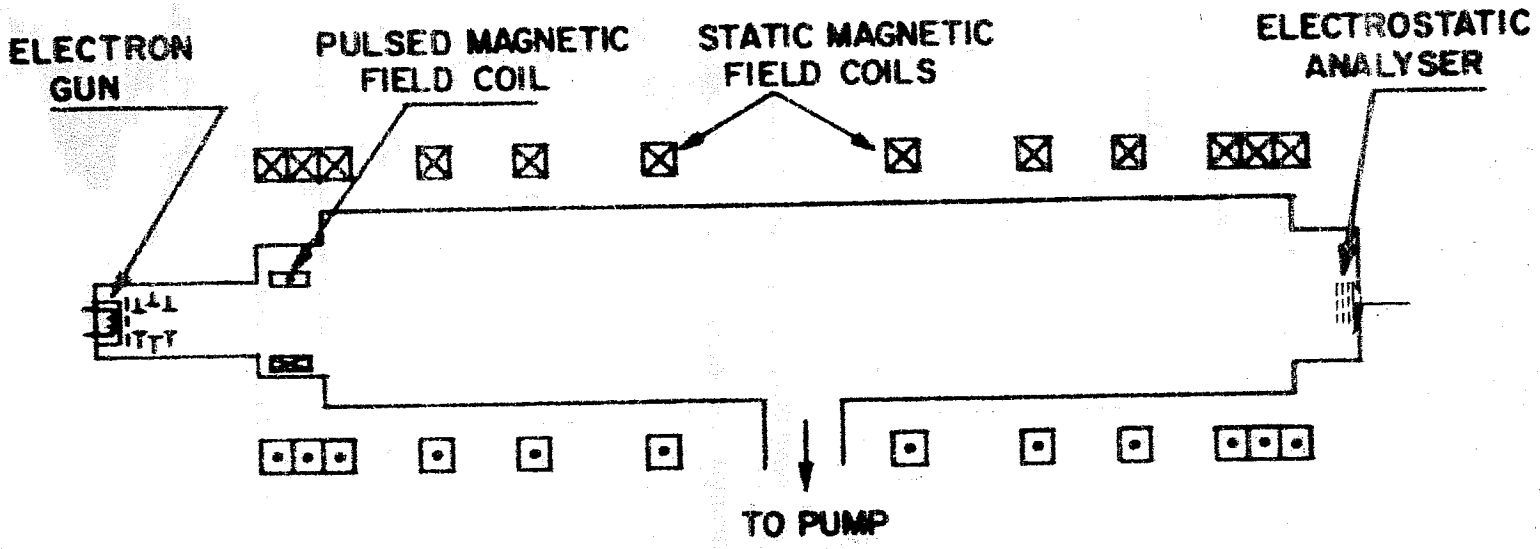

Fig. 3. Schematic of the experimental apparatus.

flushing dry nitrogen gas through the system at a pressure slightly higher than the atmospheric pressure. During this period the ion pump was isolated with the help of the isolation valve. This helped greatly in regaining the UHV conditions in the system within a short time.

2.2. Magnetic Field System :

For electron energy of $\sim$6 KeV and a midplane magnetic field of 200 gauss, the electron Larmor radius turns out to be $\sim$ 1 cm. For a minimum angle of injection of 30^{o} the required mirror field was 800 gauss. For flexibility in the experiment, a maximum field of 1000 gauss was desired.

The required magnetic field profile was obtained with the held of a set of 12 pancake coils, placed symmetrically on either side of the central plane. The pancake coils were made of 8 mm O.D and 5 mm I.D.copper tubing and all the coils had inner radius of 10 cm. Maximum constant current of 260 amps could be fed into them. To dissipate the heat generated, cold water was circulated through the coils. Five different magnetic field configurations were generated by varying the axial positions of the coils.For certain cases, current was also varied to obtain the desired field configurations. In these cases, to reduce the current through certain coils, shunts of low resistance and high current rating in the form of stainless steel strips of different thickness, width and length were used. The field configurations were numerically calculated following the method outlined in Appendix A.

A rectified power supply (300 V, 300 Amp), which could be operated in constant current or constant voltage mode with ripple content of 0.03 % was used to feed the coils for generating the desired static magnetic field.

For effective confinement of the charged particles, the injected particles must be made to feel some change in the parameters of the experimental system. For this purpose, the magnetic field value at the mirror throat near the injection point was lowered during injection. After travelling along the mirror system, the charged particles (electrons) were reflected from the opposite mirror and approached the first mirror. To confine the electrons, the magnetic field value at the mirror throat at injection end was raised to its initial value equal to the value at the other mirror point. This was achieved by means of a pulsed magnetic field superimposed on the static magnetic field at the mirror throat. Pulsed current was fed to a four turn stainless steel coil of 4 cm diameter. Stainless steel was chosen for its UHV compatibility. Since the fast magnetic field pulse could not penetrate through the 3 mm thick vacuum chamber wall, the small coil was placed inside the vacuum chamber and was fed through high voltage vacuum feed through.

The required pulse duration and the magnitude of the field value used were dependent on the energy of the electron beam. Since minimum dispersion in the beam energy was desired,

sufficient care was taken while constructing the pulse forming net work. The pulse forming network used for this purpose is described in section 2.4 of this chapter. The fall time of the pulse should be less than twice the transit time of the beam pulse through the system. Since the magnetic moment of the electrons was kept constant, the pulsed magnetic field should be homogeneous. For this purpose, the current pulse used to produce the magnetic field had to be made ripple free and with a short fall time. Thus a 100 amp current pulse of 150 nsec duration with a fall time of 30 nsec was used to produce the pulsed magnetic field. The value of the pulsed magnetic field was directly proportional to the current. By varying the current amplitude, the magnetic field value required for the experiment was selected. Fig. 7(1) shows the trace from an oscillogram of the current pulse registered with the help of a current transformer (Pearson model No.411). The magnetic field produced by this current was measured with the help of a magnetic probe, specially constructed for this purpose. The construction and the characteristics of the magnetic probe are described in section 2.5 of this chapter.

2.3. Electron Gun :

A low current electron gun was used during the experiment. The maximum beam current used was $\sim 6\ \mu A$ during the single reflection experiment with an energy of 250 - 300 ev. While conducting the confinement experiments, the beam energy was

varied upto 5 kev with a beam current of 0.2-0.4μA. Since the experiments dealt with single particle phenomenon, the density of the beam was kept low, typically of the order of 10^4 particles/cc. The beam pulse duration was 50 μsec during the single reflection experiment, while the pulse widths used for the confinement experiments were 30 nsec & 500 nsec.

Since a distribution in the electron energy leads to a distribution in the magnetic moment; one should try to have a beam with as small an energy spread as possible. As it was difficult to define a critical parameter for this, the effort was to reduce the major causes which gave rise to beam dispersion. Some of the major causes are the following[3]:

a) the velocity distribution with which electrons are thermionically emitted.

b) Fluctuations in the accelerating voltage in time scales short compared to the beam switching time.

c) Beam forming optics.

d) Geometric factors: Finite dimensions of the filament and anode causes the space charge cloud to have potential gradients especially when the beam switching takes place in a short time.

Therefore, an electrostatic electron gun was designed to give a well focussed beam. Strong focussing i.e. the use of distribution of electrostatic einzellinsen, was used. Three cylindrical electrodes were used to focus and accelerate

the beam. The central electrode was kept at a lower voltage than the other two electrodes. In certain region of small ratios of $a/_L$, the gap region of the system would be a lens with a long focal length[37]. Here 2a is the diameter of the cylindrical lense and L is the total length of two consecutive lenses along with the gap between them. The ratio of the diameters and voltages were calculated from the perveance for the particular specifications. For simple multielectrode systems, the perveance is approximated by

$$P = 61 \times 10^{-6} \left(\frac{V_1}{V_0}\right)^2 \left(\frac{2a}{L}\right)^2 \qquad (2.3.1)$$

Perveance P is expressed in micropervs. A gun with a perveance of one microperv gives 1 μA at 10 KV . In the above formula $V_1 = V_{High} - V_{low}$ and $V_o = (V_H + V_L)/2, V_1 \ll V_o$ and $2a \ll L$. In the derivation, the charge density was assumed uniform as it should be when the beam originates from a well designed gun.

A grid was placed infront of the cathode aperture at a distance of 3 mm. Both the cathode and the grid were kept at negative potential with respect to the accelerating electrode. A-300 V pulse with desired pulse duration was applied to the cathode making the grid 300 V positive with respect to the cathode. During this time a pulse of electrons escaped through the grid and was accelerated through the cylindrical electrodes. It should be noted that, for the short pulse width

operation, care had to be taken in the electrical connections to the cathode. The connecting cable length etc were minimized as stray inductance and capacitance affected the pulse shape considerably. The pulse forming net work is discussed in a subsection later in this chapter.

Focussing of the beam was considerably simplified as the gun was placed in a magnetic field. Besides, the electrostatic focussing, the magnetic field also gave a focussing effect. A zinc sulphide coated screen was employed to estimate the beam diameter along the length of the system. The pencil beam that was formed gave a spot size of 2 - 4 mm on the screen.

2.4. Pulse Forming Network for Trapping B-field:

To form a high current rectangular pulse, a transmission line (coaxial cable) terminated with its characteristic impedance Zo was used. Schematic of the line is shown in fig.4. An open ended length of coaxial cable was charged through a high resistance to a dc potential V. The line was discharged into a load resistance R_L, equal to the characteristic impedance Zo (50 Ω) of the cable, through an air spark gap. The spark gap opened after each closure to allow the line to recharge, thus enabling repetitive pulses to be produced. The pulse repetition rate could be adjusted by changing the value of the charging resistors.

Let the voltage be written as a function of time in the form $[V] = V[1]_0$, the spark gap being operated at time

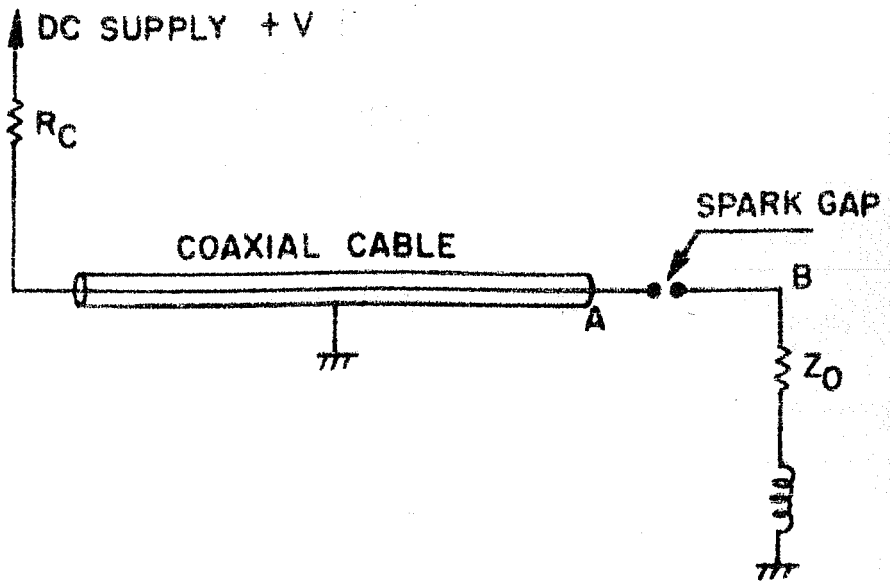

Fig. 4. Coaxial pulse forming line to generate 100 amp. current pulse of 150 nsec duration.

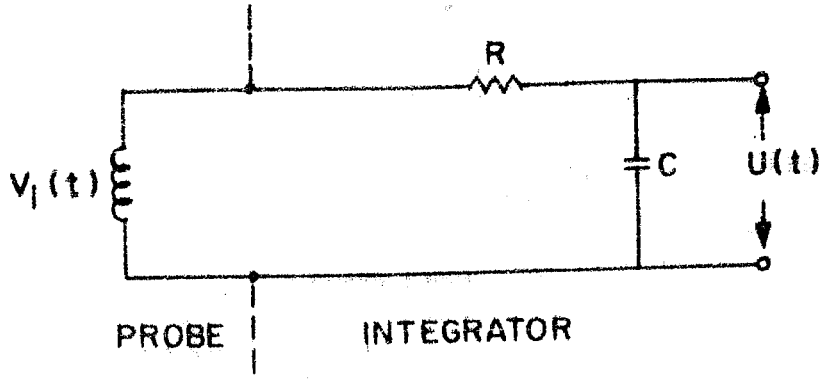

Fig. 5. Schematic of the magnetic probe circuit.

$t = 0^{20}$. The laplace transform of this voltage was then $[\bar{V}] = V/p$. On looking into the line A a certain impedance Z_{in} was seen. The signal voltage V_B which appeared across the load Z was given by the simple potential divider formula as

$$\bar{V}_B = \frac{Z}{Z + Z_{in}} [\bar{V}] \qquad (2.4.1)$$

Since the line was open circuited at the end remote from A, it followed

$$\bar{V}_B = \frac{\frac{Z}{Z+Z_o}\left(1 - e^{-2pT\ell}\right)}{1 - \frac{Z - Z_o}{Z + Z_o} e^{-2pT\ell}} [\bar{V}] \qquad (2.4.2)$$

Where T was the transit time of the pulse and l was the length of the line. For the case $Z = Z_o$, this reduced to

$$\bar{V}_B = \left(1 - e^{-2pT\ell}\right)[\bar{V}]/2 \qquad (2.4.3)$$

and when the inverse laplace transform was taken, it was found that the output pulse was rectangular in shape, had an amplitude V/2 and lasted for a time 2T i.e. twice the transit time of the pulse in the line.

To form a pulse of 150 nsec, the length of the coaxial cable needed was

$$L = Vt/2 \quad ; \text{ where } V = \frac{c}{\sqrt{\epsilon_o}}$$
$$\simeq 14 \text{ mts.}$$

where ϵ_0 is the dielectric constant of the medium. To get a current amplitude of 100 amp, the voltage required to charge the cable was 10 KV. The four turn coil to produce the magnetic field was put in series with 50 Ω resistance. The current pulse was picked up by a current transformer and is shown in fig. 7 (1). The magnetic field pulse shape was monitored and the magnitude was measured with the help of magnetic probe, described in the next section.

2.5. Fast Response Magnetic Probe:

Fig.5 shows the schematic of the magnetic probe used for measuring time varying magnetic field. When a coil of effective area A_{eff} was placed in a time varying magnetic field B, induced voltage V_i (t) across the terminals was

$$V_i(t) = A_{eff} \frac{dB}{dt} \qquad (2.5.1)$$

where A_{eff} = nS; n is the number of turns in the probe and S is the cross section $1/4\,\pi d^2$.

From equation (2.5.1), it is seen that magnetic field B is directly proportional to $\int V_i(t)\,dt$. This integral could be directly measured by coupling the probe to an integrating circuit as shown in fig.5. For pulse duration smaller than the integration time RC, the following relation could be easily obtained[13].

$$B = \frac{RC}{A_{eff}} U = 10^8 \frac{RC}{A_{eff}} U \ [\text{gauss}] \qquad (2.5.2)$$

It is clear from (2.5.2) that the magnetic field was directly proportional to the voltage drop U across the capacitor C, which could be measured directly on the oscilloscope.

The main requirements for such a probe were :

i) Minimum size to obtain good resolution in time and space.

ii) Fast electrical response $\lesssim$ 10 nsec.

iii) Correct matching of the circuit impedance, particularly between the cables connecting the coil to the scope, thus avoiding ringing.

iv) Alignment of the probe coil with respect to the field component to be measured.

v) Shielding of the probe against electrostatic noise.

When there was no integrating element, resistance $R_T = 50\,\Omega$ was connected in series with the probe to match its impedance with the characteristic impedance of the coaxial cable.

The frequency response of the coil was given by the ratio L/Ro, L was the inductance of the coil and Ro was the resistance across it. The inductance value was found to be 152 n Henry and the corresponding response time T was .152 nsec for a total resistance value of 1000 Ω.

The constructed coil had 20 turns with a diameter d = 16 mm , length l = 4 mm and $K\frac{d}{L}$ = 3 where K was a damping constant.

The capacitance value used was 5 pf. However, the total capacitance of the circuit was 175 pf. This value included the 20 pf input capacitance of the oscilloscope and 150 pf was the approximate capacitance of the coaxial cable having a length of 1.5 m. Therefore, the integrating time RC was found to be 175 nsec. Since the pulse duration was 150 nsec, the magnetic field could be related to the observed voltage with the help of (2.5.2).

Fig.6 shows the construction of the probe. The glass cover over the probe coil was coated with a thin layer of silver to avoid electrostatic pick up during the measurements. Fig.7 shows the simultaneous traces of the magnetic probe and the current pulse from the current transformer. For calibration of the magnetic probe, the current through the magnetic field production coil was varied by varying the input voltage, used for charging the pulse forming line. The probe output voltage as a function of the magnetic field is shown in fig. 8.

2.6. Electron Beam - Pulse forming Network:

It has been already mentioned that the shape of the electron beam pulse was very important. Therefore to form a 30 nsec, - 300 V rectangular pulse, a three stage lumped LC circuit was used.

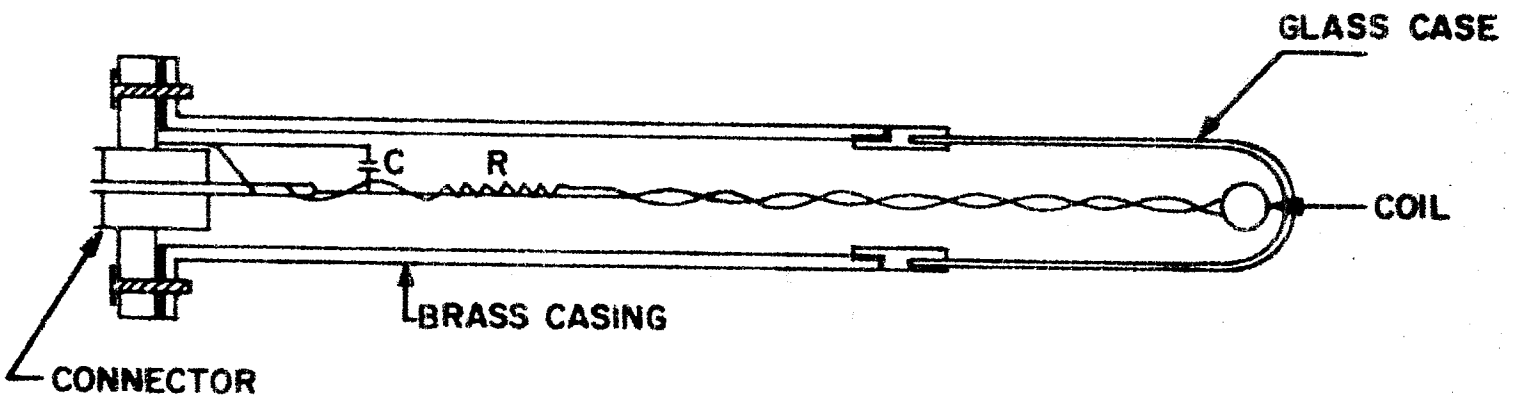

MAGNETIC INDUCTION PROBE

Fig. 6. Magnetic Induction Probe.

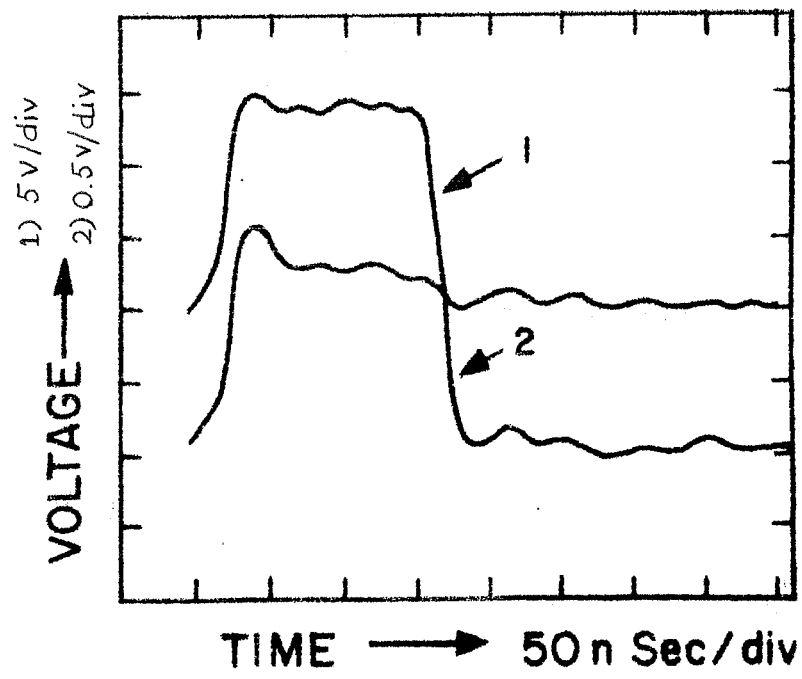

Fig. 7. Curve 1 represents the current transformer output. Curve 2 - The magnetic field produced by the same current pulse as registered by the magnetic probe.

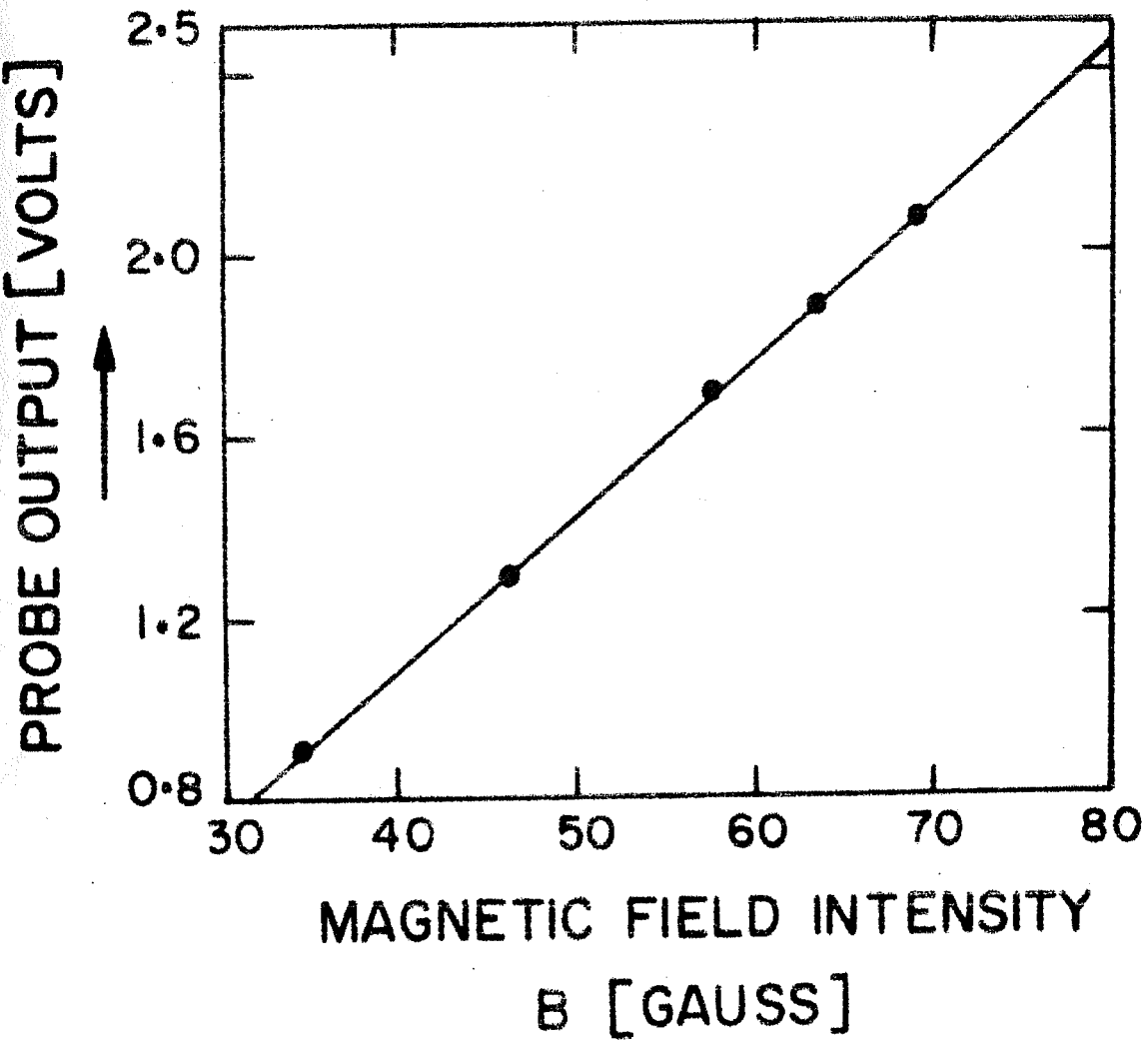

Fig. 8. Calibration curve for the magnetic probe.

The final shape of the pulse obtained with the help of a lumped circuit is made up of the sum of the individual currents in the resonant circuits[17]. As suggested by Guillemin[24], the fourier series representation of an alternating current with the wave shape of each half period approaching that of the desired pulse was calculated. The alternating current could be written in the form of

$$i = \sum_{n} i_n \quad (n = 1, 3, 5 \ldots\ldots) \qquad (2.6.1)$$

where $i_n = k_n I \sin \omega_n t$; $\omega_n = n\pi/T$, T is the total pulse duration.

Because of symmetry the even harmonics of the fourier series do not contribute to the total current i. From the equivalent form of Guillemin Voltage fed network[20], the In and Cn were calculated. The values of the inductances of the equivalent form were multiplied by Zo T and the values of the capacitances by T/Zo. Zo was the characteristic impedance of the network, given by the ratio of the initial capacitor voltage to the current amplitude I. The discharge current of the circuit was very similar to i of eq. (2.6.1) and switched by SCRs, it was similar to the single pulse of the desired shape. In such a lumped circuit, the shape generally depends on the number of elements and losses in the circuit. As the pulse width was increased, to form a better pulse, the number of lumped

circuits needed increased. For a very short pulse, the wiring of the circuit had to be carefully done to reduce losses in the circuit and also to reduce the effect of stray capacitance and inductance on the pulse shape.

In practice, to form the pulse, the capacitors of the storage network were charged upto the required voltage of -300 V. Then the charging unit was disconnected and the storage network was discharged through a series of SCRs. Fast response SCRs (GB 30 1 A) were used for producing the short duration fast rising pulse. Since each of these SCRs could accomodate a voltage of 150 V, three SCRs in series were used. The SCRs were triggered with the help of a voltage pulse derived from the current pulse for the production of the pulsed magnetic field. The triggering of the SCRs was delayed by 100 nsec with respect to the magnetic field pulse, so as to synchronize the entrance of the electron beam with the applied magnetic field.

As shown in fig 9, in series connection of SCRs, difference in delay and fall time could result in voltage imbalance during the turn on period. This would mean that if all the devices have different time delay in turning on, then the full voltage drop would appear across the device which has the largest delay. The trigger pulse was applied to SCR_1, it turned on and the voltage across it dropped from 100 V to 0.8 volts. Then C_1 discharged through SCR_2 gate and it turned on. Similarly SCR_3

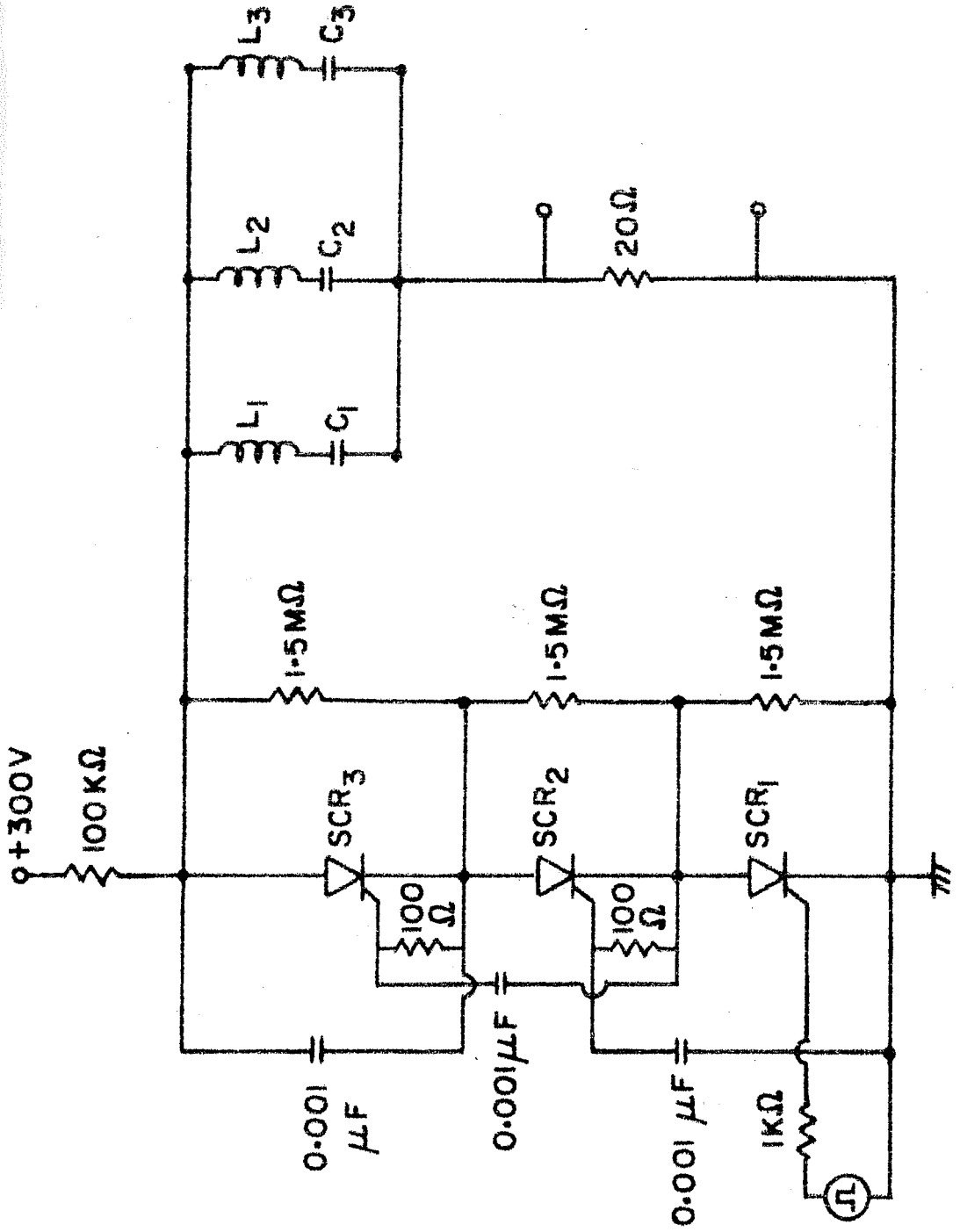

Fig. 9. Circuit diagram for the 30 nsec pulse forming network. L_2, C_2 and L_3, C_3 correspond to L_3, C_3 and L_5, C_5 of Guillemin voltage fed network respectively.

was also turned on. The 1.5 MΩ resistances were used to ensure similar voltage drop across the three SCRs. The final voltage drop across the load due to the current pulse gave the voltage pulse which was fed to the cathode of the electron gun as described earlier in this chapter.

Longer duration pulse (500 nsec) was also used during the experiment. In that case, care was taken to synchronize the magnetic field pulse with the voltage pulse in such a way that the field pulse was always within the voltage pulse duration. The number of electrons trapped in the system did not change as only a part of the electrons would see the change in the magnetic field. The electrons, not trapped in the system, anyway, did not contribute to the decay current[14].

2.7. Diagnostics and Data acquisition system:

The conventional diagnostic methods applied in the experiments are as follows:

2.7.1. Electrostatic Retarding Potential Analyser (RPA): To measure the parallel energy of the charged particles, an electrostatic retarding potential analyser was used. The schematic of the device is depicted in fig.10. It consisted of three grids and a collector housed in a cylindrical casing with an aperture whose area could be varied. To measure the energy of the electrons, retarding potential was applied to the central grid. The remaining two grids on either side of the central grid were kept at the ground potential. This was done to reduce

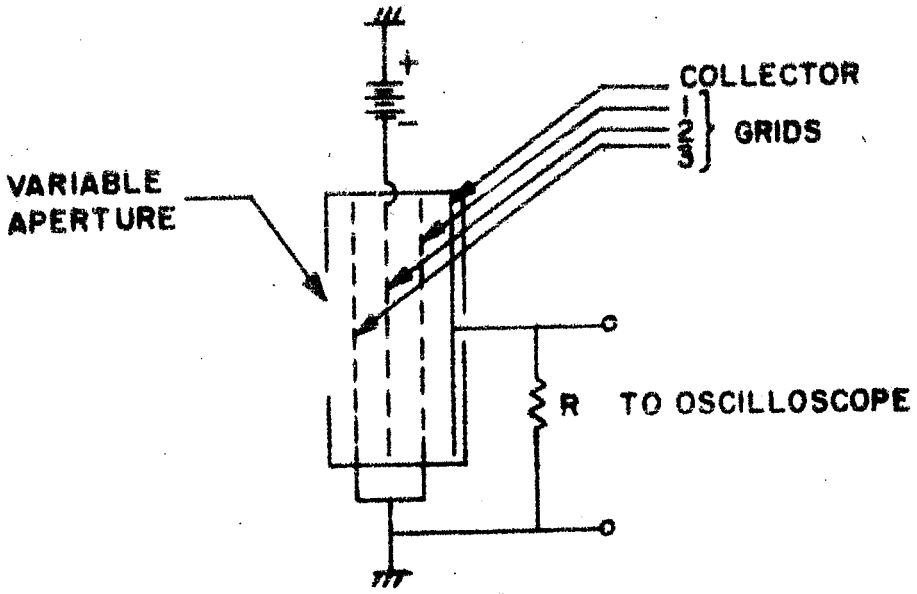

Fig. 10. Schematic of the electrostatic analyser.

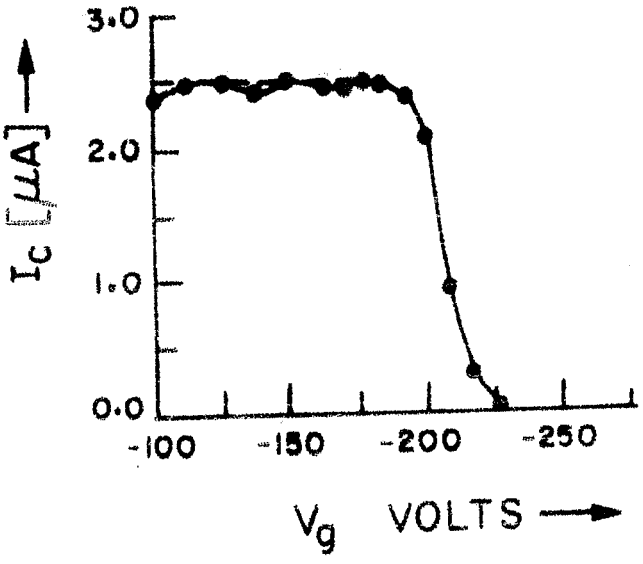

Fig. 11. Sample collector current Vs. retarding voltage plot. Dotted line shows how data was interpreted.

the effect of the retarding potential on the electrons, which passed through the grids and were collected by the collector. The current due to the collected electrons gave a voltage drop across a resistance and could be displayed on the oscilloscope screen.

While designing the RPA, the field distortions such as capacitor fringe fields, field leakage through the aperture and retarding field perturbations from the grid were minimised and therefore assumed to be unimportant. There exist several mechanisms for electrons to be emitted from a surface, although most of the mechanisms involve only a small percentage of the electrons emitted[46]. Since the effect of secondary emission was not significant on the observed signal, secondaries from particles with large incident angles were also ignored. The material used for the construction of the analyser was stainless steel.

Fig.11 shows a typical curve of the collector current as a function of the retarding voltage. For a monoenergetic beam, the fall in the current value was abrupt near the cut off value of the retarding voltage. However, for certain values of applied voltage, small dips were observed probably due to small secondary emission. But, since these dips were never more than 5%, they were approximated by the dotted curve for all practical purposes. Fig. 12 shows the cut off retarding voltage as a function of the beam voltage. It is seen that the experimental curve falls slightly above the unit slope.

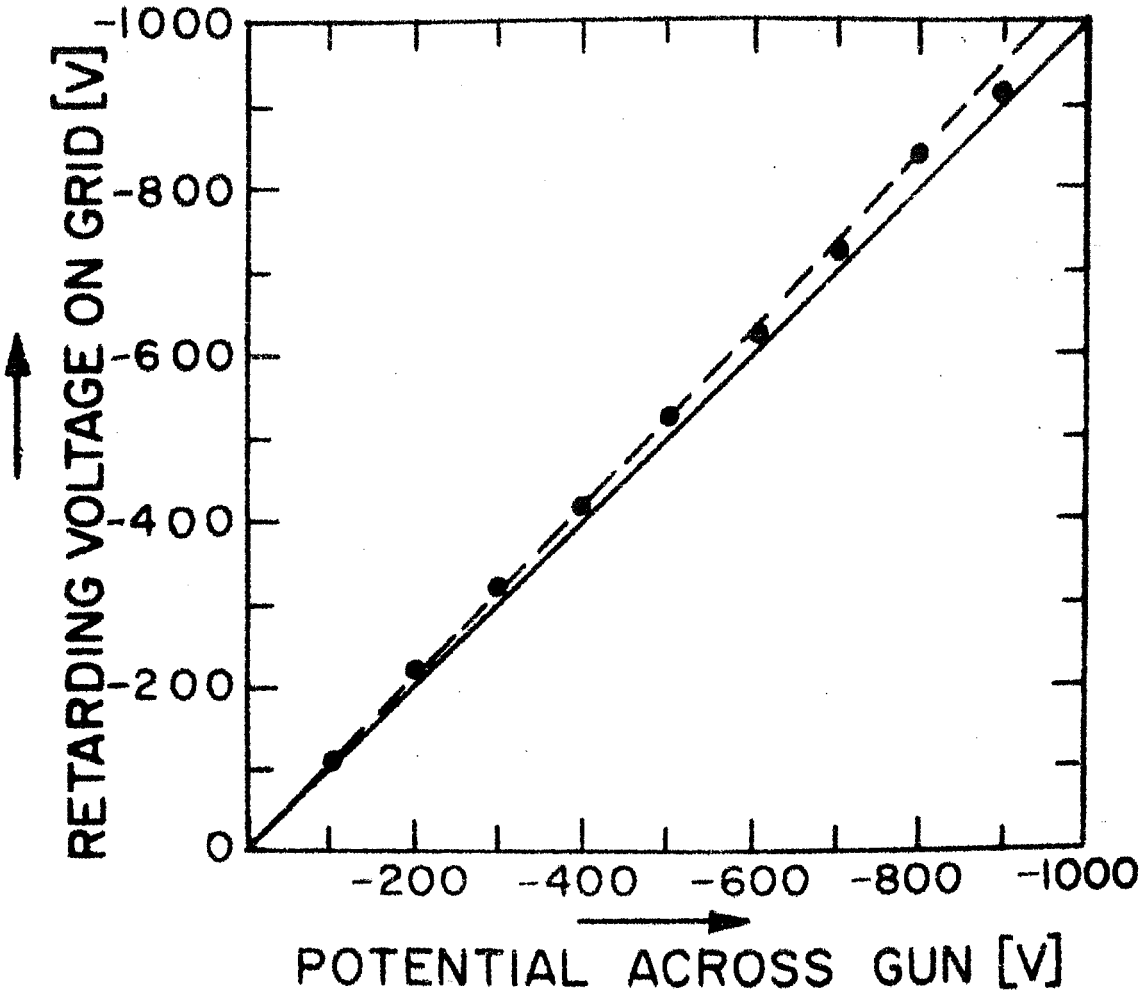

Fig. 12. Calibration curve for retarding potential analyser. Solid line shows the unit slope which is below the experimental curve.

While performing experiments with plasma stream, the same retarding potential analyser was used with one more grid on it to measure the directed ion energy. This grid was used to select the particles to be analysed. During the experiment, the number density was reduced with the help of a 30 % transparent grid to avoid electrical break down between the grids in the presence of the plasma.

2.7.2. Electrostatic Probes: In one of the experiments, the reflected beam was measured at the mid plane of the system. For this purpose a single faced electrostatic probe in the form of a collector, made out of stainless steel was used. But it was observed, that when the beam impinged on the insulated surface of the collector, a small amplitude spurious signal due to capacitive coupling appeared. To avoid this, the collector was modified slightly. Two collectors with their insulated surfaces facing each other were employed to serve the purpose. Electrostatic Langmuir probes[9] were employed to measure the directed velocity by measuring the time of flight of the pulsed plasma stream. For the measurement of the floating potential, high impedance electrostatic probes were used.

2.7.3. Data Acquisition System: During the trapping experiment, the RPA was placed outside the mirror throat and the current due to electrons leaking out of the mirror was measured. The data was digitized and recorded on a magnetic tape. Fig. 13 shows a block diagram of the system used for data acquisition.

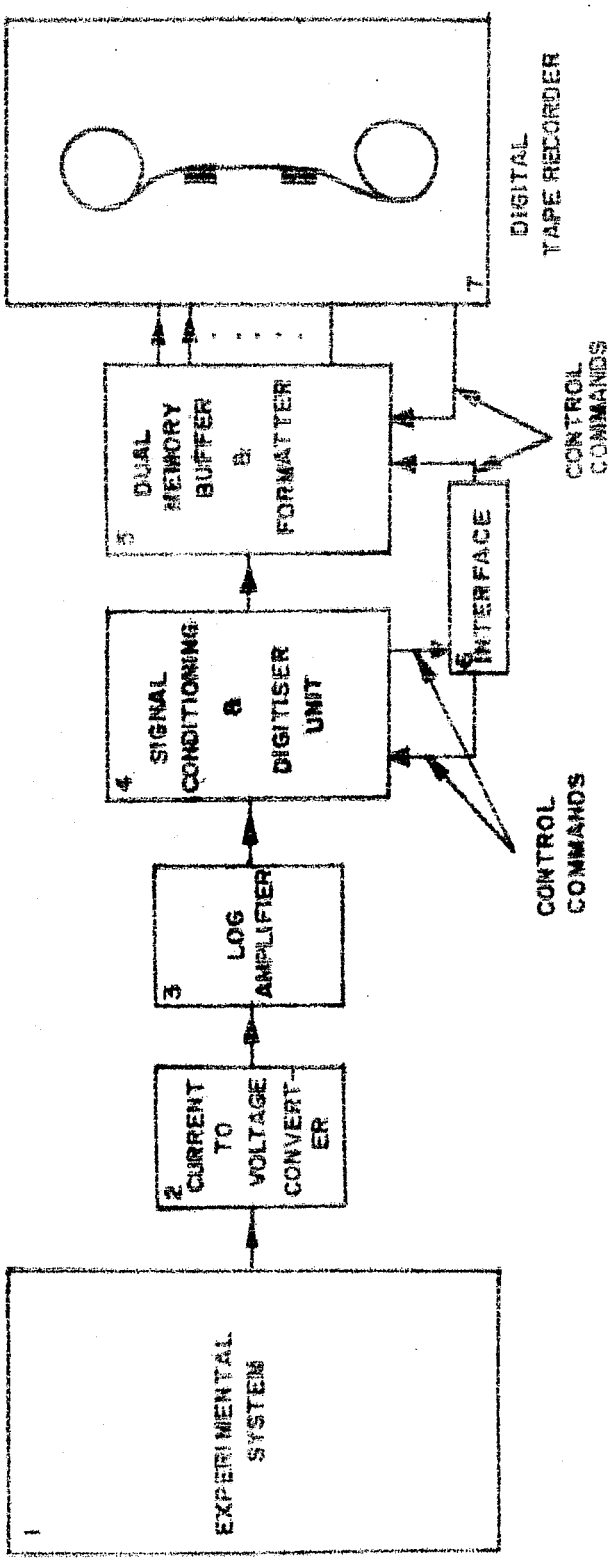

Fig. 13. Block diagram of the data acquisition system.

The signal from the collector of the RPA was fed to the current to voltage converter. Op. amp. 8007 with high input impedance and low bias current ($\sim 10^{-12}$ amp) was used, since the signal level itself was small ($\lesssim 10^{-6}$ amp). The collector signal was fed to the inverting end of the op. amp. Thus the output signal from the converter was inverted.

The signal from the current to voltage converter was fed to a log amplifier. Fig. 14 shows the circuit diagram of the log amplifier. The ratio $\frac{R1 + R2}{R2}$ was chosen such that the output voltage gain was 2.5 V/decade. It is wellknown, that a log amplifier, unlike an operational amplifier, cannot be adjusted by simply grounding the input. This is simply because the log of zero approaches minus infinity. It was therefore necessary to zero the off set voltage of A_1 and A_2 seperately and then to adjust the scale factor[29].

To check the response of the log amplifier, the output voltage was plotted as a function of known input voltage. Fig. 15 shows the response of the circuit as a log amplifier.

The signal from log-amplifier was digitised by means of an A/D converter and was recorded on a digital tape recorder. Recorded data was analysed with the help of IBM 360 computer. The digitisation error for the signal was $\sim 1\%$. A detailed discussion of the data analysis method is given in chapter IV.

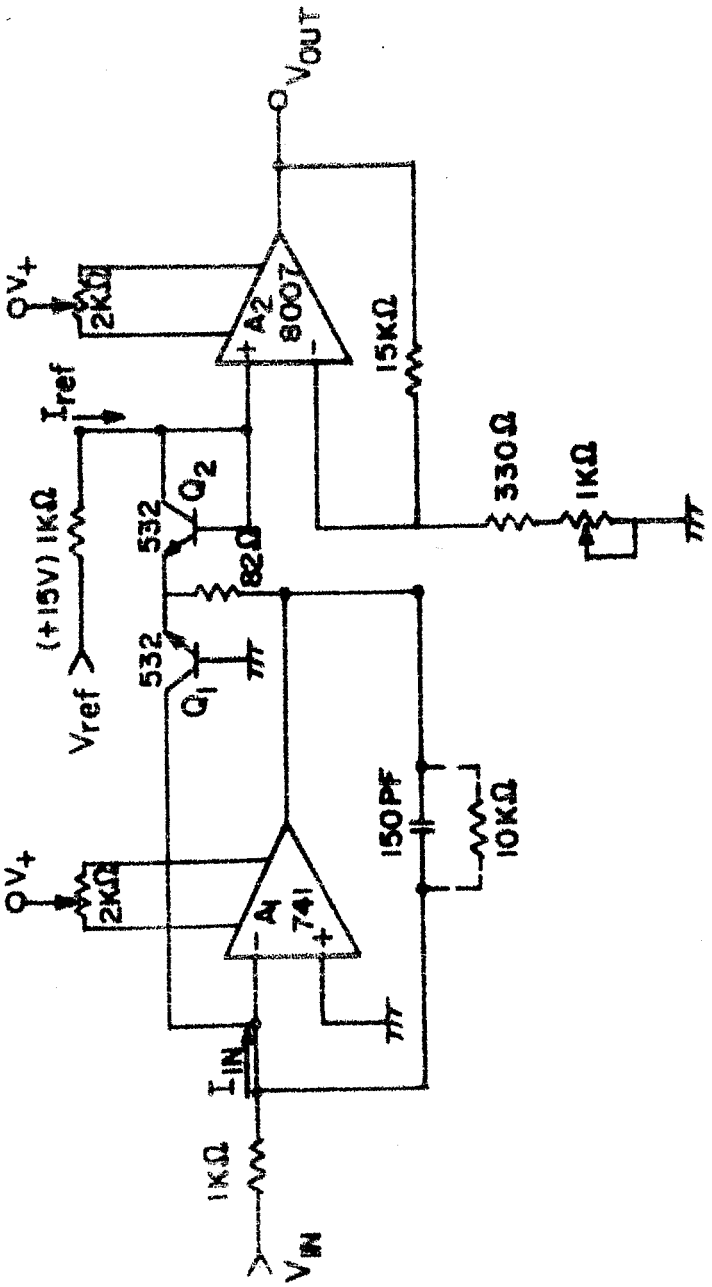

Fig. 14. Circuit diagram of the Log-amplifier.

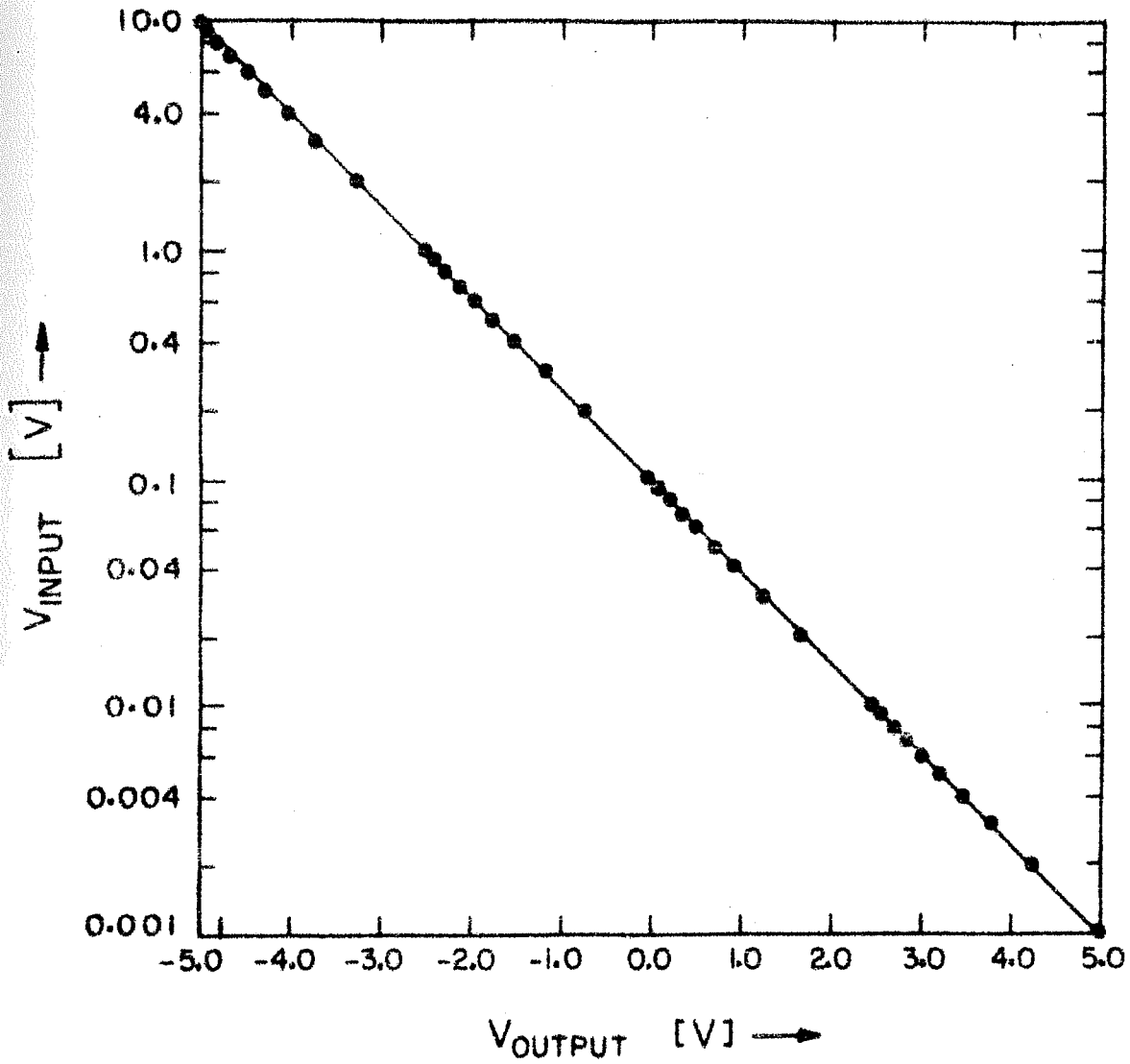

Fig. 15. Log-amplifier response over four decades.

CHAPTER III

ELECTRON AND PLASMA REFLECTION FROM ADIABATIC AND STRONGLY NONADIABATIC MIRRORS

As we have noticed from the earlier works[5,18], the finite bounds of the motion of a charged particle in a trap depends upon the conservation of the adiabatic invariant. During a single reflection also, the change in the value of the magnetic moment depends on the half width of the mirror, initial Larmor radius of the particles in the midplane of the magnetic mirror and on the magnetic field gradient scale length. Therefore, it is worthwhile to experimentally investigate the behaviour of charged particles in a magnetic mirror during a single reflection. Here, in this chapter we describe such an experimental study and the results obtained. Plasma reflection is also studied under similar conditions.

3.1. Experimental Method:

For reflection from a magnetic mirror, the particles have to posses transverse velocity such that $V_{\perp o}/V_{\parallel o} \geq 1/\sqrt{R_m}$ at the midplane of the mirror system. Here $V_{\perp o}$ and $V_{\parallel o}$ are the perpendicular and the parallel velocity components respectively at the midplane of the mirror and R_m is the mirror ratio. This demanded imparting additional perpendicular energy to particles which was achieved by allowing the particles to pass through a region of transverse electric field.

To see the effect of the particle traversal through a region of transverse electric field, one could write the equation of a charged particle in such a field in presence of a magnetic field. The region of transverse electric field extended only over a small distance ($\sim$2 cms) and therefore, the magnetic field was considered homogeneous over this distance. Let the axial magnetic field be in the Z direction. Then the equation of motion could be written simply as

$$m\dot{\vec{V}} = e\vec{E} + e/c\ \vec{V} \times \vec{B}_o \qquad (3.1.1)$$

The three components of this equation are

$$\begin{aligned} m\dot{V}_z &= 0 \\ m\dot{V}_y &= -e/c\ V_x B_o \\ m\dot{V}_x &= eE_x + e/c\ V_y B_o \end{aligned} \qquad (3.1.2)$$

Here the electric field was in the X direction and B_o was the magnetic field value.

It could easily be seen that the axial velocity along the Z axis was constant.

$$V_Z = \text{const} = V_o \qquad (3.1.3)$$

The two perpendicular components of the velocity could be written in the following manner :

$$\begin{aligned} (\dot{V}_x + i\dot{V}_y) &= \frac{e}{m}E_x - \frac{e}{mc}i(V_x + iV_y)B_o \\ &= \frac{e}{m}E_x - i\Omega(V_x + iV_y) \end{aligned} \qquad (3.1.4)$$

where Ω was the particle (electron)gyrofrequency. Eq. (3.1.4) could be rewritten as

$$\ddot{\rho} = \frac{eE_x}{m} - i\Omega\dot{\rho} \; ; \text{ where } \dot{\rho} = (V_x + iV_y) \qquad (3.1.5)$$

This equation could also be written in the following way

$$\frac{d}{dt}\left(\dot{\rho}\, e^{i\Omega t}\right) = \frac{eE_x}{m} e^{i\Omega t}$$

$$\dot{\rho} = e^{-i\Omega t}\int_0^t dt' \frac{eE_x}{m} e^{i\Omega t'} + \dot{\rho}_o e^{-i\Omega t} \qquad (3.1.6)$$

The second term in the equation came from the fact that the particle had initial perpendicular velocity before entering the region of transverse electric field. Then

$$\dot{\rho} = \frac{eE_x}{i\Omega m} + \dot{\rho}_o e^{-i\Omega t}$$

$$|\dot{\rho}|^2 = \left|\frac{eE_x}{im\Omega} + \dot{\rho}_o e^{-i\Omega t}\right|^2 \qquad (3.1.7)$$

Put $t = Z/V_o$, then the above expression transformed into

$$|\dot{\rho}|^2 = \left|\frac{eE_x}{im\Omega} + \dot{\rho}_o e^{-i\Omega Z/V_o}\right|^2 \qquad (3.1.8)$$

If we assume that the electric field was inclined to the magnetic field, then

$$\dot{V}_z = \frac{e}{m} E_z$$

$$\therefore Z - Z_o = V_o t + \tfrac{1}{2}\left(e/m\, E_z\right) t^2 \qquad (3.1.9)$$

Given $(Z-Z_0) = \Delta Z$, we could solve for the residence time of the particle.

$$1/2\, A t^2 + V_0 t - \Delta Z = 0$$

$$t = \frac{-V_0 \pm \sqrt{V_0^2 + 2A(\Delta Z)}}{A} \quad ; \text{ where } A = e/m\, E_z$$

$$V_z^2 = V_0^2 + 2\,\frac{eE_z}{m^2}(\Delta Z) \tag{3.1.10}$$

The time 't' might be used in the expression for $|\dot{\rho}|^2$

$$|\dot{\rho}|^2 = \left[(\dot{\rho}_0 \cos\Omega t)^2 + \left(\frac{eE_x}{m\Omega} + \dot{\rho}_0 \sin\Omega t\right)^2\right] \tag{3.1.11}$$

with $t = -\frac{V_0}{A} + \frac{1}{A}\sqrt{V_0^2 + 2A(\Delta Z)}$

Hence $t \simeq -\frac{V_0}{A} + \frac{V_0}{A}\left[1 + \frac{1}{2}\left(2A\frac{\Delta Z}{V_0^2}\right)\right]$

$$\simeq \frac{\Delta Z}{V_0} + \frac{V_0}{A}\,\frac{\frac{1}{2}\left(-\frac{1}{2}\right)}{2!}\left(2A\frac{\Delta Z}{V_0^2}\right)^2$$

$$\simeq -\frac{\Delta Z}{V_0}\,\frac{1}{2}\left(\frac{\Delta Z}{V_0}\right)^2 \frac{A}{V_0^2} \tag{3.1.12}$$

To a first approximation

$$t = \Delta Z / V_0$$

Then, $V_\perp^2 = \left[V_{\perp 0}^2 + \frac{2eE_x}{m\Omega} V_{\perp 0} \sin\Omega\frac{\Delta Z}{V_0} + \left(\frac{CE_x}{B_0}\right)^2\right]$

$$= \left[V_{\perp 0}^2 + 2V_{\perp 0}\frac{CE_x}{B_0}\sin\Omega\frac{\Delta Z}{V_0} + \left(\frac{CE_x}{B_0}\right)^2\right] \tag{3.1.13}$$

It could be seen from the above equation that if $V_{\perp 0}^2$ was zero then the maximum energy gained was the $\vec{E} \times \vec{B}$ i.e. the drift

energy. This energy gain occured because the particles passing through transverse static electric field felt a time varying field by virtue of their motion along the magnetic field line.

The maximum value of $\sin \Omega \frac{\Delta Z}{V_o} = 1$. Therefore the maximum transverse energy would be proportional to $V_\perp$ given by

$$V_\perp^2 (max) = \left\{ V_{\perp o} + \left(\frac{cE_x}{B_o} \right) \right\}^2 \qquad (3.1.14)$$

Thus it is seen that by applying proper electric and magnetic field one could give the required pitch angle to the charged particle which could result in reflection from the mirror.

3.2. Experimental Results and Discussion:

3.2.1 Reflection of an Electron Beam: The reflection experiment was conducted for 5 different mirror configurations and the magnetic field profiles are shown in fig. 16. A low energy beam (250 ev) of electrons with a beam current of 6 μA, was injected into the system paraxially from one end of the system. The local magnetic field value at the injection point was $3/4^{th}$ the maximum magnetic field value. Since the experiment dealt with single reflection of particles, the gun was placed inside the mirror system. The location of the beam was two centimeters off the axis at the point of injection. The diagnostics have been described already in the previous chapter.

The parallel energy of the electron beam was measured by applying retarding voltage on the central grid of the RPA. When

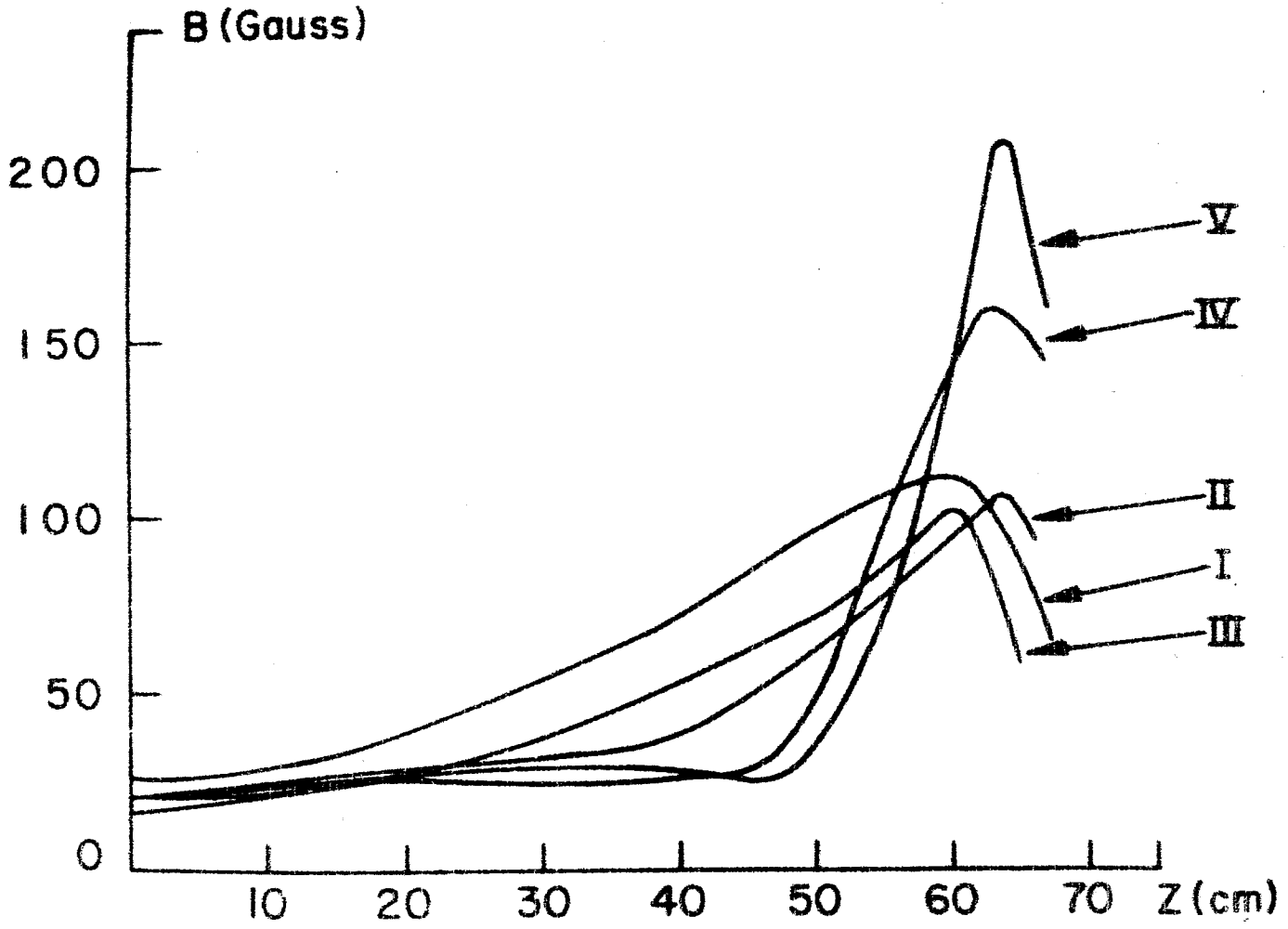

Fig. 16. Magnetic field distribution from centre of the system to one of the mirrors for the various mirror configurations with different mirror ratios and magnetic field scale lengths.

this voltage nears the electron parallel energy, the collector current falls to zero, thus determining the parallel energy of the beam. The slope of these curves give the dispersion in the parallel beam energy as shown in fig. 17.

$$\text{since } I \propto n(\mathcal{E}) = \int_{-\infty}^{\mathcal{E}} f(\mathcal{E})\, d\mathcal{E} \qquad (3.2.1)$$

where I is the current collected, which is proportional to n, the number density, the distribution function f ($\mathcal{E}$) can be written as $\frac{\partial G(\mathcal{E})}{\partial \mathcal{E}}$, where G ($\mathcal{E}$) is a function of energy and also can be written as a function of the pitch angle θ. Thus the slope of the curve gives the dispersion in the parallel energy. The dispersion for different cases was measured and was estimated to be not more than 10-12%.

The axial variation of electron parallel energy in a slowly varying magnetic field was determined and was found to decrease linearly as the field value increased. Experimentally obtained U_{11} (parallel energy) as a function of magnetic field at different axial positions for magnetic field configuration I is shown in fig. 18. The linear decrease of the parallel energy with the increase in the magnetic field could be explained easily in the following manner.

In a slowly varying magnetic field, the parallel component of the energy of the particles is converted to the perpendicular component of the energy of the particles as they move towards a stronger magnetic field region. This is simply because the

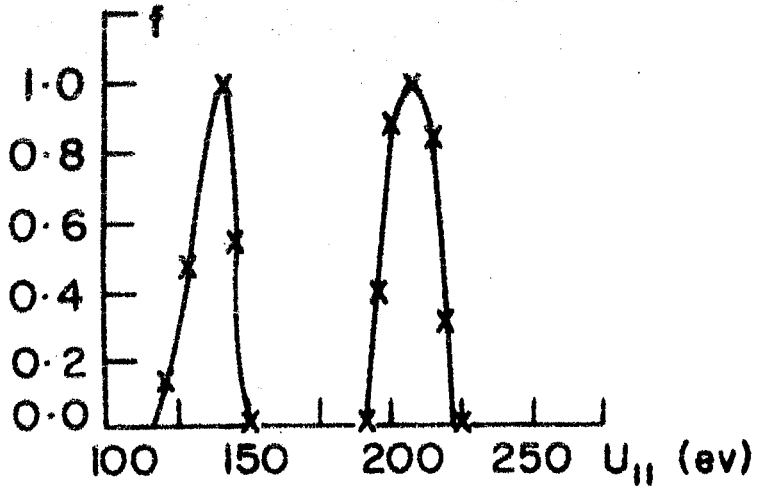

Fig. 17. Particle distribution in accordance with the parallel energy. Figure shows particle distributions for parallel energy values 140ev and 210ev.

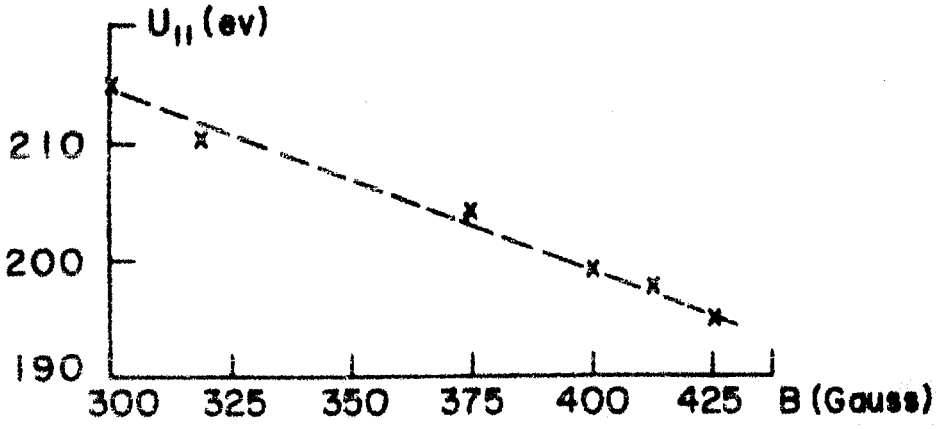

Fig. 18. Parallel energy of the electrons as a function of the axial magnetic field.

energy of the particles is conserved. From the energy conservation law, one can write the following simple relation.

$$U - \mu B = U_{||} \qquad (3.2.2)$$

where $U, U_{||}$ are the total and parallel particle energy, μ — magnetic moment of the charged particle and B is the static magnetic field. It can be noted that on the left hand side of the equation, except B all the other quantities are constants. One can therefore predict a linear relation between $U_{||}$ and B and the linearity speaks of the constancy of the magnetic moment.

The incident beam current and the reflected beam current were measured with the help of the directional probes near the mid plane. Both the currents were simultaneously displayed on the scope. The signal on the probe surface facing the electron gun was made zero so as to let the whole beam cross the probe undisturbed and the maximum reflection current on the other probe surface facing the mirror opposite to the electron gun was measured. Because of the azimuthal drift of the beam, it was possible to measure the reflected beam current at a different space point. The drift velocity was $\sim 10^{7}$ cm/sec, for the beam energy, magnetic field and the scale length of the magnetic field used during the experiment. The ratio of the reflected current to the incident current was defined as the reflection coefficient. The effect of the mirror ratio and the adiabaticity parameter on the reflection coefficient was measured. For this

purpose, the reflection coefficient was measured for all the five different mirror field configurations. Fig. 19 and fig. 20 depict the variation of the reflection coefficient as a function of the mirror ratio and the adiabaticity parameter. The adiabaticity parameter was defined as $\xi_L = r_L \frac{1}{B} \frac{dB}{dz}$. However, as r_L (Larmor radius) of a particle depends on the perpendicular velocity and $\frac{1}{B}\frac{dB}{dz}$ is the scale length in the parallel direction, ξ_L should be multiplied by a factor $V_{\parallel}/V_{\perp}$. This would reduce the value of ξ_L which is shown in fig. 20. But the functional dependence would still remain unchange. In both these curves, it is observed that the reflection coefficient goes through a minimum and then saturates at a slightly lower level than the value for the most adiabatic mirror case.

To support the reflection measurements, floating potential measurements were conducted at the mid plane of the system. A high impedance probe was inserted into the system at the midplane. During the course of work the electron energy was 200-300 ev and the pulse duration was $\sim 50\,\mu$sec. Since the transit time for the electrons through the system was $\sim 12\,\mu$sec the experiment could be considered as a steady state experiment. Therefore, after the reflection of the electrons one could expect an accumulation of electrons in the system[45]. Depending on the reflectivity of the mirror, the accumulation would vary and floating potential would change from one mirror configuration

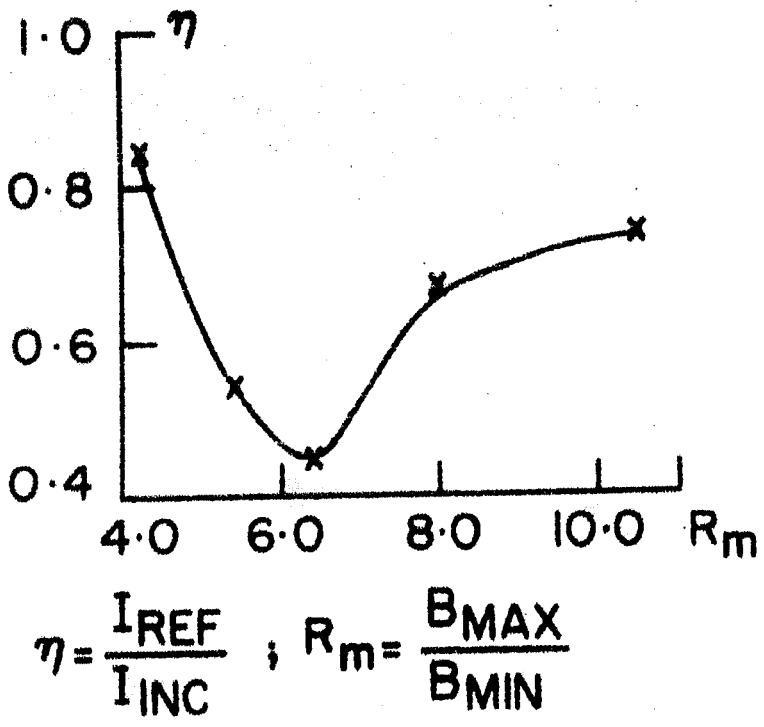

Fig. 19. Dependence of the reflection coefficient (η) on the mirror ratio R_m.

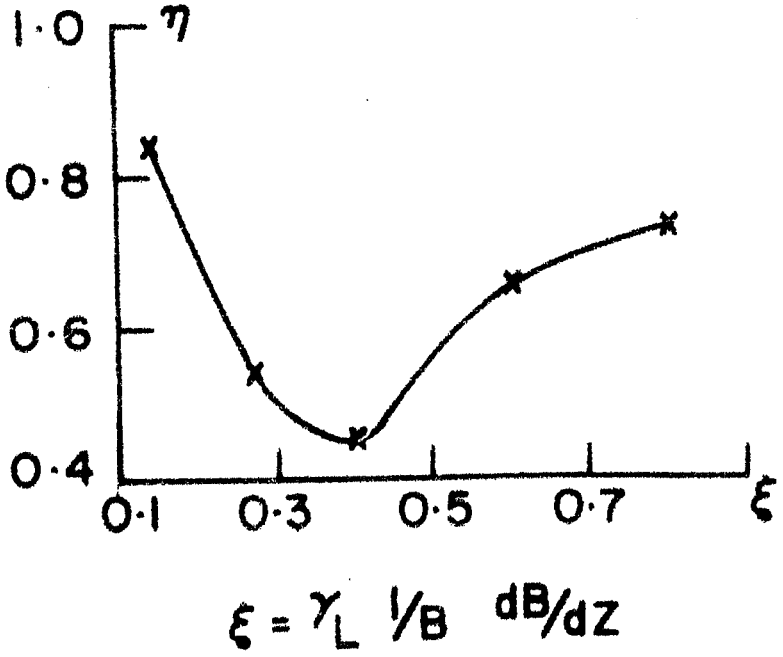

Fig. 20. The reflection coefficient as a function of the adiabaticity parameter ξ.

to another. The floating potential was measured and plotted as a function of mirror ratio, which is shown in fig.21. It is observed that the value of the mirror ratio where the minimum of this curve occured, coincided with the minimum on the reflectivity curve. The value of the floating potential saturated after passing through the minimum. This suggested that the reflectivity of the mirror became more effective for higher mirror ratios (highly nonadiabatic case).

The effect of the magnetic field value on the reflectivity of the mirror was also investigated. The base value of the magnetic field was increased keeping the pitch angle constant. As the base value of the magnetic field was increased, the Larmor radius of the particle decreased. The magnetic field gradient scale length would remain constant for a given field configuration. This amounts to a decrease in the nonadiabaticity in the system. The maximum field value was limited by the current passing through the magnetic field producing coils. This set of experiments was conducted for the configuration V. Fig. 22 shows the effect of the magnetic field on the reflection coefficient. Here, the magnetic field values correspond to the values at the mid plane of the system. The value of the reflection coefficient decreased as the magnetic field was increased.

The reflection coefficient was measured as a function of the beam current. For this, the emission current was increased

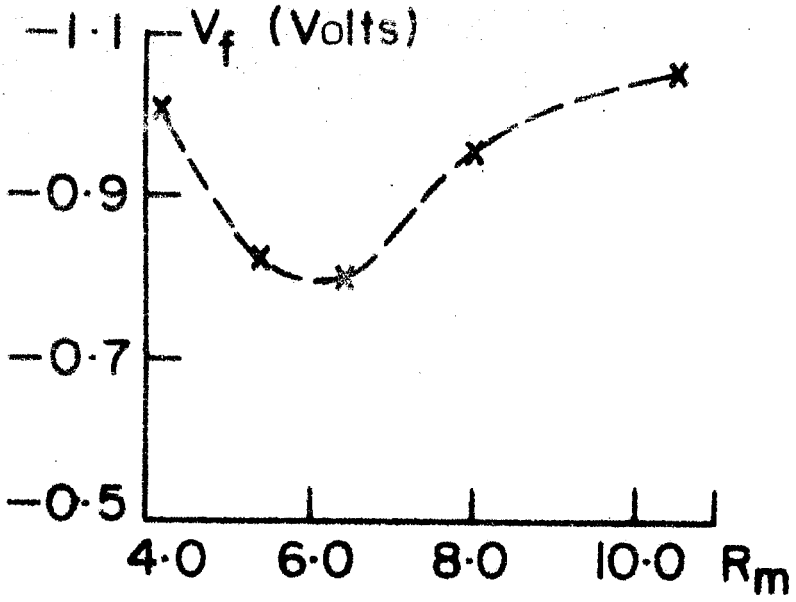

Fig. 21. Floating potential at the centre of the system as a function of the mirror ratio R_m.

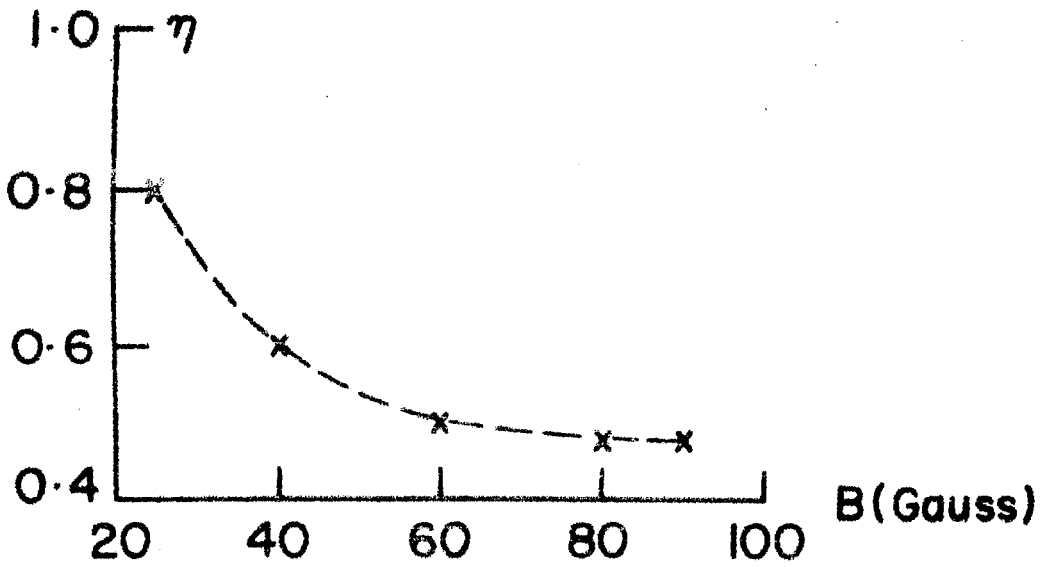

Fig. 22. Reflection coefficient η as a function of the base magnetic field.

and thereby the beam density was increased. The reflection coefficient as a function of the beam current was measured for the configuration V. It is shown in fig. 23. It was observed that the reflection coefficient increased abruptly as the beam current was increased. However at higher values of the beam current, the increase in the value of reflection coefficient was very small and flatened out thereby remaining almost steady Since the increase in the reflection coefficient occured after a critical particle density, it could be attributed to the collective behaviour of particles.

However, from fig. 22, it was observed that even the adiabaticity effected the reflection. When the system was relatively less nonadiabatic, the reflection coefficient had fallen to 45 %. Therefore, it was not only collective behaviour which played a role in increasing the reflection coefficient but the strong nonadiabaticity also played a role in this case.

3.2.2. Plasma Reflection from the Magnetic Mirror: Similar experiments were conducted with a plasma pulse also. For this purpose a plasma gun was placed instead of the electron gun in the system. The plasma gun was of a very simple construction. A discharge was initiated due to overvoltage breakdown over the surface of a nylon rod. Because of the magnetic field pressure on the plasma (hydrogen), that was formed, it was accelerated away from the gun. To initiate the discharge a 5μF condenser was charged upto a voltage of 5 KV. Since the discharge current

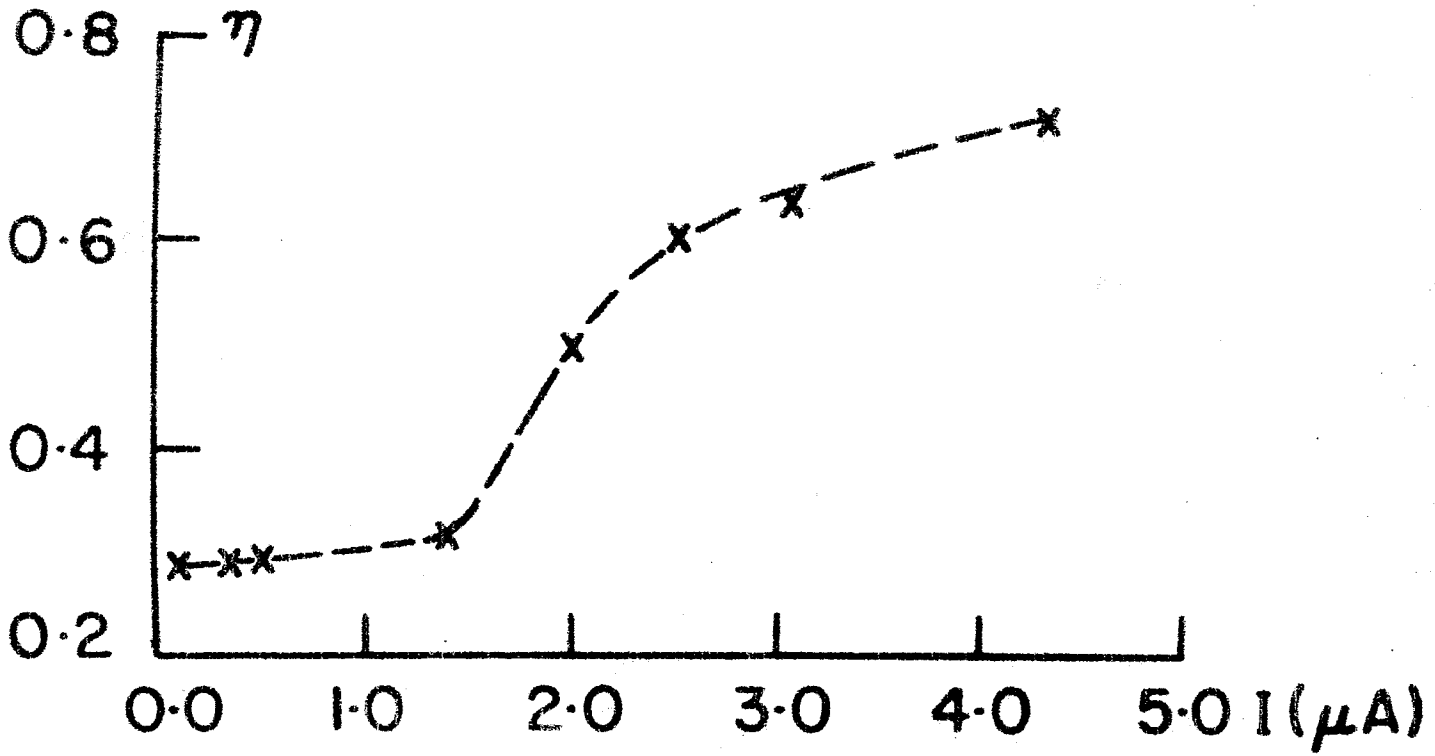

Fig. 23. Dependence of the reflection coefficient η on the beam current I for the electron beam.

pulse was of oscillatory type, it was critically damped by introducing a resistance in the circuit. Fig. 24 shows the schematic of the arrangement. The discharge current was measured with the help of a Rogowskii coil and is shown in fig.25 (curve 1). The critically damped discharged current was $\sim$8 K Amp. and the pulse duration was typically $\sim$ 15μ sec.

The parameters of the plasma pulse were measured with the help of conventional diagnostic techniques. To find out the directed velocity, time of flight measurements were conducted. The plasma signal was collected by a probe at two different axial positions away from the plasma gun. Knowing the time delay between the two signals, the velocity could be calculated. To make sure that the plasma pulses were indentical, the discharge current signal was monitored for each shot. Fig. 25 (curve 2,3) are two different signals from the probe placed at two different positions. The axial distance between the two points of observation was 30 cm. Knowing the time delay between the two peaks one can calculate the directed velocity and it was $\sim 7 \times 10^6$ cm/sec. Fig. 25 (curve 1) as mentioned earlier shows the discharge current pulse. Actually, they are two traces, superimposed on each other. This, in a way, demonstrates the repeatibility of the pulse. While measuring the ion current the collector was biased at -50 V.

To measure the directed ion energy, the electrostatic analyser was used. The existing analyser with three grids was

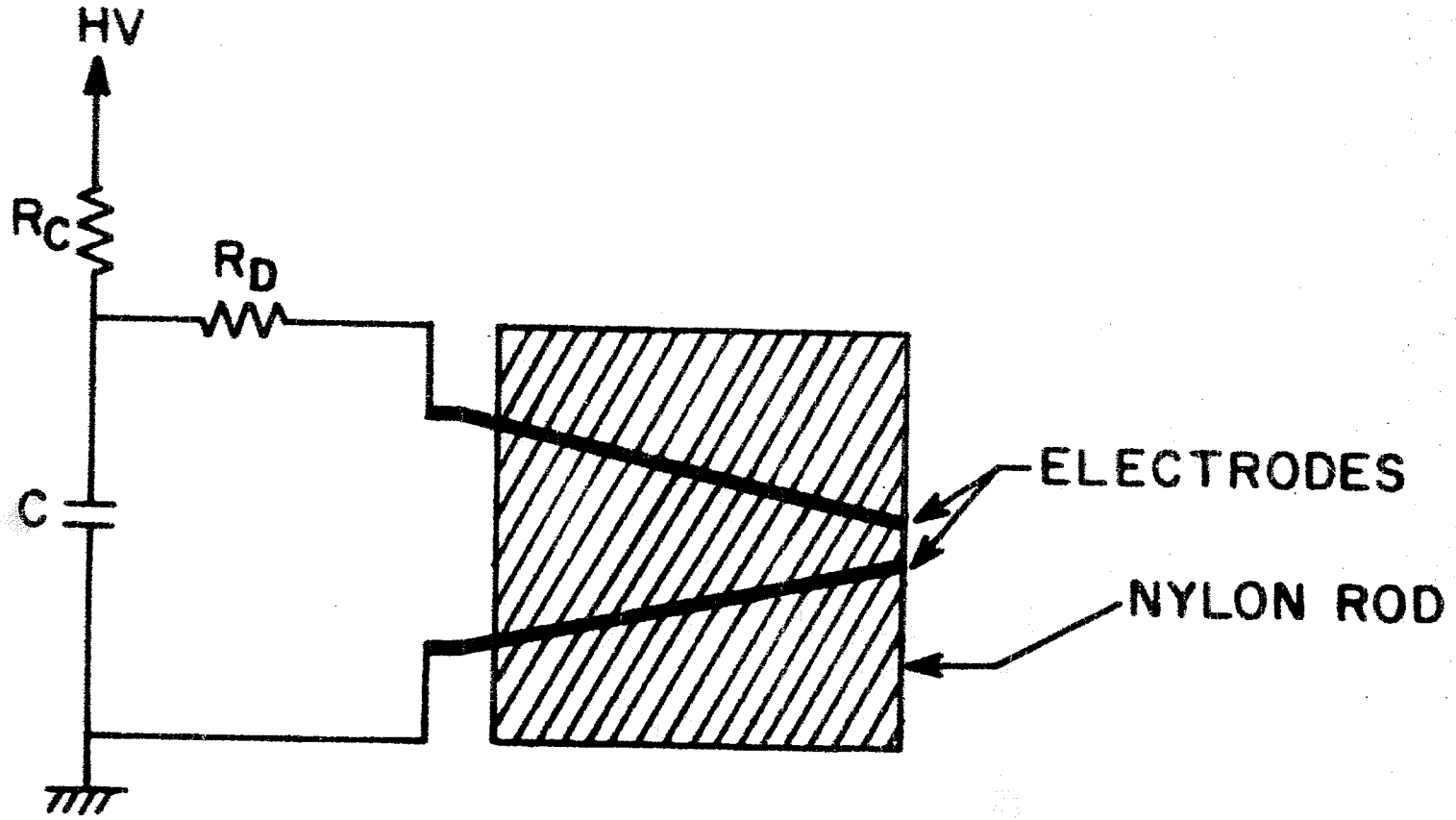

Fig. 24. Schematic of the plasma gun.

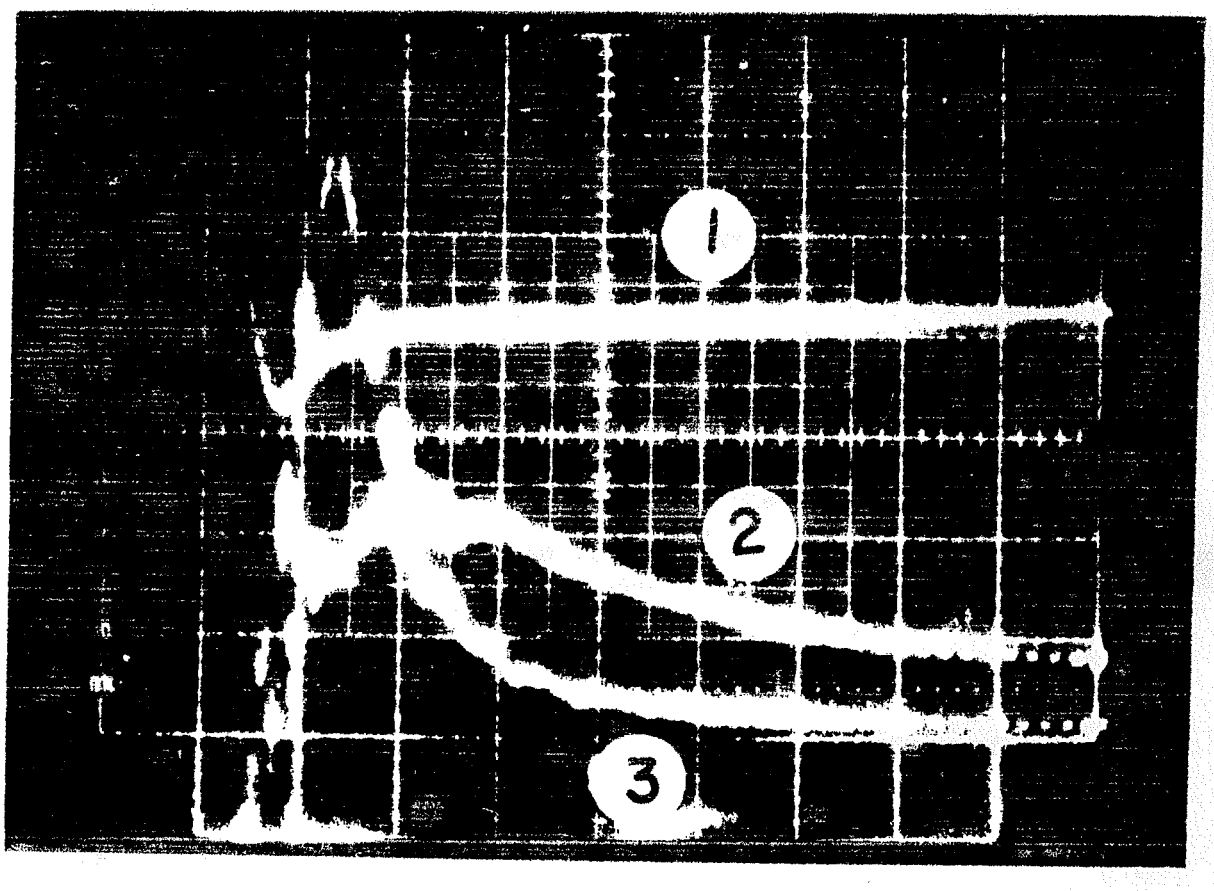

Fig. 25. Oscilloscope display of the plasma signals.
1) Superposition of discharge currents corresponding to the traces 2 and 3.
2) Ion current registered by the electrostatic probe inside the mirror system.
3) Ionic component of the plasma lost through the mirror.

modified and a fourth grid was added to analyse the plasma. The first and the third grid were kept at ground potential and a negative potential was applied to the second grid to cut off the electrons. Thus, only the ions could enter into the analyser. The retarding voltage to analyse the ions was applied on the fourth grid. The cut off of the signal at the collector for a particular voltage on the grid gave the value for ion energy. The directed ion energy measured in this way was 30 - 40 ev. The plasma density was also measured during the experiment and was $n_i \simeq 10^{11}$ cm^{-3}.

To find the reflectivity of the mirror, the incident current and the transmitted current were measured. The collector at the midplane was not employed during the experiment with an idea of eliminating the perturbations caused by the presence of the collector. Since the discharge current pulse duration was $\sim$15 μ sec, the plasma column length exceeded half the system length. The incident and the transmitted currents were measured with the help of a movable collector, which was placed infront of and after the mirror point from one end of the system. Knowing the transmission coefficient one could calculate the reflectivity of the mirror. This exercise was carried out for all the five mirror configurations and the respective reflection coefficients were calculated. Fig. 26 shows the reflection coefficient as a function of the mirror ratio. It was observed that the functional dependence in this

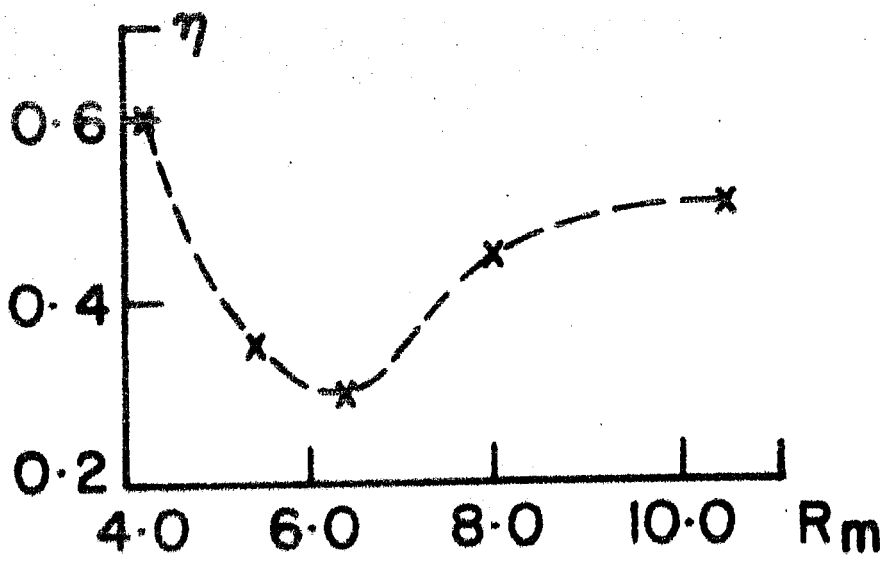

Fig. 26. Reflection coefficient η as a function of the mirror ratio.

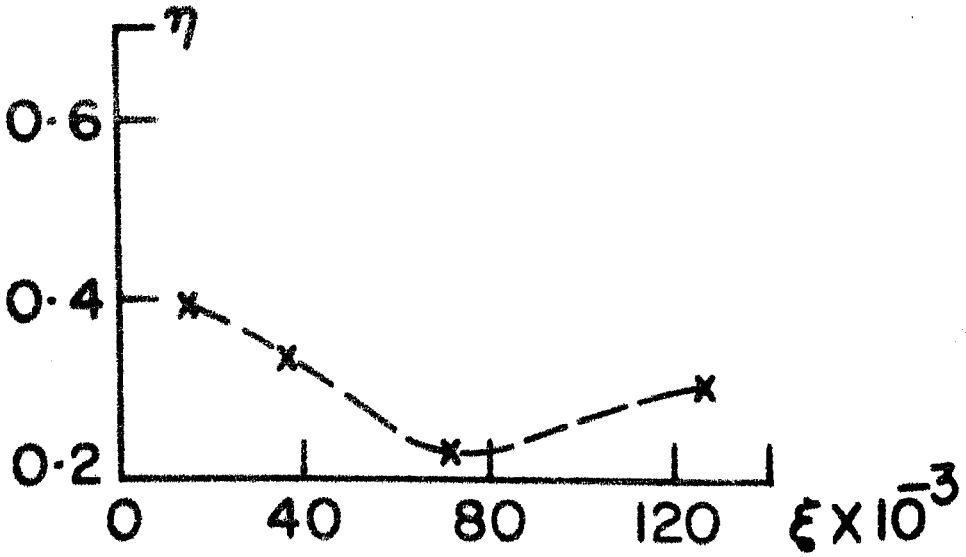

Fig. 27. Reflection coefficient η as a function of the adiabaticity parameter ξ .

case was similar to that of the electron beam. However, the absolute value of the reflection coefficient was much lower in this case. Since the plasma produced was isotropic, one would expect the reflection coefficient to be much smaller than in the case of the electrons where the pitch angle of the particles was controlled externally.

The effect of adiabaticity parameter on the reflection coefficient was measured for field configuration III. For this purpose the collector was enclosed in a 6 cm long cylinder with a variable aperture. The aperture of the cylinder decides the maximum Larmor radius of the ions that contributes to the collector current. The aperture of the cylinder was varied from ϕ 3.5 cm to ϕ 0.4 cm, thus selecting the ions with different Larmor radii.The adiabaticity parameter was calculated. The variation of the reflection coefficient on the adiabaticity parameter is shown in fig. 27. During the measurements the magnetic field value at the centre of the trap was kept at 50 gauss.

The floating potential during the plasma experiment was measured along the axis on either side of the mirror point. The successive shots from the gun were tried to be kept identical by keeping the discharge voltage constant. Numerous shots were used for each point of measurement. Slight fluctuations of the values were observed. The measurements were conducted for configurations III and V. The plots are shown in fig.28.

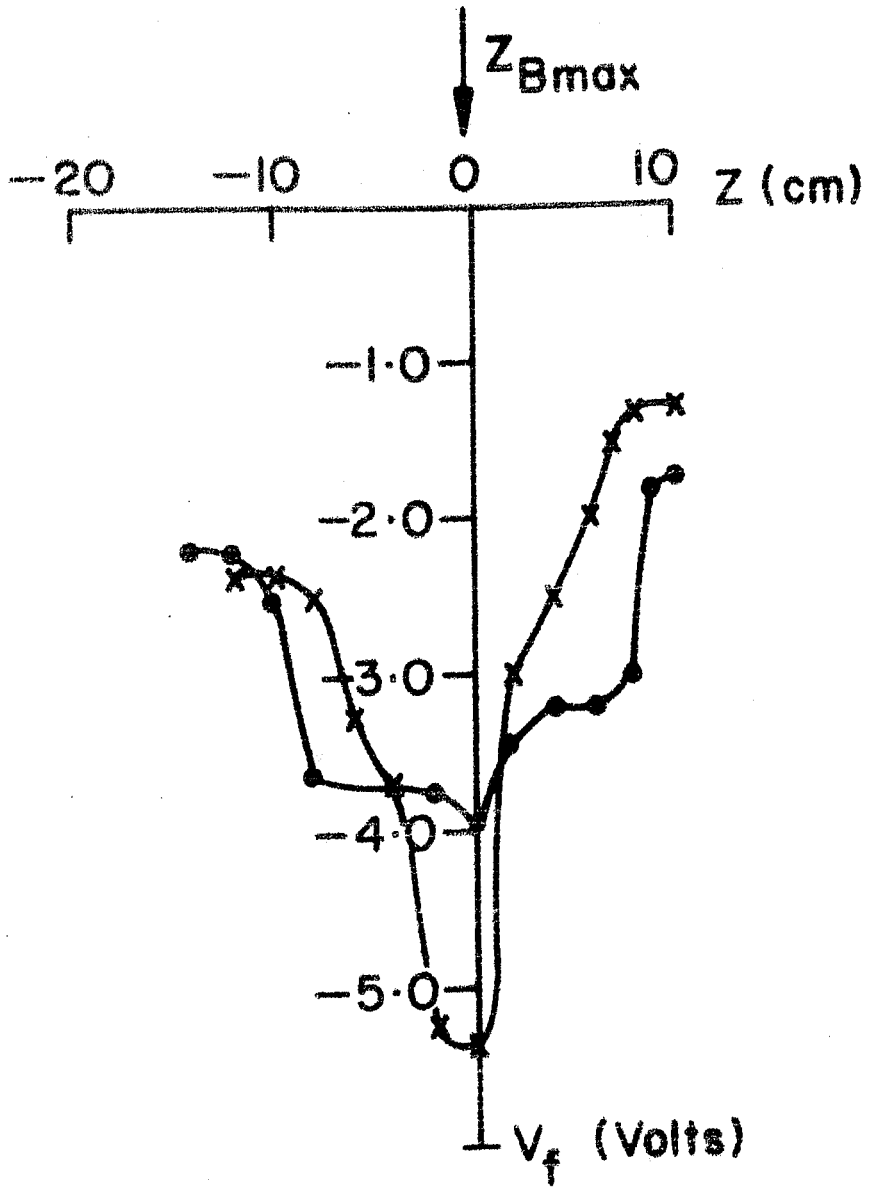

Fig. 28. Axial profile of the floating potential around the mirror point for the magnetic field configurations III and V during the plasma experiments. Z_{max} denotes the mirror point.

In the diagram the mirror system is to the left of Z_{max}. For the most nonadiabatic mirror configuration, the curve shows a sharp negative peak. This could be because of the localized accumulation of the electrons near the turning point.

The experiments were conducted at a pressure range of $2\text{-}4 \times 10^{-5}$ torr and the time for collisional scattering for electrons of the given energy during the electron beam experiment was $\sim 50\,\mu$sec, where as the single transit time for the electrons was never more than 12 μsec. So for single reflection, theoretically one should expect total reflection as the energy dispersion was small for the electron beam. The corresponding pitch angle dispersion due to the interaction of the particle with the transverse electric field was calculated. In the adiabatic case the loss due to scattering by the micro-inhomogeneities in the static magnetic field was possible but has not been estimated. As the system becomes increasingly nonadiabatic (by increasing the magnetic field gradient scale length i.e. by decreasing the mirror width), the $\Delta\mu/\mu$ ratio increases and the reflection coefficient decreases and goes through a minimum. The increase in the reflectivity when the system becomes strongly nonadiabatic can be explained in the following way using the results from the plasma experiment.

The normal mirror reflection was enhanced by the additional electrostatic reflection due to the potential hill for the electrons, thus increasing the effective reflection coefficient.

3.3. Conclusions:

Thus from the above experiment one could conclude that the mirror reflectivity reduces as the nonadiabaticity parameter increases. However, the electrostatic layer formation at steep magnetic field gradients when the beam densities go above some critical value causes enhanced reflection; making the nonadiabatic mirror as effective in plasma confinement as the conventional mirror.

CHAPTER IV

SINGLE PARTICLE CONFINEMENT IN MAGNETIC MIRROR

To study the behaviour of charged particle motion in a slowly varying magnetic field, an experiment was conducted in the device described earlier with some modifications demanded by the experiment. The major motivation in perforning the experiment was to look for the theoretically predicted multiple life times during the nonadiabatic escape of particles from the adiabatic mirror. To observe the life time determined by the nonadiabatic effects, it was necessary to r educe collision-induced particle loss to a minimum. This was achieved: i) by increasing the beam energy (thereby decreasing the collision crossection for the charged particles) and ii) by reducing the residual gas pressure in the system to $\sim 5 \times 10^{-8}$ Torr. The latter required the addition of a sputter ion pump to the system.

The electron gun was placed 3 cm off axis on one end of the system, 14 cm away from the mirror throat. The gun could be moved radially with the help of a radial motion feed-through. The magnetic field at the injection point was 3.5 times less than the maximum magnetic field. Normally the cathode and grid were held at the same dc potential. For generating the electron beam, the cathode was made negative relative to the grid by applying a rectangular pulse of appropriate voltage

of a given duration. Two types of pulses were used during the experiment, one of duration ~500 nsec, and other of much smaller duration ~30 nsec, the later being generated by means of a pulse forming line as described earlier in the chapter on instrumentation. The beam energy could be varied from 0.2 to 5 kev.

For trapping the particles in the system the magnetic field at the mirror throat was reduced to facilitate the entry of the particles into the system during the injection of the particles. A rectangular current pulse of appropriate amplitude ($\lesssim$ 100 amp) and of 150 nsec duration was applied to a four turn coil situated at the maximum of the static magnetic field.Usually the amplitude of the pulsed magnetic field was about one fifth or less of the static magnetic field value at the mirror throat. This resulted in reduction of the magnetic field in the mirror region near injection point thus allowing electrons to enter the mirror trap. The current pulse was synchronised with the electron beam pulse such that part of the electron beam always saw the increased field on its way back after the reflection from the opposite mirror and thus got trapped.

4.1 Experimental Measurements.

Observations were directed primarily towards measuring the decay current from the trap for particles injected with a particular value of the energy and the pitch angle. The observations were taken for different values of the static magnetic

field for same values of particle energy and pitch angle. Three different magnetic field configurations were used during the experiment. Although the magnetic field configuration was changed, the mirror ratio for all the three cases was same and had a value of 4. The field configurations are shown in fig.29. Different sets of observations were taken for different values of the particle energy and for different scale lengths of spatial variation of the magnetic field.

The particle energy was measured with the help of an electrostatic retarding potential analyser and the dispersion was found to be 10 - 12 % for the parallel component of the energy of the electrons. The density of the injected electrons in the trap was typically $\sim 10^4$ particles/cm^3. Since no collective effects were observed at this density, it was considered satisfactory at such low pressures.

The magnetic moment of the particles was to be kept constant as far as possible. Therefore the dispersion in the pitch angle was a very important factor to be measured. In the determination of the pitch angle the following method was adopted: The pulsed magnetic field was kept at a definite value and the static magnetic field was varied. The magnetic field ratio between the value at the point of injection and the reduced value at the mirror was calculated. The particles which would be trapped in the main mirror system should have a pitch angle value greater than 30° at the mid plane, since the mirror ratio was four.

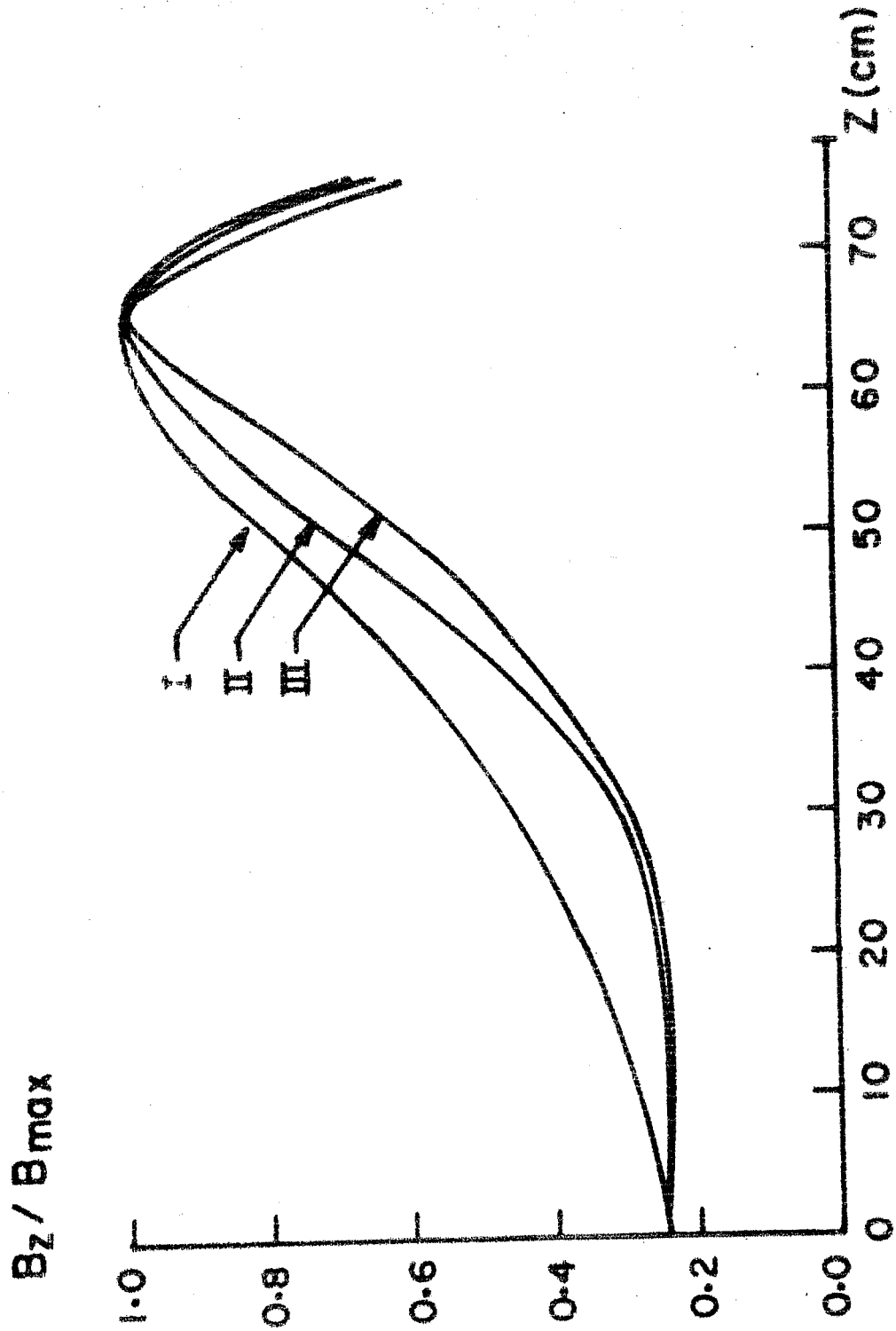

Fig. 29. Axial distribution of the magnetic field (from the centre of the system to one of the mirrors)

$R_m = 4$; i) $\alpha^{-1} = 13$ cm; ii) $\alpha^{-1} = 11$ cm; iii) $\alpha^{-1} = 8$ cm.

For smaller pitch angles, the particles, that enter the system would enter the loss cone and would be lost. The particles, to enter the main experimental chamber, must fall in the loss cone of the local mirror formed between the point of injection and the mirror throat. While entering the system electrons see a lower magnetic field. Therefore, those electrons whose velocity vector made an angle of more than 30^{o} with the static magnetic field lines at the mid plane of the experimental system could be trapped in the system. The upper limit of the pitch angle was determined by the lowest value of the magnetic field used during the experiment and the corresponding value of the pulsed magnetic field. The lower limit was given by the loss cone for the mirror. Finally the pitch angle was determined by the relative position of gun axis and the magnetic field lines near the gun. Measurements on beam width yielded an upper limit of 30' for the dispersion in pitch angle around the mean value of 33^{o} and 35^{o} for the two different pitch angles used during the experiment.

To measure the life time of the electrons, the electrostatic analyser was placed outside the mirror throat opposite the injection side, to sample particles leaking out of the trap. The signal, obtained due to the leakage of particles, on the collector was fed into a current to voltage converter and the inverted signal from the output was fed to a log amplifier. As mentioned earlier the log amplifier had a gain of 2.5 V per decade

over a range of four decades.The output signal from the log amplifier was fed into an A/D converter and the digitized data was recorded on a magnetic tape. The digitization rate was 20 μ sec. With the help of proper conversion factors, the input signal proportional to the collector current was obtained.

4.2. Data Acquisition and Analysis:

When only one life time characterized the exponential decay current, the life time could be obtained from the semilog plot of the decay signal as a function of time. In general, however, the semilog plot was not linear (fig. 30) and it suggested the existence of more than one life times characterising the decay curve. To see if this was indeed the case and to determine the life times, the decay signal was analysed in terms of a sum of exponentials with different e-folding times and amplitude. If I_i represents the current at the time t_i, then I_i may be written as a sum of N exponential functions as

$$I_i = \sum_{k=1}^{N} A_k \exp\left(-t_i/\zeta_k\right) \qquad (4.2.1)$$

where ζ_k are the different life times and A_k are the corresponding amplitudes, I_i could be rearranged in the following form:

$$I_i = \sum_{k=1}^{N} \exp\left(-t_i \sum_{m=k}^{N} \nu_m\right) \sum_{l=k}^{N} a_l$$

$$= \sum_{k=1}^{N} \prod_{m=k}^{N} \exp\left(-\nu_m t_i\right) \sum_{l=k}^{N} a_l \qquad (4.2.2)$$

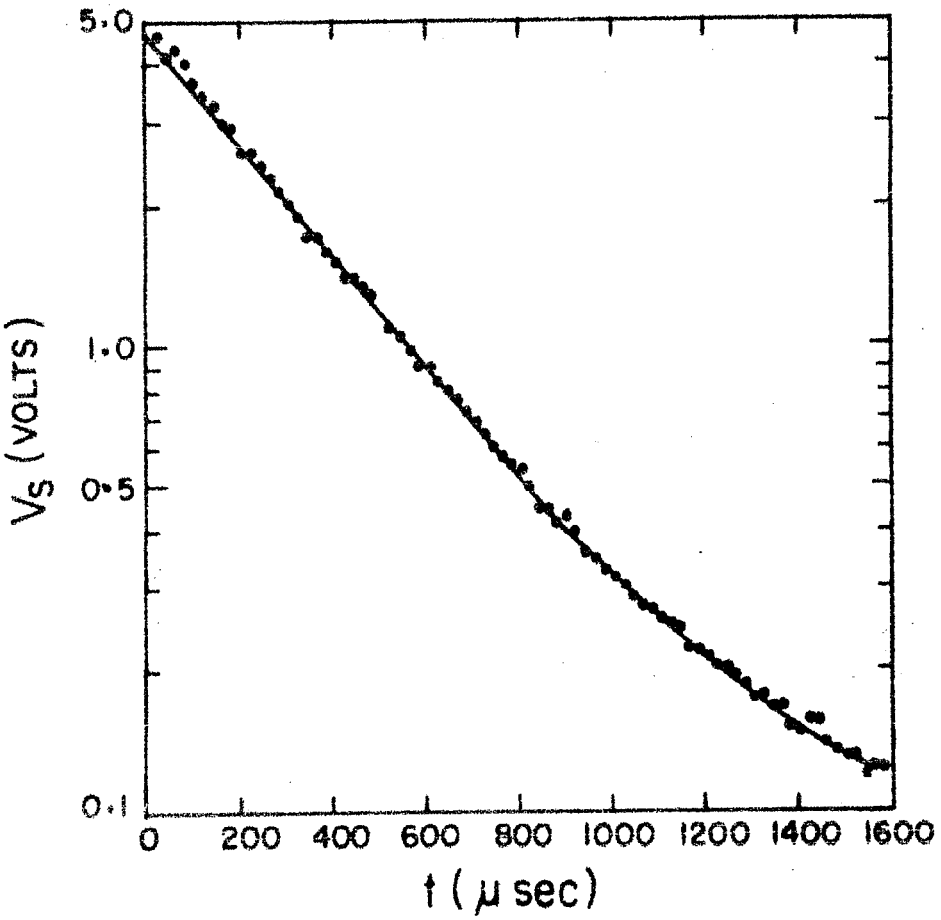

Fig. 30. The voltage proportional to the experimentally observed leakage current on a semilog scale as a function of time. Apparent fitting of a straight line through them is not possible.

where $A_k = \sum_{\ell=k}^{N} a_\ell$ and $1/\tau_k = \sum_{m=k}^{N} \nu_m$

For simplifications in the numerical analysis later, the functional form I_i was rearranged in the following manner:

$$I_i = \sum_{K=1}^{N} \prod_{m=k}^{N} \exp(-\nu_m t_i) \sum_{\ell=k}^{N} a_\ell$$

$$= (a_1 + a_2 + \cdots - a_n) \prod_{m=1}^{N} \exp(-\nu_m t_i) + (a_2 + a_3 + \cdots a_n) \prod_{m=2}^{N} \exp(-\nu_m t_i) + \cdots a_n \exp(-\nu_n t_i)$$

$$= a_1 \prod_{m=1}^{N} \exp(-\nu_m t_i) + a_2 \left[\prod_{m=1}^{N} \exp(-\nu_m t_i) + \prod_{m=2}^{N} \exp(-\nu_m t_i) \right]$$

$$+ \cdots a_n \left[\prod_{m=1}^{N} \exp(-\nu_m t_i) + \prod_{m=2}^{N} \exp(-\nu_m t_i) + \cdots \right.$$

$$\left. \cdots \exp(-\nu_n t_i) \right]$$

$$= \sum_{k=1}^{N} a_k \left\{ \sum_{j=1}^{N} \left[\prod_{m=j}^{N} \exp(-\nu_m t_i) \right] \right\} \quad (4.2.3)$$

The values of the parameters a_m and ν_m were obtained by fitting the function $I_i(t)$ defined by equation (4.2.3) to the experimentally obtained current decay curve. The fitting was done

by minimisation of the function χ^2 defined as

$$\chi^2 = \sum_i W_i \left[S_i(t_i) - I_i(t_i) \right]^2 \qquad (4.2.4)$$

where $S_i(t_i)$ was the observational data at a time t_i. I_i was the fitting function with amplitude normalized to the initial amplitude at $t = 0$ and W_i was the weight factor for data at t_i.

The minimisation of χ^2 was carried out with respect to the coefficients a_m, ν_m, $m = 1$ to N. Without loss of generality the life times could be numbered so that they could be ordered as

$$\tau_1 \leqslant \tau_2 \leqslant \tau_3 \cdots\cdots \leqslant \tau_n \qquad (4.2.5)$$

From the theory, it is expected that the corresponding amplitudes A_k would be in the following order:

$$A_1 \geqslant A_2 \geqslant A_3 \cdots\cdots \geqslant A_n \qquad (4.2.6)$$

These physically meaningful inequalities lead to the following limits on values of ν_m and a_m

$$\nu_m \geqslant 0 \quad ; \quad a_m \geqslant 0$$

which in turn helped in the minimisation of the χ^2 function, with respect to ν_m, a_m, $m = 1, \cdots N$.

Since the function $I_i(t_i)$ was not linear in the parameter τ_k, neither minimisation nor maximisation could be optimized by analytical differentiation and inversion (except in the trivial

case where only single exponential characterizes the decay curve, in which case the logarithmic signal could be linearly fitted). During the initial stage of the search, different programmes[32], based on Monte Carlo technique, minimisation programme using a simplex method by Nelder and Mead[39] were used before using the method of steepest descent[30] in the final stage. All these programmes were used to supplement each other during an efficient search. Each of these techniques had a characteristic efficiency which depended upon the proximity to minimisation. However, if a true minimum could be achieved, the resulting fitting parameters would be independent of how the minimum was located and the various programmes should differ only in the time and number of iterations required for convergence.

Although, in general, the fits should be independent of the specific search programme, they could often be sensitive to the weights chosen. For convenience, the weights were based on the measured data and included a number of different sources of uncertainity. Since the decay curves begin with relatively high signal and end when the signal becomes comparable with fluctuations in the background, the local accuracies over the decay curve were expected to vary greatly. Statistical fluctuations, at times, might not be sufficient to account for the observed spread of data points. The uncertainities in the individual parameters could be estimated by examining χ^2 as a function of each parameter in the neighbourhood of the minimum.

In our case the error on the data points was mainly because of the digitization error. The digitization error was same at all data points. However, the minimization calculations were done with the statistical fluctuations also. The calculated values for the unknown parameters did not change considerably.

Lanczos[35] studied the numerical implications of the exceedingly non-orthogonal properties of the exponential functions, and noted the extraordinary sensitivity of the fitted parameters to small changes in data. This causes difficulties in applications to physical problems, where the aim of the fits is not merely to approximate the data closely by a mathematical function, but also to determine accurately the physically meaningful parameters. To examine the effect of the changes, of the order of standard deviation, in data points on the fitted parameters the following method was adopted.

For a given minimisation, the standard deviations on the data points were calculated and the data points were modified by random addition or subtraction of thrice the standard deviations from them. Uniformly distributed random numbers between + 1 and -1 were used for this purpose. A new χ^2 minimisation was carried out using the modified data. New fitted parameters were compared with the original fitted parameters. The difference in two sets was $\lesssim$ 5%, thus indicating the good fit to the experimental data.

The errors on the fitted parameters were also calculated with the help of the error matrix[31]. The error matrix, also called the covariance matrix, is the inverse of the second derivative matrix of the function with respect to its free parameters which were evaluated at the function minimum. The diagonal elements of the error matrix were the squares of the individual parameter errors, including the effects of the correlations with the other parameters.

The appearance of the correlations could be understood as follows. The inverse of the error matrix, the second derivative matrix, contained the second partial derivatives with respect to one parameter at a time. These diagonal elements were not coupled therefore to any other parameters, but when the matrix was inverted, the diagonal elements of the inverse contained contribution from all the elements of the second derivative matrix.

The covariance matrix was required to be a positive definite matrix, for the step size to make sense, since only then would the quadratic form have a minimum. If the second derivative matrix was singular, the predicted minimum was not unique.

The second derivative matrix for χ^2 could be expressed as:

$$\frac{\partial^2 \chi^2}{\partial a_i \partial \nu_j} = \frac{\partial}{\partial a_i}\frac{\partial}{\partial \nu_j}\chi^2$$

$$= 2\frac{\partial \chi}{\partial a_i}\frac{\partial \chi}{\partial \nu_j} + 2\chi\frac{\partial^2 \chi}{\partial a_i \partial \nu_j} \qquad (4.2.7)$$

In case of the non linear least squares the linearization approximation consisted in taking

$$\frac{\partial^2 \chi^2}{\partial a_i \partial \nu_j} \simeq 2\chi \frac{\partial^2 \chi}{\partial a_i \partial \nu_j} \qquad (4.2.8)$$

This had the advantage of being easy to calculate and, moreover, it was always positive-definite. The covariance matrix obtained by inverting this approximate matrix did not in general converge to the true covariance matrix even though the minimization based on it converged to the true minimum.

The error matrix was calculated with help of the programmes mentioned earlier and based on this matrix, both the individual correlation coefficients and the global correlation coefficient for each variable parameter were printed out. Typical correlation coefficients were ~ 0.35. From the errors on the amplitudes a_k and $1/\nu_j$, the partial errors were calculated in the following fashion.

$$\delta a_j = \sum_{k=j}^{N} \delta a_k \quad \text{and} \quad \delta \nu_j = \sum_{K=j}^{N} \delta \nu_K = \sum_{k=j}^{N} \zeta_j \frac{\delta \nu_j}{\nu_j} \qquad (4.2.9)$$

where $\zeta_j = 1/\nu_j$.

The maximum error on the parameters was not more than 15 %.

4.3. Results and Discussion

4.3.1. Existence of Multiple Life times: As mentioned earlier, life time measurements were carried out under different

experimental conditions. The decay curves while plotted in the semilog scale, did not represent one life time. This indicated the possible existence of multiple life times. Therefore, the least square fitting technique was adopted as described in the previous section. Fig. 31 shows a comparison of the experimental data with the fitted curve for a typical case. In most of the cases two exponentials could be fitted through the data points. For a few cases, even three exponentials could be fitted indicating three life times. But the amplitude of the signal for the third life time fell within the digitization error. Therefore no analysis was possible on the third life time.

4.3.2. Relationships of life time τ and Amplitude A with Magnetic Field: For a given pitch angle and energy of the particles, the life time was measured as a function of magnetic field strength at the mirror throat. The life times obtained are tabulated in table I for one of the sets of observation. Along with the life times, the amplitude values are also tabulated. The amplitude values for the different life times showed the contribution of the particles with different life times to the total amplitude of the signal. From table I, it is seen that for a range of magnetic field values, two life times distinctly exist. Since both the energy and pitch angle had small but continuous spread, the two life times could not be attributed to distinct groups of particles having either two distinct energies, pitch angles or both.

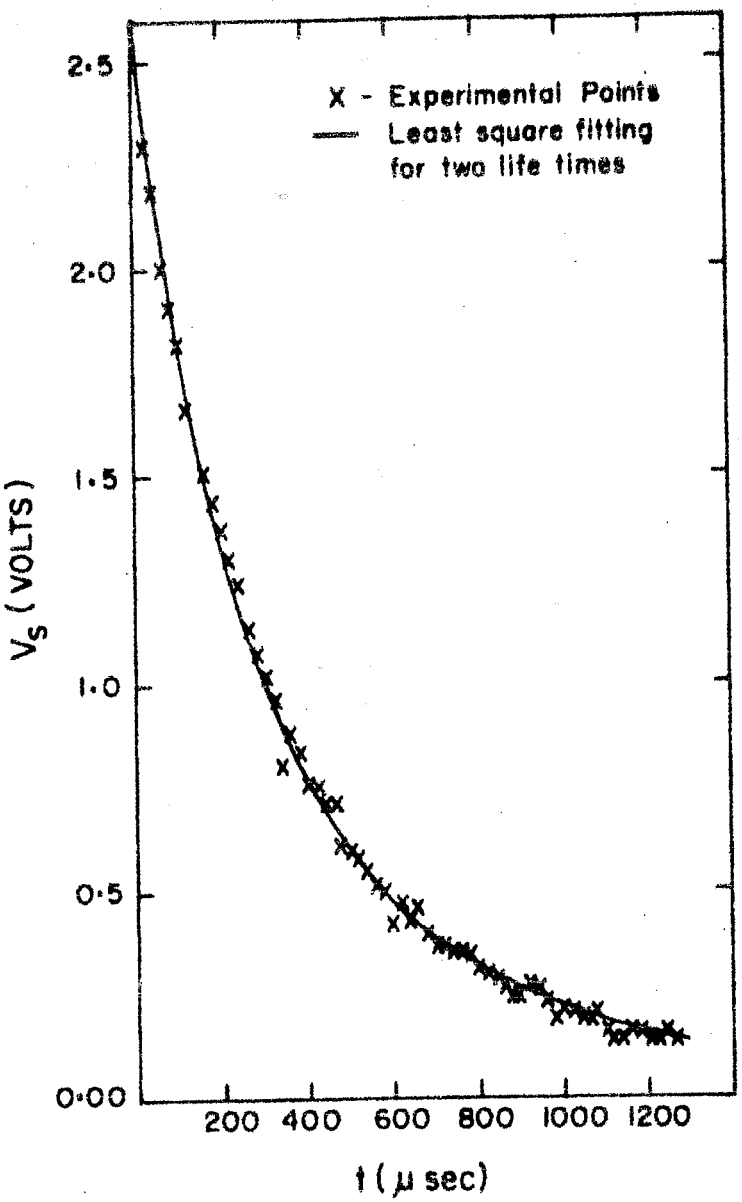

Fig. 31. The least square fitting for two life times (continuous curve) along with the experimental data points (crosses).

TABLE-I

THE VARIATION OF LIFE TIMES AND THEIR AMPLITUDES AS A FUNCTION OF THE MAXIMUM MAGNETIC FIELD VALUES AT THE MIRROR THROAT:

(E=2.2 kev; $\mathcal{L}^{-1}$ = 13 cm ; $\theta \simeq 33^{\circ}$)

B (Gauss)	T_1 (msec)	Amplitude-1	T_2 (msec)	Amplitude-2
270	0.196±0.02	0.75±0.025	0.304±0.03	0.229±0.02
335	0.207±0.03	0.705±0.08	0.33±0.041	0.21±0.05
400	0.234±0.03	0.745±0.03	0.401±0.024	0.215±0.013
465	0.246±0.037	0.769±0.023	0.45±0.05	0.229±0.013
530	0.25±0.02	0.792±0.01	0.492±0.05	0.21±0.008
595	0.256±0.03	0.82±0.03	0.43±0.03	0.18±0.02
660	0.261±0.028	0.87±0.03	0.428±0.04	0.11±0.02

The effect of the pulsed magnetic field on the charged particles while entering into the experimental space could also be investigated, although it was negligible. The time varying magnetic field produced an electric field in the perpendicular direction. The magnitude of this electric field, even for the maximum magnetic field was extremely small (few volts/cm), therefore the effect on the particles was negligible. The rise or the fall time of the magnetic field pulse ($\sim$30 nsec) was always more than the Larmor period (($\gtrsim$ 3 nsec) or the transit time ($\gtrsim$ 5 nsec) through the region under the influence of the pulsed magnetic field. Therefore, the pulsed magnetic field change was still an adiabatic change as far as the particles under consideration were concerned.

From table I, it was observed that at higher magnetic field values, the second amplitude (A_2) value decreased to very small value where as the fractional amplitude A_1 (fig. 32) increased with increasing magnetic field.

Logarithms of experimentally observed lifetimes for different sets were plotted as a function of magnetic field B_m (fig 33a-d). Straight lines were fitted through the different experimental points. It was observed that for both the life times straight lines could be fitted with a correlation coefficient of 0.9 or more for all the cases. The ratio of the slope for the second life time to that for the first were calculated and it was found to be in the range of 1.8 to 2.3.

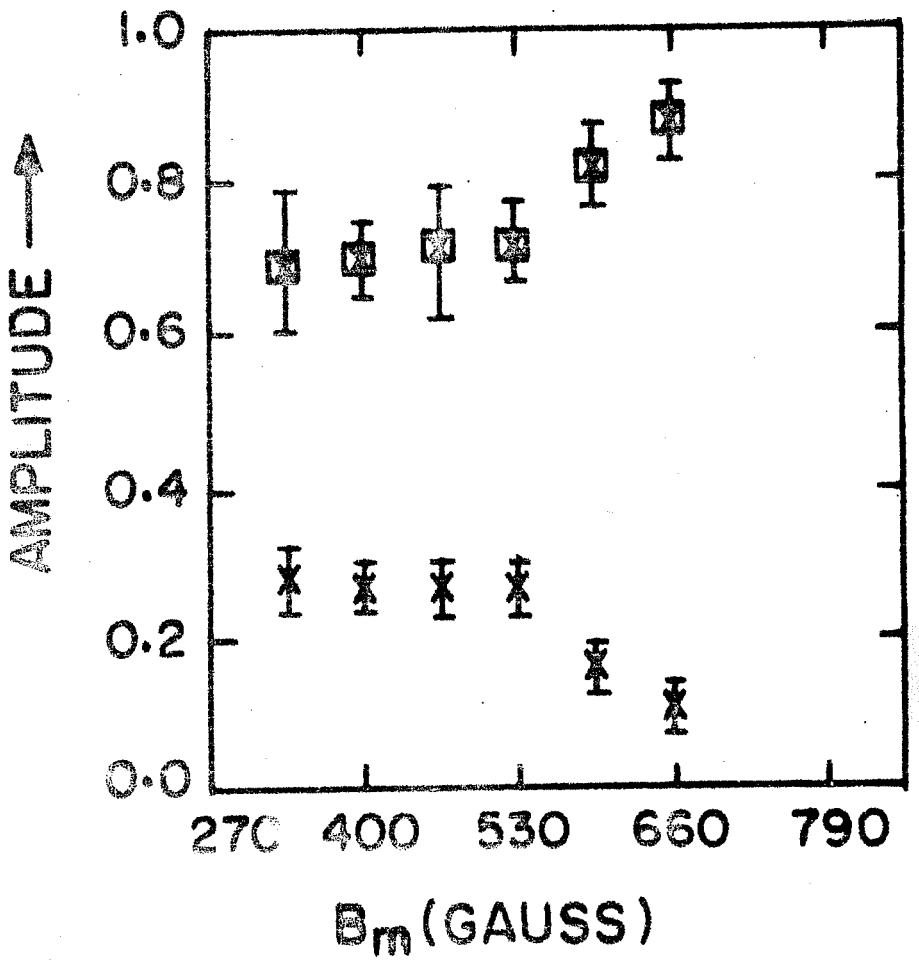

Fig. 32. Fractional amplitudes corresponding to two life times which characterise a typical decay curve (⊠ - A_1 , X - A_2).

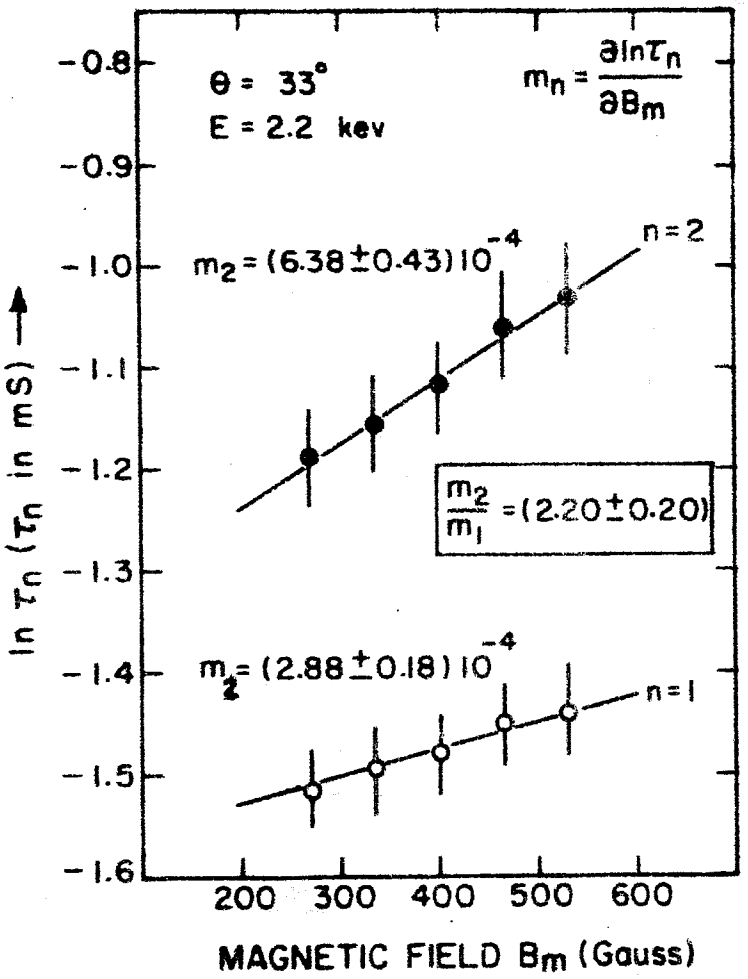

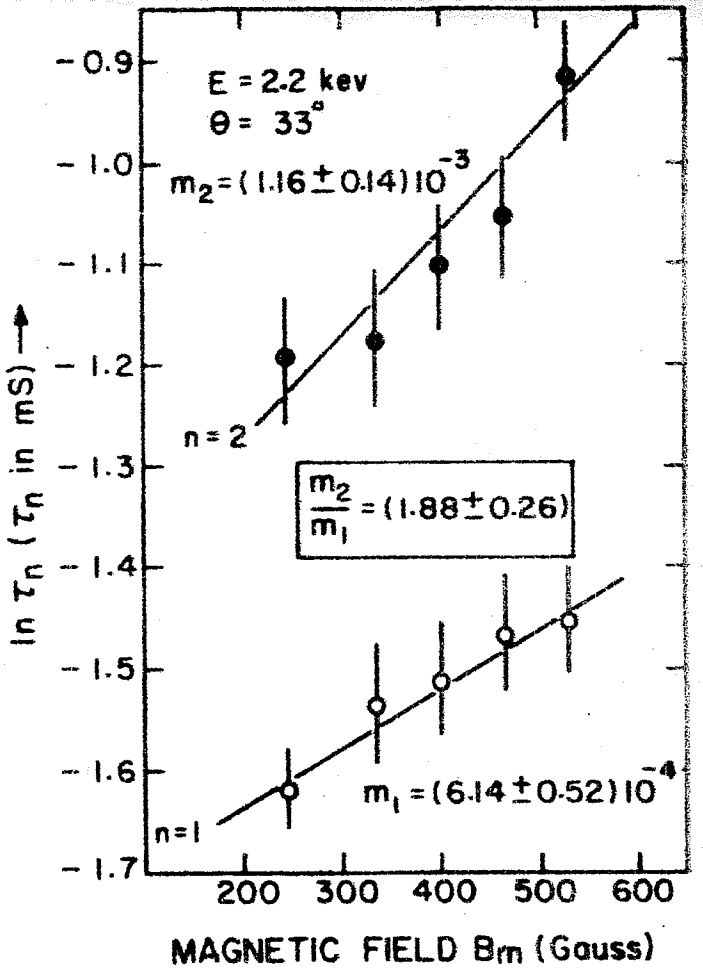

Fig. 33. $\ln \tau_n$ as a function of the maximum magnetic field B_m. Total energy E = 2.2 kev; Θ = initial pitch angle.
a) $\mathcal{L}^{-1}$ = 8 cm; b) $\mathcal{L}^{-1}$ = 11 cm. m_1 and m_2 are the slope values for τ_1 and τ_2 respectively.

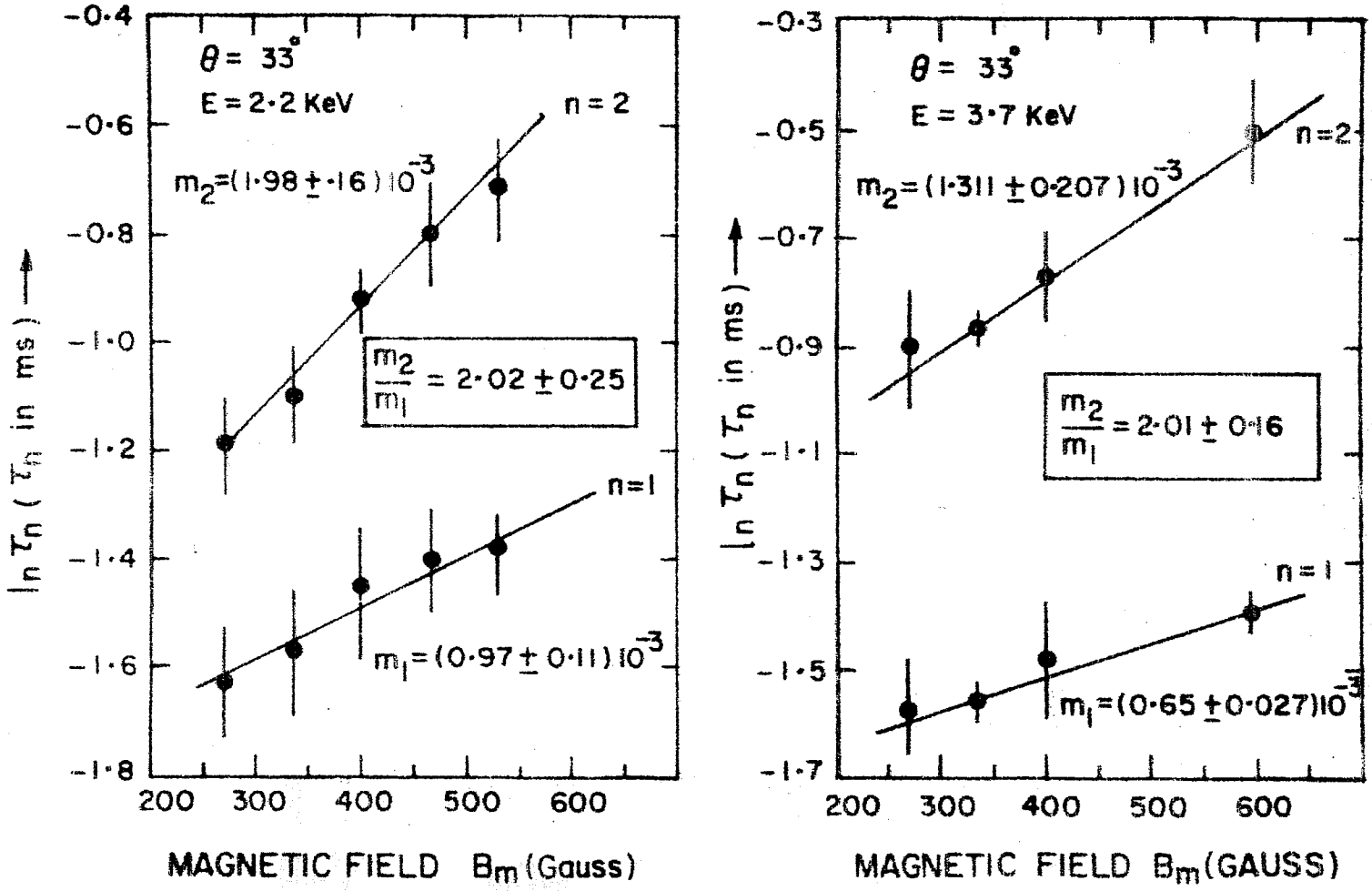

Fig. 33. $\ln \zeta_n$ as a function of maximum magnetic field B_m. θ - initial pitch angle; $\alpha^{-1} = 13$ cm.
c) E = 2.2 kev; d) E = 3.7 kev.

The experiments were conducted at two different pitch angles $\theta \simeq 33^{\circ}$ and 35° for three different magnetic field configurations as shown in fig.29. Unlike in the first case, the source was 11 cm away from the mirror throat in the second case. The scale lengths in the three different cases were different although the mirror ratio was kept constant. This was done by varying the coil positions with respect to the midplane symmetrically on either side. The charged particle energy was also varied by varying the accelerating voltage. Fig.33 a,b depict the experimental results with different magnetic field scale length (α^{-1}) while fig.33 c,d depict the results obtained by varying the energy of the injected electrons. The values of the two slopes are tabulated in table II for different cases. Along with the two slopes the ratio of the second slope to the first is also given. From the table, one can observe that the slope values increase as the scale length of the magnetic field is increased. However, the slope value decreases as the energy of the charged particles is increased. A more quantitative comparison with energy and α^{-1} can be attempted at, which is given in the next subsection. From the table it is observed that the ratio of the two slopes vary between 1.8 to 2.2 in the experiments with $\theta \simeq 33^{\circ}$ while it lies close to 2.1 except in one case for the experiments with $\theta \simeq 35^{\circ}$.

It would have been very interesting to take observations at still higher pitch angles and to see the effect on the ratio

TABLE-II

a) VARIATION OF THE SLOPES m_1 AND m_2 AS A FUNCTION OF TOTAL ENERGY E for $\mathcal{L}^{-1}$ = 13 cm; $\theta \simeq 33^{\circ}$

E(kev)	m_1	m_2	m_2/m_1
2.2	$(0.97\pm0.11)10^{-3}$	$(1.98\pm0.16)10^{-3}$	2.02 ± 0.25
2.9	$(0.95\pm0.06)10^{-3}$	$(1.7\pm0.06)10^{-3}$	1.82 ± 0.14
3.7	$(0.65\pm0.027)10^{-3}$	$(1.311\pm0.207)10^{-3}$	2.01 ± 0.16

b) VARIATION OF THE SLOPES m_1 AND m_2 AS A FUNCTION OF $\mathcal{L}^{-1}$ FOR TOTAL ENERGY E = 2.2 kev; $\theta \simeq 33^{\circ}$

$\mathcal{L}^{-1}$ (cm)	m_1	m_2	m_2/m_1
8	$(2.88\pm0.18)10^{-4}$	$(6.38\pm0.43)10^{-4}$	2.2 ± 0.2
11	$(6.14\pm0.52)10^{-4}$	$(1.16\pm0.14)10^{-3}$	1.88 ± 0.26
13	$(0.97\pm0.11)10^{-3}$	$(1.98\pm0.16)10^{-3}$	2.02 ± 0.25

c) VARIATION OF THE SLOPES m_1 AND m_2 AS A FUNCTION OF TOTAL ENERGY E for $\mathcal{L}^{-1}$=8 cm; $\theta \simeq 35^{\circ}$

E(kev)	m_1	m_2	m_2/m_1
2.2	$(5.56\pm0.18)10^{-3}$	$(11.90\pm0.5)10^{-3}$	2.14 ± 0.03
2.9	$(4.9\pm0.24)10^{-3}$	$(10.46\pm0.7)10^{-3}$	2.12 ± 0.04
3.7	$(4.54\pm0.3)10^{-3}$	$(9.95\pm0.68)10^{-3}$	2.15 ± 0.06
4.5	$(3.96\pm0.42)10^{-3}$	$(9.15\pm0.7)10^{-3}$	2.31 ± 0.1

d) VARIATION OF THE SLOPES m_1 AND m_2 AS A FUNCTION OF $\mathcal{L}^{-1}$ FOR TOTAL ENERGY E=2.9 kev; $\theta \simeq 35^{\circ}$

$\mathcal{L}^{-1}$(cm)	m_1	m_2	m_2/m_1
8	$(4.9\pm0.24)10^{-3}$	$(10.46\pm0.7)10^{-3}$	2.12 ± 0.04
11	$(6.16\pm0.18)10^{-3}$	$(12.62\pm0.62)10^{-3}$	2.05 ± 0.03
13	$(8.24\pm0.3)10^{-3}$	$(17.2\pm0.53)10^{-3}$	2.09 ± 0.038

of the two slopes. But unfortunately, in the present experimental set up, particles with higher pitch angles could not be injected into the system. This was mainly due to the physical dimension of the charged particle source and the radial dimension of the system with the neck as shown in the schematic of the experimental system in fig.3.

4.3.3. Comparison with Theory[47]: We may now recall some of the results of the theory[47], that was reviewed briefly in the first chapter. Following the analysis in the theory[47], if the adiabatic potential $\mu\Omega$ in the regions of the mirrors along a certain field line be modelled by

$$\mu\Omega = \mu\Omega_0 + (\mu\Omega_{max} - \mu\Omega)\cosh^{-2}\alpha x \qquad (4.3.1)$$

where α^{-1} is the magnetic field scale length in the mirror region and Ω_0 is the cyclotron frequency at the minimum of the well, then the probability of transmission across the potential hill for a particle of total energy $E<\mu\Omega_{max}$ according to the n^{th} Schrodinger-like mode[47] could be expressed as

$$P_n = \exp\left[-(2m)^{1/2}\frac{2\pi n}{\alpha\mu}\left\{(\mu\Omega_{max} - \mu\Omega_0)^{1/2} - (E-\mu\Omega_0)^{1/2}\right\}\right] \qquad (4.3.2)$$

whence the corresponding life time τ_n is given as

$$\tau_n = T_{eHn}\exp\left[(2m)^{1/2}\frac{2\pi neB}{mc\alpha\sqrt{E}}\left\{\left(\frac{B_m}{B}-\frac{B_0}{B}\right)^{1/2}\sin\theta - (1-\sin^2\theta\, B_0/B)^{1/2}\right\}\right] \qquad (4.3.3)$$

Where $T_{eff\,n}$ represents some effective bounce time. B is the value of the magnetic field at the point of injection. B_o is the magnetic field at the minimum of the well and B_{max} that at the maximum; Θ - the value of the pitch angle at the point of injection. The total probability of escape per unit time, then, could be written down as

$$\dot{P} = \sum_n \frac{A_n}{\tau_n} e^{-t/\tau_n} = \sum_n \frac{C(n) P_n}{T_n} e^{P_n t/T_n} \qquad (4.3.4).$$

where An are appropriate coefficients.

Since the Schrodinger-like equations[47] were uncoupled linear equations, the probability coefficients were related to the initial conditions at the time of injection and in particular to the initial distribution function in the Larmor phase[49].

The exponent in the expression for τ_n gave the slope of $\ln \tau_n$ variation with magnetic field and could be written in terms of total energy and pitch angle as follows:

$$m_n = (2m)^{1/2} \frac{2\pi e n}{mc\alpha\sqrt{E}} \left\{ \left(\frac{B_m}{B} - \frac{B_o}{B} \right)^{1/2} \sin\theta - \left(1 - \sin^2\theta \frac{B_o}{B} \right)^{1/2} \right\} \qquad (4.3.5)$$

$$= n m_1$$

that m_n is n times m_1, the slope for $\ln \tau_1$ vs B curve. From the expression (4.3.3) one could observe that i) $\ln \tau_n$ vs B curve would be a straight line with a slope m_n which would be n times the slope of $\ln \tau_1$ vs B.

ii) The magnitude of the slope would decrease with increasing energy as $E^{-\frac{1}{2}}$ and increase with increasing magnetic field scale length $\mathcal{L}^{-1}$.

The experimental results, described in the previous subsection agree with these theoretical predictions. The ratio of the slope for second life time to that for the first was found to be in the range of 1.8 to 2.3 for different sets of observations. This could be considered to be in quite a good agreement with the theoretical value of 2 as seen from relation (4.3.5). The results tabulated in Table II are also in qualitative agreement with the theoretical predictions. Since the variation of the slopes with E and $\mathcal{L}^{-1}$ is known, some quantitative comparison was done. The product of the different measurements of the slopes for different energies with respective $E^{\frac{1}{2}}$ should be constant if all other parameters are assumed to be constant. Similarly the product of the slopes with respective values of $\mathcal{L}$ would be constant for a fixed value of energy. The value $m_1\sqrt{E}$ for $\Theta \simeq 33^{\circ}$ and 35° was found out to be $(4.413 \pm .202)\ 10^{-3}$ and $(8.33 \pm .44)\ 10^{-3}$ respectively where as the value $m_1\mathcal{L}$ was found to be $(0.054 \pm 0.018)\ 10^{-3}$ and $(0.602 \pm 0.04)\ 10^{-3}$ respectively. From these values it is observed that although there is qualitative agreement between the theoretical and experimental results, the theoretical slope values corresponding to $\Theta \simeq 33^{\circ}$ differ by a great measure. At pitch angle values of $\sim 35^{\circ}$, the agreement between the theoretical and experimental values is better than in the previous case.

However it could be noted that the theoretical value for m_n became very sensitive to the value of θ when the latter lay close to the adiabatic loss cone angle. During the first set of observations, the angle of injection was estimated to be 33° at the position of the electron gun outside the trap (where the magnetic field was 3.5 times smaller than the maximum magnetic field), where as the adiabatic loss cone angle at the same position was 32° 18' 40". Therefore it was clear that the uncertainity in the specification of the pitch angle was quite large, for any meaningful comparison between the observed and calculated values of m_n. However, one could calculate the pitch angle from the observed values of the slope using the values of the energy and $\mathcal{L}^{-1}$.

Table III gives the values of the pitch angle corresponding to the various observed slopes.The slope values used here were calculated for the magnetic field values at the point of injection. We see that all these values of pitch angle lie within two narrow intervals for the two pitch angle values, namely $32^\circ 21' 49"$ - $32^\circ 26' 48"$ and $34^\circ 18' 22"$ - $34^\circ 21' 12"$. It is observed that the interval corresponding to the experimentally measured $\theta \simeq 35^\circ$ is smaller than the interval for the case of the pitch angle $\theta \simeq 33^\circ$. Thus, it could be noted that the comparison between theoretical and experimental results became more stable as one moved away from the adiabatic loss cone.

TABLE-III

THEORETICALLY CALCULATED VALUES OF θ CORRESPONDING TO THE EXPERIMENTAL VALUES OF THE FIRST SLOPE m_1 FOR DIFFERENT TOTAL ENERGIES E AND MAGNETIC FIELD SCALE LENGTHS $\mathcal{L}^{-1}$.

S.No.	E (kev)	$\mathcal{L}^{-1}$ (cm)	m_1 (experimental)	θ° (Theoretical)
1	2.2	8	0.91×10^{-3}	32° 21' 49"
2	2.2	11	0.213×10^{-2}	32° 24' 10"
3	2.2	13	0.339×10^{-2}	32° 25' 53"
4	2.9	13	0.332×10^{-2}	32° 26' 48"
5	3.7	13	0.227×10^{-2}	32° 24' 56"
6	2.2	8	1.779×10^{-2}	34° 19' 57"
7	2.9	8	1.568×10^{-2}	34° 20' 12"
8	3.7	8	1.453×10^{-2}	34° 21' 12"
9	4.5	8	1.267×10^{-2}	34° 20' 20"
10	2.9	11	1.971×10^{-2}	34° 18' 22"
11	2.9	13	2.637×10^{-2}	34° 20' 56"

4.3.4. Effective Bounce Time, T_{eff} : The form of expression for τ_n showed that its dependence on the magnetic field contained entirely in the exponential factor. The multiplying factor $T_{eff,n}$ then represents an "effective bounce time" such that the probability of escape per bounce could be given by P_n of equation (4.3.2). Table IV gives the values of $T_{eff\ 1,2}$ in the various cases. The adiabatic bounce period, T_b, was calculated in each case. The number of adiabatic bounce periods in a T_{eff} ranged between 18 to 42 for the cases where $\theta \simeq 33^\circ$ and varied from 7 to 36 in the cases with $\theta \simeq 35^\circ$. This represented the number of bounces that particle would make on the average before it escaped with a probability P_n. However, no theoretical estimate of $N = T_{eff}/T_b$ has been made yet.

4.3.5. Dependence on the Shape of the Potential Hill: The magnetic field configurations used till now in the experiment have been approximated near the mirror region by the potential of the form $\mu\Omega_{max}\ \mathrm{sech}^2(\alpha x)$. The field configuration was changed and the new field configuration is depicted in fig.34. The $\ln \tau_n$ vs B curve for this particular configuration is plotted in fig.35 for E = 2.2 kev, $\alpha^{-1} = 9$ cm and $\theta \simeq 33^\circ$. The experimental slope values for such a potential were compared with the slope values for E = 2.2 kev and $\alpha^{-1} = 8$ cm for the previous field configuration and were found to be larger by a factor of about four. However, there was a small difference in the value of the magnetic field scale length. The ratio of

TABLE IV

THE VALUES OF $T_{eff\ 1,2}/T_b$ FOR DIFFERENT VALUES OF TOTAL ENERGIES E, MAGNETIC FIELD SCALE LENGTHS α^{-1} AND PITCH ANGLES θ.

S.No.	E(kev)	α^{-1} (cm)	T_b (μsec)	$T_{eff\ 1}$ (μsec)	$T_{eff\ 1}/T_b$	$T_{eff\ 2}$ (μsec)	$T_{eff\ 2}/T_b$	θ°
1	2.2	8	8.5	203	24	254	30	33
2	2.2	11	8.6	170	20	214	25	33
3	2.2	13	8.6	151	18	179	21	33
4	2.9	13	7.6	162	21	210	28	33
5	3.7	13	6.52	170	26	272	42	33
6	2.2	8	5.12	68	13	78	15	35
7	2.9	8	4.48	107	24	114	26	35
8	3.7	8	3.94	108	27	115	29	35
9	4.5	8	3.6	122	34	132	36	35
10	2.9	11	4.48	66	15	74	17	35
11	2.9	13	4.48	33	7	35	7	35

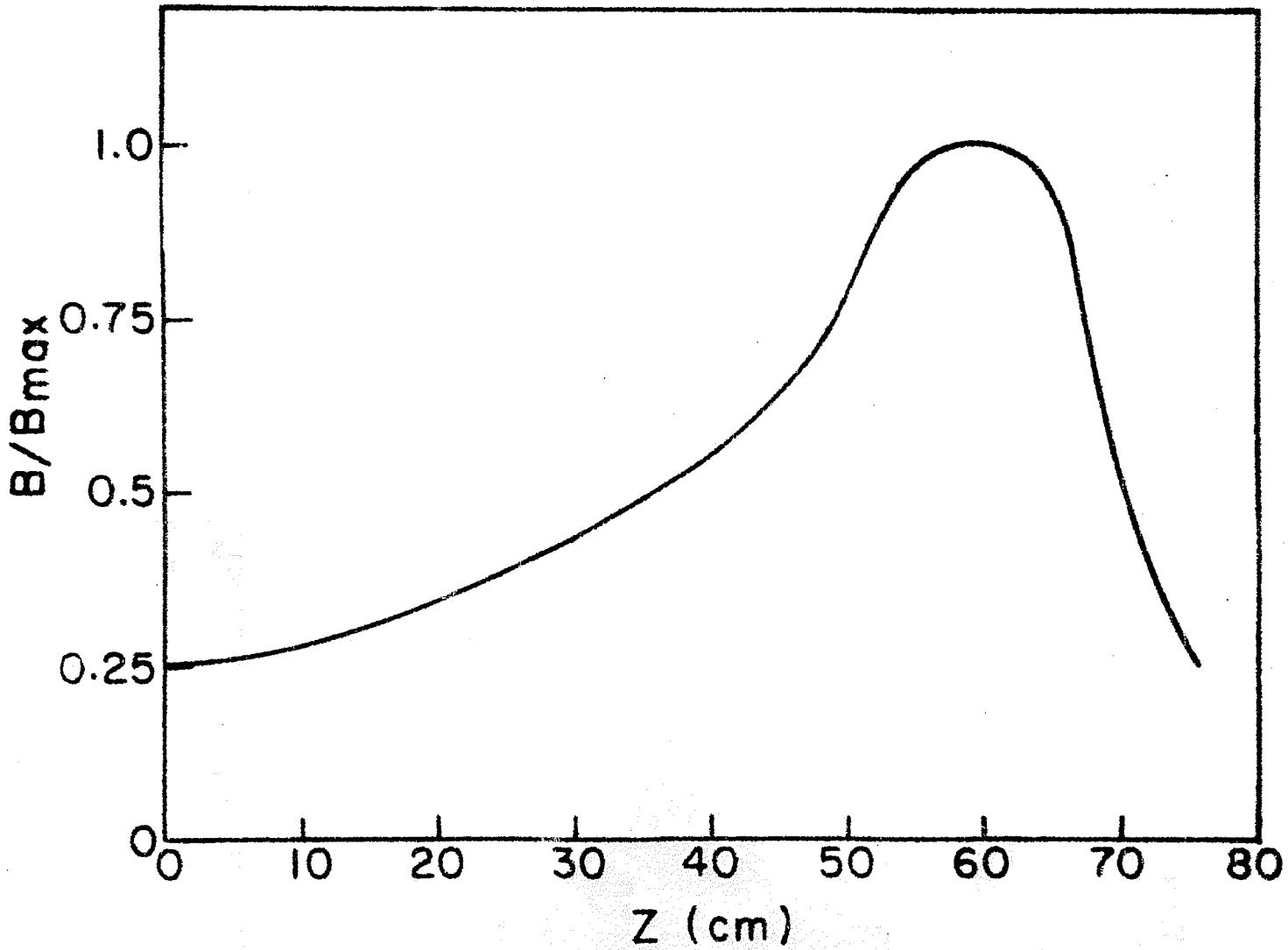

Fig. 34. Axial distribution of the magnetic field in one half of the mirror with $\mathcal{L}^{-1} = 9$ cm.

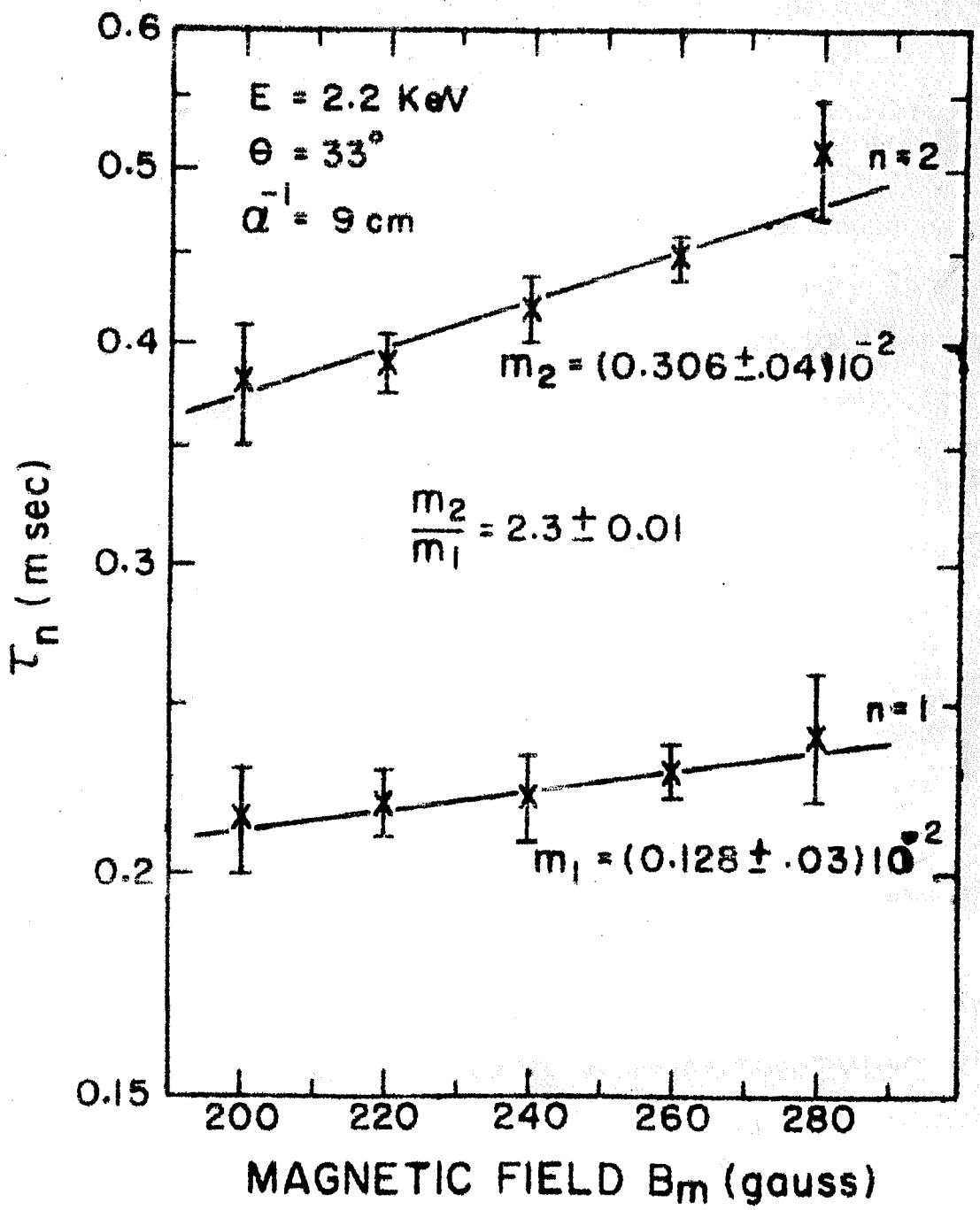

Fig. 35. Dependence of τ_n on the maximum magnetic field B_m.

the slope for the second life time to the slope for the first life time was 2.3.

The transmission probability and therefore the slope m_n could be calculated for different configurations of the potential hill (e.g. see 36). For instance, one could calculate the slope values for a square potential and compare it with the previous slope values for a given value of particle energy and pitch angle. Slope values for a square potential were found to be larger than the previous values. The present field configuration, however, could not be exactly approximated by the square potential. Following the trend of the slope values for different shapes of field configurations, one could expect higher slope values for the present configuration with a flat top in comparison to the previous field configuration.

4.3.6. Comparison with Other Theories: It was difficult to compare the experimental results with the theories discussed in the first chapter. No expression for life time was obtained in these works. For instance, one of the earlier works of Chirikov[10] and recent work of Bernstein and Rowland[7] regarded the nonadiabatic escape of particles as arising due to diffusion of particles in the μ space and into the adiabatic loss cone with a step size $\Delta\mu$, the nonadiabatic change in the magnetic moment of the particle.

Bernstein and Rowland[6] derived a Fokker-Planck equation to describe this process while Cohen, Rowlands and Foote[11] gave

expressions for $\Delta\mu$ in a mirror machine. However, no expression for the life time was obtained using this approach. It must be noted that such an approach cannot give more than one life time for a given value of the energy and the pitch angle at injection and must therefore be considered as inadequate to describe the existence of two life times that the present experimental results have established.

4.4. Conclusions:

We thus found that the experimental results did confirm the predictions of the theory[47] in some very essential aspects, namely the existence of more than one decay times, their dependence on magnetic field, the scale size of the magnetic field and the energy of the particles. The variations of the amplitudes of the decay currents corresponding to two life times, with the magnetic field was also found to be at least qualitatively in accordance with the expected behaviour[49].

CHAPTER V

SUMMARY

The work described in the previous chapters can be divided into two main sections. The first deals with the effect of nonadiabaticity on charged particles and plasma during a single reflection. The second section deals with the study of nonadiabatic loss of charged particles trapped in a mirror trap.

5.1. Results from the Single Reflection Experiment:

Effect of nonadiabaticity was considered on a beam of electrons of low energy as well as on a plasma stream. During the course of this experiment, five different mirror configurations with different mirror ratios and different magnetic field scale lengths were used. The reflection coefficient was measured as the ratio of reflected current to incident current on the collector placed near the midplane of the system. These reflection measurements were supplemented with the floating potential measurements once again near the central plane with the help of a high impedance probe. The effect of magnetic field on the reflection coefficient was observed by increasing the base value of the magnetic field. Thus by varying the magnetic field the Larmor radius was changed while the magnetic field scale length remained same for a given field configuration. This amounted to changing the adiabaticity parameter. Reflection coefficient was measured as a function of the beam current (particle density) also.

A simple plasma gun was used to study the nonadiabatic effects on plasma during a single reflection. The plasma parameters were measured using conventional diagnostics. To measure the reflection coefficient, the collector near the midplane was not used and instead the transmission efficiency was measured from which the reflectivity of the mirror was calculated assuming that the plasma loss was only through the mirror throats. This was to avoid the perturbations on the plasma by the collector at the midplane during its travel in the system. During the reflection, floating potential was measured around the mirror point on either side of it along the axis.

From all the observations made on the reflection coefficient for the plasma as well as the electron beam, we can conclude that the nonadiabatic mirror can also become as effective as an adiabatic mirror for electron beams, when the beam density goes above some critical value. From the plasma floating potential measurements near the mirror point, we see the formation of strong electrostatic potential at steep magnetic field gradients. Then the normal reflection is enhanced by additional electrostatic reflection due to the potential hill for the electrons, thus increasing the effective reflection coefficient; making the nonadiabatic mirror as effective in plasma confinement as the conventional mirrors.

5.2. Results from the Confinement Experiment :

The second part of the work (chapter IV) deals with the study of nonadiabatic particle leakage from an adiabatic mirror. The leakage current through the mirror throat was measured as a function of time for different values of particle energy and different magnetic field congigurations. The semi-log plot of the decay current as a function of time could not be approximated by single exponential decay. Therefore, numerical analysis for a least square fit was carried out. In most of the cases the experimental results were best approximated by two exponential decay times. Fractional amplitudes of the signal corresponding to the two decay times were also estimated. From $\ln \tau_n$ **vs** B curves, it was observed that the variations were linear and the ratio of the slope for the second life time to the first life time was between 1.8 to 2.3. This could be considered in good agreement with the theoretical prediction of 2. Table II shows the slope variation as a function of particle energy and magnetic field scale length. The slope values decreased as the energy of particles increased. Whereas, the slope value increased with an increase in the magnetic field scale length. This behaviour is in qualitative agreement with the theoretical predicitions[47]. However, for consistency check, the pitch angle was calculated using the experimental slope values. The pitch angle variations for the two different cases were between $32^{\circ}21'49"-32^{\circ}26'48"$ and $34^{\circ}18'22"-34^{\circ}21'12"$.

This shows that as the pitch angle is shifted away from the adiabatic loss cone, the variations in calculated pitch angle decrease. For better quantitative agreement, the experiment should be performed for larger pitch angles. But without major modifications in the experimental system, this is not possible as mentioned earlier.

Effective bounce time, T_{eff}, was experimentally obtained. This represented an "effective bounce period" such that the probability of escape per bounce was given by equation (4.3.2). The number of adiabatic bounce periods T_b in a T_{eff} was also calculated. This represented the number of bounces that a particle would make on the average before it escaped with a probability P_n. However, theoretical estimation of this number has not yet been done.

The effect of the shape of the magnetic field profile on the slope values was also investigated. Thus, the conclusions that can be made from this experimental work are : 1) The leakage of particles of a given energy E and initial value of the action invariant μ is characterised by more than one life times. 2) The two lifetimes are found to be exponential functions of confining magnetic fields, with the ratio of the exponents lying in the range of 1.8 to 2.3, which can be considered to be in good agreement with the theoretical value of 2. 3) The values of exponents, are found to vary with

energy E and magnetic field scale length α^{-1}, which is in qualitative agreement with theory. This agreement becomes more quantitative for larger values of the pitch angle. 4) Amplitude corresponding to life time τ_1, is found to increase with the magnetic field while that corresponding to τ_2 decreases until it becomes vanishingly small for sufficiently large magnetic fields.

5.3 Future Experimental Programme.

The present work described in this thesis can be considered as the basis for more experimental studies to have a better and complete understanding of the phenomenon. Continuing in the same line of experimental work, one can do the experiment at larger pitch angles. Since, it was not possible to attain higher pitch angle in the present set up, some modifications in the source region would be necessary. With the required modifications one would be able to investigate the slopes corresponding to different life times at higher pitch angles and seek for better quantitative comparison with the theory.

It can be noted that the theory mentions multiple life times for particles with same energy and initial value of the magnetic moment. It would be highly interesting, therefore, to see if there exists at least a third life time. For this, one has to increase the signal amplitude to avoid contamination of the data due to digitisation error.

From the observations made in subsection 4.3.5, it is seen that any change in the shape of the magnetic field configuration near the magnetic mirror changed the slope values for the two observed life times. To have a thorough understanding of this behaviour, experiments can be conducted in different field configurations of different shapes, keeping the field scale length constant to have a better comparison among the slope values for different field configurations of different shapes. With all these further experimentations, one would be able to study many more interesting aspects of the problem discussed in this thesis.

REFERENCES

1. Alfven H., Cosmical Electrodynamics, Oxford (1950), 19.
2. Arnold V.I., Usp. Mat. Nauk 8, (1963), 91.
3. Ash E.A., Electron Optics in Hand book of Vacuum Physics, Vol.2, Physical Electronics (ed. A.H. Beck), Pergamon Press (1968), 482.
4. Baldwin D.E., Revs. Mod. Phys. 49, (1977) 317.
5. Balebanov V.M. and Semashko N.N., Nucl. Fus., 7, (1967), 207.
6. Bernstein I.B., Adv. Plasma Phys., Vol.4. (ed. A.Simon and W.B. Thompson) Wiley, N.Y., (1971), 311.
7. Bernstein I.B and Rowland G., Phys. Fluids, 19, (1976), 1546.
8. Brevnov N.N. and Tomashchuk Yu. F., J. Nucl. Energy Pt. C: Plasma Phys. 6, (1964), 161.
9. Chen F.F., in Plasma Diagnostic Techniques (ed. R.H. Huddlestone and S.L. Leonard), Academic Press (1965), 113.
10. Chirikov B.V., J. Nucl. Energy, Pt. C : Plasma Phys. 1, (1960), 253.
11. Cohen R.H., Rowland G and Foote J.H., Phys. Fluids 21, (1978), 627.
12. Curtis L.J., Life time Measurements in Beam foil Spectroscopy (topics in Current Physics 1, ed. S. Bashkin), Springer Verlag, N.Y, (1976), 88.

13. Decker G and Honea D.L., Rept. from Centre for Plasma Phys. and thermonuclear Research, Univ. Texas, Austin, CPPT 36, ORO - 3458 - 29, (1971).

14. Dubinina A.N., Tranin L. Ya. and Chirikov B.V., Sov. Phys. JETP 22, (1966), 260.

15. Dubinina A.N. and Krasitskaya L.S., JETP Lett. 5, (1967), 184.

16. Dubinina A.N., Krasitskaya L.S. and Yudin Yu. N., Plasma Phys. 11, (1969), 551.

17. Dworschak G., Haberey F., Hildebrand P., Kneller E and Schreiber D., Rev. Sci. Instrum. 45, (1974), 243.

18. Dykhne A.M. and Chaplik A.V., Sov. Phys. JETP 13, (1961), 465.

19. Fermi E., Nuclear Physics, Univ. Chicago Press, Chicago (1950).

20. Früngel F.B.A., High Speed Pulse Technology, Vol. 1, Academic Press, New York, (1965), 235, 229.

21. Garren A., Riddell R.J., Smith L., Bing G., Henrich L.R, Northrop T.G. and Robert J.E., Proceedings of 2nd United Nations Intern. Conf. Peaceful uses of At. Energy, 31, (1958), 65.

22. Gibson G., Jordan W.C., and Lauer E.J., Phys. Fluids, 6, (1963), 116.

23. Gibson G., Jordan W.C. and Lauer E.J., Phys. Fluids, 6, (1963), 133.

24. Glasoe G.N. and Lebacqz J.V., Pulse Generators, Mac Graw-Hill, New York (1948), 201.

25. Hastie R.J., Hobbs G.D. and Taylor J.B., Plasma Physics and controlled Nucl. Fusion Research (Int. At. Energy Agency, Vienna), 1, (1969), 389.

26. Il'ina A.N. and Il'in V.D., JETP Lett. 19, (1974), 388.

27. Il'in V.D. and Il'ina A.N., Sov. Phys. - JETP, 43, (1976), 661.

28. Il'in V.D. and Il'ina A.N., Sov. Phys. - JETP, 48, (1978), 259.

29. Intersil Semi Conductor Products Catalogue, (1974), 157.

30. James F., Function Minimization, Reprinted from the Proc. of the 1972 CERN Computing and Data Processing School, CERN 72-21 (1972).

31. James F., Interpretation of the errors on parameters as given by minuit, CERN Computer Centre Library (1978), D516.

32. James F. and Roos M., A system for Function Minimization and Analysis of the Parameter Errors and correlations (Long Write up), Computer Centre Programme Library (1977) D506.

33. Kruskal M.D., Advanced Theory of Gyrating Particles in "Plasma Physics", Int. At. Energy Agency, Vienna, 1965.

34. Kulsrud R.M., Phys. Rev. 106, (1957), 205.

35. Lanczos C., Applied Analysis, (1956), 272.

36. Landau L., Lifshitz E., Quantum Mechanics (course of theor. phys. vol.3), Pergamon Press, (1977).

37. Litvinenko L.N., Moroz E.E., Sal'nikova L.P. and Shestopalov V.P., Sov. Phys. - Tech. Phys. 17, (1973), 1968.

38. Montgomery D.B., Solenoid Magnet Design, Wiley - Interscinece, (1969), 258.

39. Nelder J.A. and Mead R., Comput. J. 7 (1965), 308.

40. Northrop T.G., The adiabatic Motion of charged particles, Interscience Publishers (1963), 96.

41. Ponomarenko V.G., Tranin L. Ya., Yurchenko V.I. and Yasnetskii A.N., Sov. Phys. - JETP 28, (1969), 1.

42. Roth Reece J., Phys. Fluids 7, (1964), 536.

43. Roth Reece J., Nonadiabatic Particle Losses in axisymmetric and multipolar magnetic fields, Nasa Tech. Note NASA TN D - 3164 (1965).

44. Rodionov S.N., J. Nucl. Energy, Pt. C. Plasma Phys. 1, (1960), 247.

45. Sinel'nikov K.D., Fedorchenko V.D., Rutkevich B.N., Chernyi B.M. and Safronov B.G., Sov. Phys.-Tech. Phys. 5, (1960), 236.

46. Thesis A.J., Ph.D. Thesis, Univ. of Maryland, (1973) and references there in related to the RPA construction.

47. Varma R.K., Phys. Rev. Lett. 26, (1971), 417.

48. Varma R.K., and Horton Jr. C.W., Phys. Fluids 15, (1972), 1469.

49. Varma R.K., Pramana, 10, (1978), 89.

APPENDIX-A

MIRROR MAGNETIC FIELD DESIGN PROCEDURE

The design procedures were based on the minimisation of a weighted sum of the squared deviations from the desired field profile and the power dissipated in the coils for a given field configuration. Such a minimisation yielded a set of simultaneous equations, which in certain cases happened to be linear, depending upon the parameters with respect to which the minimisation was carried out. These simultaneous equations were then solved to obtain the desired parameters.

A system with N coaxial coils was considered and M points along the axis of these coils were chosen where the desired field strength was specified. In the analysis, the coils carried an index n and the points at which the desired field was specified, carried on index m. If the desired field at point m was designated by Bm, then the deviation dm could be written as[38]

$$d_m = B_m - \sum_{n=1}^{N} i_n b_{nm} \qquad (A.1).$$

where i_n was the current in amperes through the n^{th} coil and b_{nm} was the geometrical factor which gave the magnetic field produced at point m by n^{th} coil from a unit current flowing through it. b_{nm} could be written in the following way[38]

$$b_{nm} = \frac{0.2\pi N_n a_n^2}{\left(r_{nm}^2 + a_n^2\right)^{3/2}} \qquad (A.2).$$

Here r_{nm} represented the distance between point m and centre of the n^{th} coil along the axis. η_n was the number of turns in the coil and a_n — the radius of the coil. However, if the width and depth of the coils were not very small incomparison to its radius, b_{nm}, could be expressed as

$$b_{nm} = \frac{\eta_n a_{1n}}{2h_n(a_{2n}-a_{1n})}\left[\frac{F(\alpha_n,\beta_n+r_{nm})+F(\alpha_n,\beta_n-r_{nm})}{2}\right]$$

where

$$F(\alpha_n,\beta_n)=\frac{4\pi\beta_n}{10}\ln\frac{\alpha_n+(\alpha_n^2+\beta_n^2)^{1/2}}{1+(1+\beta_n^2)^{1/2}} \qquad (A.3)$$

Here $\alpha_n = a_{2n}/a_{1n}$ was the ratio of outer radius a_{2n} to the inner radius a_{1n} and $\beta_n = h_n/a_{1n}$ was the ratio of the half width h_n to the inner radius. If ρ_n represented the resistance of the n^{th} coil, the power dissipated in the n^{th} coil was given by

$$P_n = i_n^2 \rho_n \qquad (A.4).$$

A function χ^2 was defined as

$$\chi^2 = \sum_{m=1}^{M} W_m d_m^2 + \sum_{n=1}^{N} W_p i_n^2 \rho_n \qquad (A.5)$$

χ^2, thus represented a weighted sum of the squared deviations from the specified field configuration at all test points and the power dissipated in all the coils. When the function χ^2 was minimised with respect to a set of parameters, the resulting values of those parameters yielded a

configuration giving best fit to the specified field profile and the procedure also resulted in optimising the power dissipation.

During the course of the experiments, different field configurations were used. To design these field configurations, χ^2 was either minimised with respect to currents in different coils or with respect to axial positions of the coils for a fixed value of current.

Minimisation with respect to currents i_n $(n = 1, N)$, lead to a set of equations

$$\partial \chi^2 / \partial i_n = 0 \quad ; \quad n = 1, 2, - - - - N \qquad \text{(A.6)}$$

which could be solved to obtain currents in different coils placed at known axial positions. Using eqs (A.1) and (A.5) the set of equations represented by (A.6) could be rewritten as

$$\sum_{\substack{n=1 \\ n \neq j}}^{N} i_n A_{jn} + i_j A_{jj} = C_j \; ; \; j = 1, N \qquad \text{(A.7)}$$

where

$$\begin{aligned} C_j &= \sum_{m=1}^{M} w_m B_m b_{jm} \\ A_{jn} &= \sum_{m=1}^{M} w_m b_{nm} b_{jm} \\ A_{jj} &= \sum_{m=1}^{M} w_m b_{jm}^2 + w_p \beta_j \end{aligned} \qquad \text{(A.8)}$$

All the equations in the set of simultaneous equations represented by (A.7) were linear in currents i_j and could be solved to obtain values of currents for different coils. The set (A.7) could be represented in the form of a matrix as

$$[A] \times [I] = [C] \qquad (A.9)$$

where $[A]$ represented N X N matrix and $[C]$, the N element column vector, having elements given by (A.8), while $[I]$ represented a N element column vector having currents i_j, $j = 1, N$ as its elements. Equation (A.9) then could be solved to obtain $[I]$ as follows:

$$[I] = [C]\,[A^{-1}] \qquad (A.10)$$

where $[A^{-1}]$ is the inverse of matrix $[A]$.

The minimisation was carried out using a Fortran programme, based on the logic outlined above and developed for designing axi-symmetric magnetic field systems. The desired field profile was achieved by an iterative procedure which involved adjustment of the coil currents. The deviations at test points were all given equal weights and similarly all the power turns were given equal weights. However, the weights W_p were always chosen smaller than the weights W_m and a certain amount of optimisation was necessary in the ratio of W_p to W_m to obtain the desired fit with optimal power dissipation.

Minimisation with respect to coil positions, keeping the current fixed, lead to a set of equations

$$\partial \chi^2 / \partial X_j = 0 \quad ; \quad j = 1, 2, \ldots N \qquad (A.11)$$

where the function χ^2 could be defined as

$$\chi^2 = \sum_{i=1}^{N} W_i \left(B_i - \sum_{j=1}^{M} F_j \left(\vec{r}_{ji} \right) \right)^2 \qquad \text{(A.12)}$$

Here $F_j(\vec{r}_{ji})$ represented the geometrical factor for the field value. $\vec{r}_{ji} = \vec{X}_j - \vec{x}_i$; $\vec{X}_j$ was the axial distance of the point from the centre of the system while X_i was the axial distance of the coil from the centre of the system.

However the set of equations (A.11) were non linear and the solutions were not as simple as in the previous case. Therefore to solve these equations the method of "Steepest descent" was used. The parameters X_j could be considered as coordinates of a N - element vector $\vec{\lambda}$

$$\vec{\lambda} = \vec{\lambda}(X_1, X_2, \ldots X_N) \qquad \text{(A.13).}$$

Then the surface $\chi^2 = \chi^2(\vec{\lambda})$ would have a valley in the neighbourhood of the best fit values of the parameters such that equation (A.11) was satisfied. For achieving minimisation, an initial estimate of the vector was made. Then, quantised vector increments, in the direction of $-\vec{\nabla}\chi^2$ were given to the vector $\vec{\lambda}_j$, the magnitude of the increments being adjusted in binary approximation. A new value of $\vec{\lambda}_{j+1}$ was obtained from the previous value $\vec{\lambda}_j$ using the following relation

$$\vec{\lambda}_{j+1} = \vec{\lambda}_j - \epsilon_{j+1} \frac{\vec{\nabla}\chi^2(\vec{\lambda}_j)}{|\vec{\nabla}\chi^2(\vec{\lambda}_j)|} \qquad (A.14)$$

and the process of interaction was repeated till the minimum was approached, thus satisfying the criterion for the approach to the minimum. ϵ_{j+1} is the small increment mentioned above.

Based on the above idea, Fortran programme was developed for χ^2 minimisation using the "Steepest descent" method. As in the previous case, the deviations at the test points were all given equal weights and similarly all the power terms were given equal weights.

As mentioned in chapter 2.2, all the coils had equal number of turns with equal radii. Therefore the constant current mode of operation was more economical for the given set of coils. Because, to operate in the variable current mode, different shunts of different values had to be incorporated with the coils to obtain the desired field configurations, thus dissipating a part of the power consumed. The discripancy between the calculated and measured values at different axial positions was $\lesssim 5\%$.